

Theory of elastic neutrino-electron scattering

OLEKSANDR TOMALAK^{1,2,3} AND RICHARD J. HILL^{1,2}

¹*Department of Physics and Astronomy, University of Kentucky, Lexington, KY 40506, USA*

²*Fermilab, Batavia, IL 60510, USA*

³*Institut für Kernphysik and PRISMA Cluster of Excellence, Johannes Gutenberg Universität, Mainz, Germany*

July 9, 2019

Theoretical predictions for elastic neutrino-electron scattering have no hadronic or nuclear uncertainties at leading order making this process an important tool for normalizing neutrino flux. However, the process is subject to large radiative corrections that differ according to experimental conditions. In this paper, we collect new and existing results for total and differential cross sections accompanied by radiation of one photon, $\nu e \rightarrow \nu e(\gamma)$. We perform calculations within the Fermi effective theory and provide analytic expressions for the electron energy spectrum and for the total electromagnetic energy spectrum as well as for double- and triple-differential cross sections w.r.t. electron energy, electron angle, photon energy, and photon angle. We discuss illustrative applications to accelerator-based neutrino experiments and provide the most precise up-to-date values of neutrino-electron scattering cross sections. We present an analysis of theoretical error, which is dominated by the $\sim 0.2 - 0.4\%$ uncertainty on the hadronic correction.

Contents

1	Introduction	4
2	Neutrino-electron scattering	5
2.1	Kinematics for neutrino-electron scattering	5
2.2	Effective neutrino-charged lepton operators	6
2.3	Effective neutrino-lepton and neutrino-quark interactions beyond leading order	8
3	Virtual QED corrections	8
3.1	QED vertex correction	9
3.2	Closed fermion loops: leptons and heavy quarks	10
3.3	Light-quark contribution	12
4	Real photon emission	13
4.1	Radiation of one photon	13
4.2	Triple-differential distribution	14
4.3	Double-differential distribution in electron energy and electron angle	15
4.4	Double-differential distribution in electromagnetic energy and electron angle	16
4.5	Double-differential distribution in photon energy and electron energy	17
4.6	Double-differential distribution in photon energy and photon angle	18
4.7	Photon energy spectrum	19
4.8	Electron energy spectrum	19
4.9	Electromagnetic energy spectrum	22
4.9.1	Below electron endpoint: $E_{\text{EM}} \leq E'_0 = m + \frac{2\omega^2}{m+2\omega}$	22
4.9.2	Above electron endpoint: $E_{\text{EM}} > E'_0 = m + \frac{2\omega^2}{m+2\omega}$	24
4.10	Absolute cross section	24
5	Illustrative results	24
5.1	Total cross section: energy dependence and error analysis	24
5.2	Electron and total electromagnetic energy spectra	26
5.3	Electron angular spectrum	26
6	Conclusions and outlook	27
A	QCD correction to QED vacuum polarization	29
B	Triple-differential distribution	30
C	Double-differential distribution in electron energy and electron angle	32
D	Double-differential distribution in electromagnetic energy and electron angle	33
E	Double-differential distribution in photon energy and electron energy	34
F	Double-differential distribution in photon energy and photon angle	34
G	Photon energy spectrum	36
H	Electron energy spectrum	37
I	Electromagnetic energy spectrum below electron endpoint	38

J	Electromagnetic energy spectrum above electron endpoint	40
K	Total cross section	41
L	Averaged over flux neutrino cross sections	42
	References	47

1 Introduction

In the Standard Model of particle physics, neutrinos are massless particles. However, experiments with solar [1–6], atmospheric [7, 8], reactor [9–13] and accelerator [14–16] neutrinos,¹ establish that neutrinos oscillate and have nonzero mass [17, 18], thus providing a convincing example of physics beyond the Standard Model. Fundamental questions about this definitive portal to new physics remain unanswered: What is the origin of neutrino mass? Are lepton number and CP symmetries violated? Do sterile neutrinos exist? What is the absolute scale and ordering of neutrino masses? New experiments aim to address these questions but rely on a precise description of neutrino interactions with the ordinary matter (electrons and nuclei) used to detect them.

Interactions with atomic nuclei compose the bulk of neutrino scattering events at accelerator neutrino experiments. Although interactions with atomic electrons are rarer, they are nonetheless valuable. The neutrino-electron scattering process plays an important dual role: first, owing to a clean experimental signature and a small cross-section uncertainty, the process provides an incisive constraint on neutrino flux [19, 20]; second, the bulk of next-to-leading order (NLO) radiative corrections can be evaluated analytically and thus serve as a prototype for the more complicated cases of neutrino-nucleon and neutrino-nucleus scattering.

Radiative corrections to elastic neutrino-electron scattering of order α were calculated first in Ref. [21], where only soft-photon bremsstrahlung was considered. In Ref. [22], an analytical phase-space integration technique was developed to include hard-photon bremsstrahlung, and the electron energy spectrum for neutrino-electron scattering accompanied by one radiated photon was obtained. The leading-order (LO) cross section in the low-energy limit of the Weinberg theory [23] was evaluated in Ref. [24]. References [25, 26] presented the electron energy spectrum in the limit of small electron mass accounting for corrections of order α , and including other electroweak NLO radiative corrections. The electromagnetic energy spectrum was considered in Refs. [27, 28]. Reference [29] reproduced results of Refs. [22, 25] by numerically performing the phase-space integration, and accounted for the electron mass suppressed interference term; Ref. [29] also presented a numerical evaluation of the electromagnetic energy spectrum. The hard photon correction to the total elastic cross section was studied in Refs. [30, 31]. Different aspects of radiative corrections in elastic neutrino-electron scattering were also discussed in Refs. [27–44]. See Refs. [45, 46] for recent reviews.

In this work, we analytically evaluate relevant distributions and spectra in elastic (anti-)neutrino-electron scattering starting from four-fermion effective field theory (EFT). We take neutrino-lepton and neutrino-quark EFT coefficients from Ref. [47] and calculate virtual corrections in the $\overline{\text{MS}}$ renormalization scheme. Exploiting the technique of Ref. [22], we evaluate the electron energy spectrum and present this calculation in a relatively compact form. We generalize this technique for the evaluation of the electromagnetic energy spectrum as well as triple and double-differential cross sections. We discuss a new treatment of “hadronic penguin” diagrams; this contribution dominates the error budget for neutrino-electron scattering, and impacts other neutral current neutrino processes, such as coherent neutrino-nucleus scattering [48]. As illustrative applications using accelerator neutrino beams [16, 49–51] we consider the impact of radiative corrections on energy spectra, and compare observables employing electron energy versus total electromagnetic energy. For possible low-energy applications, we provide results in analytic form keeping all charged lepton mass terms. The complete mass dependence could be useful in the analysis of future reactor and solar neutrino experiments [52–56].

The paper is organized as follows. Section 2 considers the kinematics of neutrino-electron scattering and computes the tree-level scattering process including electroweak corrections to the low-energy four-fermion interaction. Section 3 computes virtual corrections to elastic scattering. Section 4 represents the bulk of the paper and computes QED corrections involving real radiation. Section 5 presents illustrative results for total cross sections and electron energy versus total electromagnetic energy spectra. Section 6 presents our conclusions and outlook. In the main text of the paper, we describe the general strategy

¹ For the purposes of this paper, “accelerator” neutrinos have energy large compared to the electron mass.

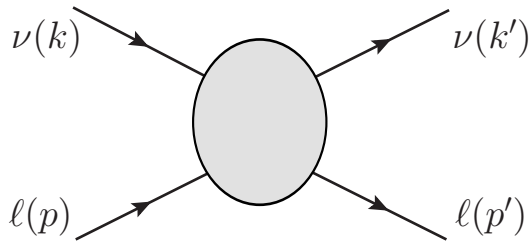


Figure 1: Neutrino-electron scattering kinematics.

of the computations and focus on results in the limit of small electron mass (i.e., neutrino beam energy much larger than electron mass). Appendices provide general expressions retaining all electron mass terms. Appendix A summarizes higher-order perturbative QCD corrections to heavy-quark loops that are discussed in Section 3.2. Appendix L displays flux-averaged spectra in experimental conditions of DUNE, MINERvA, NOvA and T2K experiments.

2 Neutrino-electron scattering

We begin in Section 2.1 by reviewing the kinematics of neutrino scattering on atomic electrons. Throughout this Section we consider general charged leptons ℓ , but in following Sections we specialize to the phenomenologically most relevant case of the electron, $\ell = e$. We introduce the relevant basis of four-fermion effective operators in Section 2.2 and discuss their coefficients in Section 2.3.

2.1 Kinematics for neutrino-electron scattering

Consider the scattering of neutrinos on atomic electrons. We neglect the atomic binding energy and momentum compared to the energy and momentum transferred in the scattering process. Consequently, the initial electron is taken to be at rest in the laboratory frame, where the kinematics is given by $p^\mu = (m, 0)$ (initial electron with $p^2 = m^2$), $p'^\mu = (E', \mathbf{k} - \mathbf{k}')$ (final charged lepton with $p'^2 = m'^2$), $k^\mu = (\omega, \mathbf{k})$ (initial neutrino), $k'^\mu = (\omega', \mathbf{k}')$ (final neutrino), see Figure 1. The neutrino mass scale is much lower than the electron mass and typical neutrino beam energy, and we neglect the neutrino mass m_ν throughout. We will let $q^\mu = p'^\mu - p^\mu$ denote the momentum transfer to the charged lepton and write $m_e = m$ for the electron mass.

Elastic scattering is described by two independent kinematical variables. It is convenient to introduce the invariant momentum transfer,

$$q^2 = (p' - p)^2, \quad (1)$$

and the squared energy in the centre-of-mass reference frame,

$$s = (p + k)^2. \quad (2)$$

Note that production of heavier charged leptons in neutrino-electron scattering is possible when the neutrino beam energy is high enough. Using $s = m^2 + 2m\omega \geq m'^2$ we see that $\omega \geq (m'^2 - m^2)/(2m) \approx 10.9$ GeV to produce a muon ($m' = m_\mu$), while $\omega \geq 3089$ GeV for the production of τ ($m' = m_\tau$).

The neutrino scattering angle in the laboratory frame, Θ_ν , can be expressed in terms of the final neutrino energy ω' as

$$\cos \Theta_\nu = \frac{\omega\omega' - m(\omega - \omega') - \frac{m^2 - m'^2}{2}}{|\mathbf{k}||\mathbf{k}'|} = 1 + \frac{m}{\omega} - \frac{m}{\omega'} - \frac{m^2 - m'^2}{2\omega\omega'}. \quad (3)$$

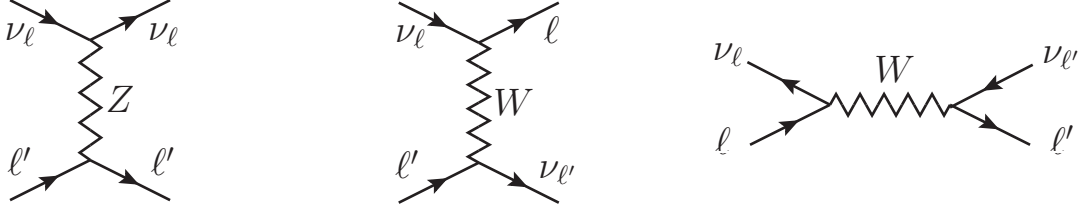


Figure 2: Leading-order contributions to neutrino-lepton scattering in the Standard Model. The graph with the exchange of Z boson contributes to the neutrino and antineutrino scattering. ℓ and ℓ' denote charged leptons of any flavor in this Figure.

The final neutrino energy varies between backward and forward scattering in the range:

$$\frac{m\omega}{m+2\omega} + \frac{m^2 - m'^2}{2(m+2\omega)} \leq \omega' \leq \omega + \frac{m^2 - m'^2}{2m}, \quad (4)$$

corresponding to the charged lepton energy range:

$$m + \frac{m'^2 - m^2}{2m} \leq E' \leq m + \frac{2\omega^2}{m+2\omega} + \frac{m'^2 - m^2}{2(m+2\omega)}. \quad (5)$$

The angle between recoil charged lepton direction and the neutrino beam direction, Θ_e , is given by

$$\cos \Theta_e = \frac{\omega E' - m^2 - m(\omega - E') + \frac{m^2 - m'^2}{2}}{\omega |\mathbf{p}'|}, \quad (6)$$

and scattering is possible only in the forward cone bounded by Θ_e^{\max} :

$$\cos \Theta_e^{\max} = \sqrt{\frac{m'^2 - m^2}{m^2} \frac{(2\omega + m)^2 - m'^2}{4\omega^2}}. \quad (7)$$

The scattering angle expression simplifies for the elastic process ($m' = m$) to

$$\cos \Theta_e = \frac{m + \omega}{\omega} \sqrt{\frac{E' - m}{E' + m}}, \quad (8)$$

when it varies between 0 and 1, i.e., the electron is scattered always into the forward hemisphere.

2.2 Effective neutrino-charged lepton operators

Neutrino-electron scattering is described by the exchange of weak vector bosons W and Z (with masses M_W and M_Z respectively) in the Standard Model, cf. Figure 2 for contributing Feynman diagrams. At energies below the electroweak scale, the interactions of neutrinos and charged leptons are determined by an equivalent effective Lagrangian [57–59]. Neglecting corrections suppressed by $1/M_W^2$, the effective Lagrangian consists of momentum-independent four-fermion operators.

At tree level, the matching onto this effective Lagrangian \mathcal{L}_{eff} is readily obtained,

$$\mathcal{L}_{\text{eff}} = -\frac{g^2}{M_W^2} (J_{W^+})^\mu (J_{W^-})_\mu - \frac{g^2}{2M_Z^2} (J_Z)^\mu (J_Z)_\mu, \quad (9)$$

where $J_{W^-}^\mu$, $J_{W^+}^\mu = J_{W^-}^{\dagger\mu}$ and J_Z^μ are charged and neutral currents in the Standard Model Lagrangian coupling to W^+ , W^- and Z respectively, and g is the electroweak $\text{SU}(2)_L$ coupling constant. Focusing on leptonic versus quark operators, we have

$$J_{W^-}^\mu = \frac{1}{\sqrt{2}} \sum_{\ell} \bar{\ell} \gamma^\mu P_L \nu_{\ell}, \quad (10)$$

$$J_Z^\mu = \frac{1}{\cos\theta_W} \sum_\ell \left[\left(-\frac{1}{2} + \sin^2\theta_W \right) \bar{\ell} \gamma^\mu P_L \ell + \sin^2\theta_W \bar{\ell} \gamma^\mu P_R \ell + \frac{1}{2} \bar{\nu}_\ell \gamma^\mu P_L \nu_\ell \right], \quad (11)$$

where $P_L = (1 - \gamma_5)/2$ and $P_R = (1 + \gamma_5)/2$ are projection operators onto left-handed and right-handed fermions and θ_W denotes the weak mixing angle satisfying $M_W/M_Z = \cos\theta_W$. After Fierz rearrangement of the charged current contribution, the result may be written as

$$\mathcal{L}_{\text{eff}} = - \sum_{\ell, \ell'} \bar{\nu}_\ell \gamma^\mu P_L \nu_\ell \bar{\ell}' \gamma_\mu (c_L^{\nu_\ell \ell'} P_L + c_R P_R) \ell' - c \sum_{\ell \neq \ell'} \bar{\nu}_{\ell'} \gamma^\mu P_L \nu_\ell \bar{\ell} \gamma_\mu P_L \ell', \quad (12)$$

with coefficients $c_L^{\nu_\ell \ell'}$, c_R and c :

$$c_L^{\nu_\ell \ell'} = 2\sqrt{2}G_F \left(\sin^2\theta_W - \frac{1}{2} + \delta_{\ell\ell'} \right), \quad c_R = 2\sqrt{2}G_F \sin^2\theta_W, \quad c = 2\sqrt{2}G_F, \quad (13)$$

where we have introduced the Fermi constant $G_F = g^2/(4\sqrt{2}M_W^2)$, and where the Kronecker symbol $\delta_{\ell\ell'}$ satisfies $\delta_{\ell\ell'} = 1$ for $\ell = \ell'$ and $\delta_{\ell\ell'} = 0$ for $\ell \neq \ell'$. Note that coefficients c and c_R are the same for all combinations of lepton flavors, while the coefficient $c_L^{\nu_\ell \ell'}$ depends on whether the neutrino and charged lepton have the same flavor.

Neglecting the neutrino magnetic moment contribution [60–66], the leading-order cross section of neutrino-lepton scattering can be expressed, in all possible cases, as [24, 25, 29, 67–92]

$$\frac{d\sigma_{\text{LO}}^{\nu_\ell \ell' \rightarrow \nu_\ell \ell'}}{d\omega'} = \frac{m}{4\pi} \left[\left(c_L^{\nu_\ell \ell'} \right)^2 I_L + c_R^2 I_R + c_L^{\nu_\ell \ell'} c_R I_R^L \right], \quad (14)$$

$$\frac{d\sigma_{\text{LO}}^{\bar{\nu}_\ell \ell' \rightarrow \bar{\nu}_\ell \ell'}}{d\omega'} = \frac{m}{4\pi} \left[\left(c_L^{\nu_\ell \ell'} \right)^2 I_R + c_R^2 I_L + c_L^{\nu_\ell \ell'} c_R I_R^L \right], \quad (15)$$

$$\left. \frac{d\sigma_{\text{LO}}^{\nu_\ell \ell' \rightarrow \nu_{\ell'} \ell}}{d\omega'} \right|_{\ell \neq \ell'} = \frac{m}{4\pi} c^2 I_L, \quad (16)$$

$$\left. \frac{d\sigma_{\text{LO}}^{\bar{\nu}_\ell \ell \rightarrow \bar{\nu}_{\ell'} \ell'}}{d\omega'} \right|_{\ell \neq \ell'} = \frac{m}{4\pi} c^2 I_R, \quad (17)$$

with kinematical factors:

$$I_L = \frac{(k \cdot p)(k' \cdot p')}{m^2 \omega^2} = 1 + \frac{m^2 - m'^2}{2m\omega} \rightarrow 1, \quad (18)$$

$$I_R = \frac{(k \cdot p')(k' \cdot p)}{m^2 \omega^2} = \frac{\omega'^2}{\omega^2} \left(1 + \frac{m'^2 - m^2}{2m\omega'} \right) \rightarrow \frac{\omega'^2}{\omega^2}, \quad (19)$$

$$I_R^L = -\frac{mm'(k \cdot k')}{m^2 \omega^2} = -\frac{m'}{\omega} \left(1 - \frac{\omega'}{\omega} + \frac{m^2 - m'^2}{2m\omega} \right) \rightarrow -\frac{m}{\omega} \left(1 - \frac{\omega'}{\omega} \right), \quad (20)$$

where the limit of elastic process, i.e., $m' = m$, is presented in the last step. The neutrino-energy spectra in Eqs. (14–17) are equivalent to the recoil electron energy spectra due to energy conservation: $m + \omega = E' + \omega'$. In particular, $d\sigma/dE' = d\sigma/d\omega'$. We later apply this observation to compute differential cross sections with respect to total electromagnetic energy in the presence of radiative corrections. To study the angular spectrum, the differential cross section can be obtained by exploiting

$$dE' = \frac{4m\omega^2 (m + \omega)^2 \cos\Theta_e d\cos\Theta_e}{\left[(m + \omega)^2 - \omega^2 \cos^2\Theta_e \right]^2}. \quad (21)$$

Table 1: Effective couplings (in units 10^{-5} GeV^{-2}) in the Fermi theory of neutrino-fermion scattering with 4 quark flavors at the scale $\mu = 2 \text{ GeV}$. The error due to the uncertainty of Standard Model parameters is shown.

$c_L^{\nu\ell\ell'}, \ell = \ell'$	$c_L^{\nu\ell\ell'}, \ell \neq \ell'$	c_R	c_L^u	c_R^u	c_L^d	c_R^d
2.39736(26)	-0.90166(26)	0.76834(24)	1.14118(18)	-0.51112(16)	-1.41508(11)	0.25591(8)

We observe that the contribution from the interference term I_R^L is suppressed by the charged lepton mass. The neutrino and antineutrino scattering are related by the substitution $I_L \leftrightarrow I_R$ ($k \leftrightarrow k'$) or equivalently $c_L^{\nu\ell\ell'} \leftrightarrow c_R$.

Note that $\nu_\ell \ell \rightarrow \nu_\ell \ell$ and $\bar{\nu}_\ell \ell \rightarrow \bar{\nu}_\ell \ell$ cross sections involving one flavor seem to be not positive definite for energies comparable with the charged lepton mass due to the helicity-flip interference term $c_L^{\nu\ell\ell} c_R$. However, the cross section is always positive in the physical region of scattering $m\omega/(m+2\omega) < \omega' < \omega$ and can vanish only in case of forward recoil electrons with maximum energy $E' = m + \omega^2/(m+2\omega)$ [93, 94] in the scattering of an electron antineutrino of energy $\bar{\omega}$:

$$\bar{\omega} = \left(\frac{c_L^{\nu\ell\ell}}{c_R} - 1 \right) \frac{m}{2}. \quad (22)$$

2.3 Effective neutrino-lepton and neutrino-quark interactions beyond leading order

Higher-order electroweak and QCD contributions modify couplings in the effective Lagrangian of Eq. (12). The evaluation of virtual NLO corrections to elastic neutrino-charged lepton scattering also involves interaction with quarks and gluons; see Sections 3.2 and 3.3. The relevant neutral current part of the effective neutrino-quark Lagrangian is

$$\mathcal{L}_{\text{eff}}^q = - \sum_{\ell, q} \bar{\nu}_\ell \gamma^\mu P_L \nu_\ell \bar{q} \gamma_\mu (c_L^q P_L + c_R^q P_R) q, \quad (23)$$

with (neutrino flavor independent) left- and right-handed couplings c_L^q and c_R^q respectively. At tree level,

$$c_L^q = 2\sqrt{2}G_F (T_q^3 - Q_q \sin^2 \theta_W), \quad c_R^q = -2\sqrt{2}G_F Q_q \sin^2 \theta_W, \quad (24)$$

where T_q^3 denotes the quark isospin (+1/2 for $q = u, c$, -1/2 for $q = d, s$) and Q_q its electric charge in units of the positron charge (+2/3 for $q = u, c$, -1/3 for $q = d, s$). For numerical analysis, we employ low-energy effective couplings from Ref. [47]. For definiteness, we take inputs in four-flavor QCD ($n_f = 4$) at renormalization scale $\mu = 2 \text{ GeV}$ in the $\overline{\text{MS}}$ scheme and do not distinguish between couplings to u (d) and c (s) quarks.²

The effective Lagrangians of Eqs. (12) and (23), and the corresponding charged current quark operators [47], determine neutrino scattering rates at GeV energy scales, up to corrections suppressed by powers of electroweak scale particle masses. Electroweak scale physics is encoded in the values of the operator coefficients from Table 1. Real photon radiation and virtual corrections involving the photon and other light particles must still be calculated within the effective theory.

3 Virtual QED corrections

In this Section, we present virtual corrections, considering QED vertex corrections involving virtual photons in Section 3.1 and closed fermion loop contributions from leptons and heavy quarks in Section 3.2. We estimate the correction coming from light-quark loops in Section 3.3.

² In Ref. [47], one-loop matching to the Standard Model is performed at the electroweak scale accounting for the leading QCD corrections with one exchanged gluon inside quark loops and neglecting masses of all fermions except the top quark compared to the electroweak scale. The matching is accompanied by renormalization group evolution to GeV scales to resum large electroweak logarithms in the effective couplings.

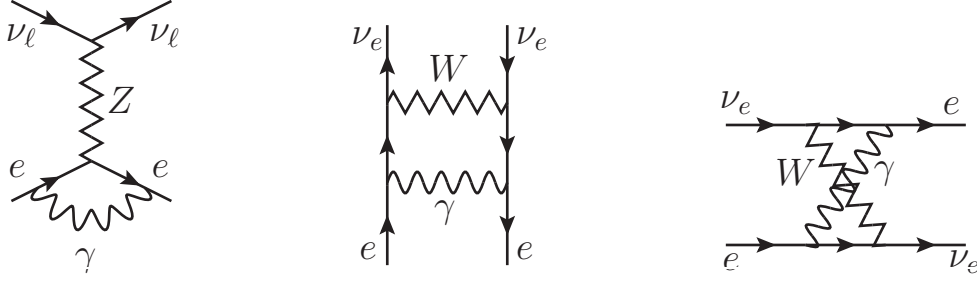


Figure 3: Virtual corrections to elastic neutrino-electron scattering in the Standard Model corresponding to the vertex correction in effective theory.

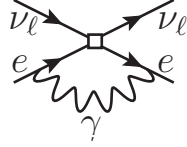


Figure 4: QED vertex correction to elastic neutrino-electron scattering in effective theory.

3.1 QED vertex correction

We consider one-loop virtual corrections in elastic (anti-)neutrino-electron scattering $\nu_\ell e \rightarrow \nu_\ell e$ ($\bar{\nu}_\ell e \rightarrow \bar{\nu}_\ell e$). Within the Standard Model, the vertex correction is given by the diagrams in Figure 3, while only the single diagram in Figure 4 contributes in the effective theory. The usual field renormalization factors must be applied to external legs.

First, we evaluate the one-loop vertex correction to the matrix element of left-handed (L) and right-handed (R) charged lepton currents $J_\mu^{\text{L,R}} = \bar{e}(p') \gamma_\mu P_{\text{L,R}} e(p)$ from Eq. (12). We perform the integration in $d = 4 - 2\epsilon$ dimensions of space-time to regularize the ultraviolet divergence:

$$\delta J_\mu^{\text{L,R}} = -e^2 \int \frac{id^d L}{(2\pi)^d} \frac{\bar{e}(p') \gamma^\lambda (\not{p}' - \not{L} + m) \gamma_\mu P_{\text{L,R}} (\not{p} - \not{L} + m) \gamma^\rho e(p)}{(L^2 - \lambda^2) ((p-L)^2 - m^2) ((p'-L)^2 - m^2)} \left(g_{\lambda\rho} - (1 - \xi_\gamma) \frac{L_\lambda L_\rho}{L^2 - a\xi_\gamma \lambda^2} \right), \quad (25)$$

where $\not{k} \equiv k_\mu \gamma^\mu$ for any four-vector k , ξ_γ is the photon gauge parameter, and a is an arbitrary constant associated with the photon mass regulator. The small photon mass λ is introduced to regulate infrared (IR) divergences. The corresponding field renormalization factor of external charged leptons is

$$Z_\ell = 1 - \frac{\alpha}{4\pi} \frac{\xi_\gamma}{\epsilon} - \frac{\alpha}{4\pi} \left(\ln \frac{\mu^2}{m^2} + 2 \ln \frac{\lambda^2}{m^2} + 4 \right) + \frac{\alpha}{4\pi} (1 - \xi_\gamma) \left(\ln \frac{\mu^2}{\lambda^2} + 1 + \frac{a\xi_\gamma \ln a\xi_\gamma}{1 - a\xi_\gamma} \right). \quad (26)$$

Neglecting Lorentz structures whose contractions with the neutrino current vanish at $m_\nu = 0$, the resulting correction can be expressed as

$$(Z_\ell - 1) J_\mu^{\text{L,R}} + \delta J_\mu^{\text{L,R}} = \frac{\alpha}{\pi} (f_1 J_\mu^{\text{L,R}} + f_2 j_\mu^{\text{L,R}}), \quad (27)$$

in terms of form factors f_1 and f_2 and the additional currents j_μ^{L} and j_μ^{R} :

$$j_\mu^{\text{L}} = \frac{1}{2} \bar{e}(p') \left(\gamma_\mu \gamma_5 + \frac{i\sigma_{\mu\nu} q^\nu}{2m} \right) e(p), \quad (28)$$

$$j_\mu^{\text{R}} = \frac{1}{2} \bar{e}(p') \left(-\gamma_\mu \gamma_5 + \frac{i\sigma_{\mu\nu} q^\nu}{2m} \right) e(p). \quad (29)$$

Here $\sigma_{\mu\nu} = \frac{i}{2}[\gamma_\mu, \gamma_\nu]$.

Using Eqs. (25) and (26), the UV finite and gauge-independent virtual correction is given in Eq. (27) by one-loop QED form factors [95, 96]:

$$f_1(\beta) = -\frac{1}{2\beta} \left(\beta - \frac{1}{2} \ln \frac{1+\beta}{1-\beta} \right) \ln \frac{\lambda^2}{m^2} + \frac{1}{\beta} \left[\frac{3+\rho}{8} \ln \frac{1+\beta}{1-\beta} - \frac{1}{8} \ln \frac{1+\beta}{1-\beta} \ln \left(2 \frac{1+\rho}{\rho} \right) \right] - \frac{1}{2\beta} \left(\text{Li}_2 \frac{\beta-1+\rho}{2\beta} - \text{Li}_2 \frac{\beta+1-\rho}{2\beta} \right) - 1, \quad (30)$$

$$f_2(\beta) = \frac{\rho}{4\beta} \ln \frac{1+\beta}{1-\beta}, \quad (31)$$

which are expressed in terms of the recoil electron velocity β and the parameter ρ :

$$\beta = \sqrt{1 - \frac{m^2}{E'^2}}, \quad \rho = \sqrt{1 - \beta^2} = \frac{m}{E'}. \quad (32)$$

The vertex correction (27) to the unpolarized cross section can be expressed as a sum of factorizable and nonfactorizable terms:

$$d\sigma_v^{\nu_\ell e \rightarrow \nu_\ell e} = \frac{\alpha}{\pi} \delta_v d\sigma_{\text{LO}}^{\nu_\ell e \rightarrow \nu_\ell e} + d\sigma_{v, \text{NF}}^{\nu_\ell e \rightarrow \nu_\ell e}. \quad (33)$$

The factorizable correction is given by

$$\delta_v = 2f_1. \quad (34)$$

The nonfactorizable term $d\sigma_{v, \text{NF}}^{\nu_\ell e \rightarrow \nu_\ell e}$ is obtained by modifying kinematical factors I_i in Eqs. (14, 15) as $I_i \rightarrow I_i + \frac{\alpha}{\pi} f_2 \delta^v I_i$ where

$$\delta^v I_L = \delta^v I_R = \frac{1}{2} I_R^L - \frac{\omega'}{\omega}, \quad (35)$$

$$\delta^v I_R^L = 2 \left(I_L + I_R - \frac{\omega'}{\omega} \right) - I_R^L. \quad (36)$$

The resulting vertex correction to the unpolarized cross section of Eq. (33) is in agreement with Refs. [29, 37]. In the limit of massless electron, the Pauli form factor vanishes, $f_2(\beta) \rightarrow 0$, and the correction becomes exactly factorizable.

3.2 Closed fermion loops: leptons and heavy quarks

In addition to the corrections involving virtual photons in Section 3.1, we must account for the corrections with a closed fermion loop (so called ‘‘penguin’’ diagrams) of Figure 5. These corrections correspond to the neutrino ‘‘charge radius’’ contribution and effects of γ - Z mixing in the Standard Model, cf. Figure 6. They represent the EFT determination of the kinematical dependence of electroweak corrections, cf. Refs. [25, 27].

In this Section, we consider the loop contribution from an arbitrary fermion with mass m_f and charge Q_f (in units of the positive positron charge) and effective left- and right-handed couplings c_L^f and c_R^f respectively, as in Eqs. (12) and (23). Note that the coupling c_L^f for charged leptons ($f = \ell$) depends on the neutrino flavor. This perturbative treatment applies to loops involving charged leptons or heavy quarks ($m_f \gg \Lambda_{\text{QCD}}$). Light quarks require a nonperturbative treatment, as discussed in Section 3.3 below. Starting from the $n_f = 4$ flavor theory discussed in Section 2.3, we treat the charm quark as heavy and the up, down and strange quarks as light.

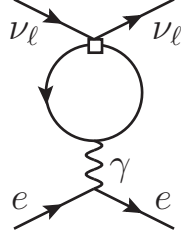


Figure 5: Long-range dynamics in elastic neutrino-electron scattering in the effective theory. Loops with all interacting fields in the theory are summed up.

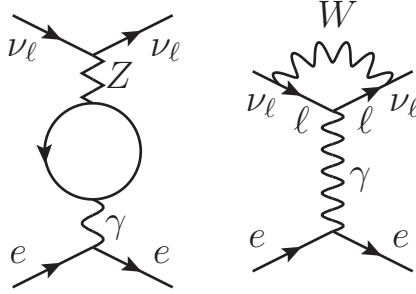


Figure 6: Long-range dynamics in elastic neutrino-electron scattering in the Standard Model: γ - Z mixing and penguin-type diagram.

The correction can be expressed as a modification of electron left- and right-handed currents, $c_{L,R}J_\mu^{L,R} \rightarrow c_{L,R}J_\mu^{L,R} + c_{L,R}^f \delta J_\mu^{L,R}$:

$$\delta J_\mu^{L,R} = Q_f e^2 \bar{e}(p') \gamma^\lambda e(p) \frac{-g_{\lambda\rho}}{q^2} \int \frac{id^d L}{(2\pi)^d} \frac{\text{Tr}[\gamma^\rho (\not{L} + m_f) \gamma_\mu P_{L,R} (\not{L} - \not{q} + m_f)]}{(L^2 - m_f^2) ((L - q)^2 - m_f^2)}, \quad (37)$$

and does not depend on the photon gauge. Corrections to either left- or right-handed currents are vector-like and may be written

$$\delta J_\mu^L = \delta J_\mu^R = Q_f \frac{\alpha}{2\pi} \Pi(q^2, m_f) (J_\mu^L + J_\mu^R). \quad (38)$$

At renormalization scale μ in the $\overline{\text{MS}}$ scheme, the form factor Π is

$$\Pi(q^2, m_f) = \frac{1}{3} \ln \frac{\mu^2}{m_f^2} + \frac{5}{9} + \frac{4m_f^2}{3q^2} + \frac{1}{3} \left(1 + \frac{2m_f^2}{q^2}\right) \sqrt{1 - \frac{4m_f^2}{q^2}} \ln \frac{\sqrt{1 - \frac{4m_f^2}{q^2}} - 1}{\sqrt{1 - \frac{4m_f^2}{q^2}} + 1}, \quad (39)$$

and corresponds to vacuum polarization in QED [97–101].

The resulting “dynamical” correction to the unpolarized cross section, $d\sigma_{\text{dyn}}^{\nu_\ell e \rightarrow \nu_\ell e}$, can be expressed in the following form:

$$d\sigma_{\text{dyn}}^{\nu_\ell e \rightarrow \nu_\ell e} = \frac{\alpha}{\pi} \sum_{f \neq uds} Q_f \Pi(q^2, m_f) d\tilde{\sigma}_{\text{dyn},f}^{\nu_\ell e \rightarrow \nu_\ell e} + d\sigma_{\text{dyn},uds}^{\nu_\ell e \rightarrow \nu_\ell e}. \quad (40)$$

The contribution from three light flavors $d\sigma_{\text{dyn},uds}^{\nu_\ell e \rightarrow \nu_\ell e}$ is discussed below in Section 3.3. The reduced cross section $d\tilde{\sigma}_{\text{dyn},f}^{\nu_\ell e \rightarrow \nu_\ell e}$ is obtained by replacing $\nu_\ell e$ couplings in Eqs. (14, 15) as

$$\left(c_L^{\nu_\ell \ell'}\right)^2 \rightarrow c_L^{\nu_\ell \ell'} \left(c_L^f + c_R^f\right), \quad (41)$$

$$(c_R)^2 \rightarrow c_R \left(c_L^f + c_R^f\right), \quad (42)$$

$$c_L^{\nu_\ell \ell'} c_R \rightarrow \frac{1}{2} \left(c_L^{\nu_\ell \ell'} + c_R\right) \left(c_L^f + c_R^f\right). \quad (43)$$

The sum in Eq. (40) extends over all charged leptons (e, μ, τ) and heavy quarks (c) in the theory (a factor $N_c = 3$ is obtained in the sum over colors for heavy quarks). We also include QCD corrections due to exchanged gluons inside the quark loop; see Refs. [102–105] and Appendix A for exact expressions.

The momentum transfer in elastic neutrino-electron scattering is suppressed by the electron mass,

$$0 \leq -q^2 < 2m\omega. \quad (44)$$

For neutrino beam energies smaller than 10 GeV, this implies $|q^2| \lesssim 0.01 \text{ GeV}^2$. Consequently, the contribution of loops with heavy quarks can be well approximated substituting $\Pi(q^2, m_f) \rightarrow \Pi(0, m_f)$.

3.3 Light-quark contribution

At small q^2 , QCD perturbation theory cannot be applied to evaluate the light-quark contribution in Figure 5. We instead evaluate this contribution by relating it to measured experimental quantities.

For GeV energy neutrino beams, momenta in the range (44) are small compared to hadronic mass scales and we thus evaluate the relevant hadronic tensor at $q^2 = 0$. Neglecting NLO electroweak corrections to the quark coefficients of Eqs. (24), the light-quark contribution in Eq. (40) may be written,

$$d\sigma_{\text{dyn},uds}^{\nu_\ell e \rightarrow \nu_\ell e} = \frac{\alpha}{\pi} \left(\hat{\Pi}_{3\gamma}^{(3)}(0) - 2 \sin^2 \theta_W \hat{\Pi}_{\gamma\gamma}^{(3)}(0) \right) d\tilde{\sigma}_{\text{dyn},uds}^{\nu_\ell e \rightarrow \nu_\ell e}. \quad (45)$$

The reduced cross section $d\tilde{\sigma}_{\text{dyn},uds}^{\nu_\ell e \rightarrow \nu_\ell e}$ is obtained replacing $\nu_\ell e$ couplings in Eqs. (14, 15) as

$$\left(c_L^{\nu_\ell \ell'}\right)^2 \rightarrow 2\sqrt{2}G_F c_L^{\nu_\ell \ell'}, \quad c_R^2 \rightarrow 2\sqrt{2}G_F c_R, \quad c_L^{\nu_\ell \ell'} c_R \rightarrow \sqrt{2}G_F \left(c_L^{\nu_\ell \ell'} + c_R\right). \quad (46)$$

The quantity $\Pi_{\gamma\gamma}$ is defined by the vacuum correlation function,

$$(q^\mu q^\nu - q^2 g^{\mu\nu}) \Pi_{\gamma\gamma}(q^2) = 4i\pi^2 \int d^d x e^{iq \cdot x} \langle 0 | T \{ J_\gamma^\mu(x) J_\gamma^\nu(0) \} | 0 \rangle, \quad (47)$$

where $J_\gamma^\mu = \sum_q Q_q \bar{q} \gamma^\mu q$ is the quark electromagnetic current. Similarly, $\Pi_{3\gamma}$ is given by

$$(q^\mu q^\nu - q^2 g^{\mu\nu}) \Pi_{3\gamma}(q^2) = 4i\pi^2 \int d^d x e^{iq \cdot x} \langle 0 | T \{ J_3^\mu(x) J_\gamma^\nu(0) \} | 0 \rangle, \quad (48)$$

where $J_3^\mu = \sum_q T_q^3 \bar{q} \gamma^\mu q$ is (the third component of) the quark isospin current. The current-current correlation functions $\hat{\Pi}_{ij}^{(3)}(0)$ are evaluated at $q^2 = 0$ for $n_f = 3$ flavors, in the $\overline{\text{MS}}$ scheme.

Unlike the light-quark contribution to the photon propagator, involving only $\hat{\Pi}_{\gamma\gamma}$, the correction to neutral current neutrino-electron scattering involves also $\hat{\Pi}_{3\gamma}$, and cannot be directly related to the total hadron production cross section in e^+e^- collisions. However, an approximate relation between $\hat{\Pi}_{\gamma\gamma}^{(3)}$ and $\hat{\Pi}_{3\gamma}^{(3)}$ holds in the limit of $\text{SU}(3)_f$ flavor symmetry for three light quarks [106, 107]. In general, the flavor sums read

$$\hat{\Pi}_{\gamma\gamma}^{(3)} = \sum_{i,j} Q_i Q_j \Pi^{ij} = \frac{4}{9} \Pi^{uu} + \frac{1}{9} \Pi^{dd} + \frac{1}{9} \Pi^{ss} - \frac{4}{9} \Pi^{ud} - \frac{4}{9} \Pi^{us} + \frac{2}{9} \Pi^{ds}, \quad (49)$$

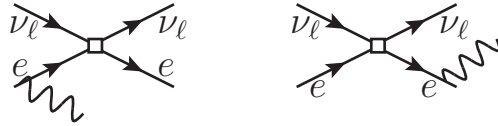


Figure 7: One-photon bremsstrahlung in elastic neutrino-electron scattering.

$$\hat{\Pi}_{3\gamma}^{(3)} = \sum_{i,j} T_i^3 Q_j \Pi^{ij} = \frac{1}{2} \left(\frac{2}{3} \Pi^{uu} + \frac{1}{3} \Pi^{dd} + \frac{1}{3} \Pi^{ss} - \Pi^{ud} - \Pi^{us} + \frac{2}{3} \Pi^{ds} \right). \quad (50)$$

$SU(3)_f$ symmetry implies $\Pi^{uu} = \Pi^{dd} = \Pi^{ss}$ and $\Pi^{ud} = \Pi^{us} = \Pi^{ds}$, and consequently, the simple relation [106] $\hat{\Pi}_{3\gamma}^{(3)}(0) \approx \hat{\Pi}_{\gamma\gamma}^{(3)}(0)$. This allows us to express the entire light-quark contribution to the unpolarized cross section $d\sigma_{\text{uds}}^{\nu_\ell e \rightarrow \nu_\ell e}$ in terms of the single observable $\hat{\Pi}_{\gamma\gamma}^{(3)}(0)$.

For numerical evaluation, we use the dispersive analysis of e^+e^- cross section data and measurements of hadronic τ decays combined with a model of the high-energy contribution in Refs. [108–110],

$$\hat{\Pi}_{\gamma\gamma}^{(3)}(0)|_{\mu=2\text{ GeV}} = 3.597(21). \quad (51)$$

For comparison to the $SU(3)_f$ symmetry approximation, we may consider an alternative $SU(2)_f$ ansatz that sets $\Pi^{uu} = \Pi^{dd}$, $\Pi^{ss} = 0$ and neglects disconnected, OZI-suppressed, terms, $\Pi^{ud} = \Pi^{us} = \Pi^{ds} = 0$. The flavor sums (49) and (50) then yield $\hat{\Pi}_{3\gamma}^{(3)} = 9\hat{\Pi}_{\gamma\gamma}^{(3)}/10$, only a 10% correction to the $SU(3)_f$ symmetry limit. In the final error budget, we consider a more conservative 20% uncertainty on this relation,

$$\hat{\Pi}_{3\gamma}^{(3)}(0) = (1 \pm 0.2) \hat{\Pi}_{\gamma\gamma}^{(3)}(0). \quad (52)$$

Renormalization scale dependence of the light-quark contribution (45) is perturbatively calculable. For $\mu \neq 2\text{ GeV}$, the additional correction corresponds with $3\Pi(0, m_f = 2\text{ GeV})$ of Eq. (39) for each quark (accounting for $N_c = 3$ quark colors).

4 Real photon emission

Section 4.1 provides basic expressions for one-photon bremsstrahlung. We then study relevant differential observables accounting for both soft and hard photons. We start with the electron energy, electron angle, and photon energy triple-differential cross section in Section 4.2. Integrating over one energy variable, we obtain double-differential distributions in Sections 4.3 and 4.4. The double-differential cross section w.r.t. two energy variables is described in Section 4.5. We provide the distribution w.r.t. photon energy and photon angle in Section 4.6. Integrating it over the photon angle, we provide the photon energy spectrum in Section 4.7. Finally, we discuss the real soft-photon correction to elastic neutrino-electron scattering and present electron and electromagnetic energy spectra in Sections 4.8 and 4.9, respectively. We also provide the absolute scattering cross section in Section 4.10. Throughout this Section 4, we present all expressions in the limit of small electron mass, and provide expressions for general mass in the Appendix. For the energy spectra in Sections 4.8 and 4.9, we provide a general discussion of momentum regions at arbitrary mass, but present the massless limit and relegate details to the Appendix.

4.1 Radiation of one photon

The one-photon bremsstrahlung amplitude $T^{1\gamma}$, cf. Figure 7, contains terms corresponding to radiation from the initial electron $T_i^{1\gamma}$ and from the final electron $T_f^{1\gamma}$:

$$T^{1\gamma} = T_i^{1\gamma} + T_f^{1\gamma}. \quad (53)$$

The amplitude $T_i^{1\gamma}$ is obtained from the tree-level amplitude with the substitution

$$e(p) \rightarrow e\varepsilon_\rho^* \frac{\not{p} - \not{k}_\gamma + m}{(p - k_\gamma)^2 - m^2} \gamma^\rho e(p), \quad (54)$$

where k_γ is a photon momentum and ε_ρ^* is the photon polarization vector. The amplitude $T_f^{1\gamma}$ is obtained from the tree-level amplitude with the substitution

$$\bar{e}(p') \rightarrow e\varepsilon_\rho^* \bar{e}(p') \gamma^\rho \frac{\not{p}' + \not{k}_\gamma + m'}{(p' + k_\gamma)^2 - m'^2}. \quad (55)$$

Evaluating the spin-averaged squared matrix element, $\sum_{\text{spin}} |T^{1\gamma}|^2$, we obtain for the bremsstrahlung cross sections:

$$d\sigma_{\text{LO}}^{\nu_\ell e \rightarrow \nu_\ell e \gamma} = \frac{\alpha}{4\pi} \frac{m\omega}{\pi^3} \left[(c_L^{\nu_\ell e})^2 \tilde{\text{I}}_L + c_R^2 \tilde{\text{I}}_R + c_L^{\nu_\ell e} c_R \tilde{\text{I}}_R^L \right], \quad (56)$$

$$d\sigma_{\text{LO}}^{\bar{\nu}_\ell e \rightarrow \bar{\nu}_\ell e \gamma} = \frac{\alpha}{4\pi} \frac{m\omega}{\pi^3} \left[(c_L^{\nu_\ell e})^2 \tilde{\text{I}}_R + c_R^2 \tilde{\text{I}}_L + c_L^{\nu_\ell e} c_R \tilde{\text{I}}_R^L \right], \quad (57)$$

where terms $\tilde{\text{I}}_i$ contain the phase-space integration:

$$\tilde{\text{I}}_i = \int \frac{R_i}{m^2 \omega^2} \delta^4(k + p - k_\gamma - k' - p') \frac{d^3 \vec{k}_\gamma}{2k_\gamma} \frac{d^3 \vec{k}'}{2\omega'} \frac{d^3 \vec{p}'}{2E'}, \quad (58)$$

and kinematical factors R_i are expressed in terms of particle momenta as

$$R_L = -\text{I}_L \left[\frac{p^\mu}{(p \cdot k_\gamma)} - \frac{p'^\mu}{(p' \cdot k_\gamma)} \right]^2 m^2 \omega^2 + \frac{(k \cdot p')(k' \cdot p')}{(k_\gamma \cdot p')} - \frac{(k \cdot p)(k' \cdot p)}{(k_\gamma \cdot p)} + \frac{(k \cdot p)(k' \cdot p')}{(k_\gamma \cdot p')} - \frac{(k \cdot p)(k' \cdot p')}{(k_\gamma \cdot p)} \\ + \frac{(k' \cdot p')(k \cdot k_\gamma)}{(k_\gamma \cdot p)} \left(1 + \frac{m^2}{(k_\gamma \cdot p)} - \frac{(p \cdot p')}{(k_\gamma \cdot p')} \right) + \frac{(k \cdot p)(k' \cdot k_\gamma)}{(k_\gamma \cdot p')} \left(1 - \frac{m'^2}{(k_\gamma \cdot p')} + \frac{(p \cdot p')}{(k_\gamma \cdot p)} \right), \quad (59)$$

$$R_R = -\text{I}_R \left[\frac{p^\mu}{(p \cdot k_\gamma)} - \frac{p'^\mu}{(p' \cdot k_\gamma)} \right]^2 m^2 \omega^2 + \frac{(k \cdot p')(k' \cdot p')}{(k_\gamma \cdot p')} - \frac{(k \cdot p)(k' \cdot p)}{(k_\gamma \cdot p)} + \frac{(k' \cdot p)(k \cdot p')}{(k_\gamma \cdot p')} - \frac{(k' \cdot p)(k \cdot p')}{(k_\gamma \cdot p)} \\ + \frac{(k \cdot p')(k' \cdot k_\gamma)}{(k_\gamma \cdot p)} \left(1 + \frac{m^2}{(k_\gamma \cdot p)} - \frac{(p \cdot p')}{(k_\gamma \cdot p')} \right) + \frac{(k' \cdot p)(k \cdot k_\gamma)}{(k_\gamma \cdot p')} \left(1 - \frac{m'^2}{(k_\gamma \cdot p')} + \frac{(p \cdot p')}{(k_\gamma \cdot p)} \right), \quad (60)$$

$$R_R^L = -\text{I}_R^L \left[\frac{p^\mu}{(p \cdot k_\gamma)} - \frac{p'^\mu}{(p' \cdot k_\gamma)} \right]^2 m^2 \omega^2 - \frac{2mm'(k \cdot k_\gamma)(k' \cdot k_\gamma)}{(p \cdot k_\gamma)(p' \cdot k_\gamma)}. \quad (61)$$

Kinematical factors I_L , I_R , I_R^L are given in terms of momentum invariants in Eqs. (18-20), and are evaluated in the kinematics of $2 \rightarrow 3$ scattering. Neutrino and antineutrino scattering are related by the substitution $R_L \leftrightarrow R_R$ (equivalently, $k \leftrightarrow k'$). The IR-divergent parts of R_L and R_R correspond to integrals R and \hat{R} in Ref. [25], respectively.

4.2 Triple-differential distribution

We evaluate the bremsstrahlung cross section using the integration technique of Ref. [22] and provide expressions for the triple-differential cross section w.r.t. electron angle, electron energy and photon energy keeping all electron mass terms in Appendix B. In the limit of small electron mass,³ the result can be approximated by the following substitutions in Eqs. (56, 57):⁴

$$\tilde{\text{I}}_L \xrightarrow{\omega \gg m} \left[\frac{(\omega - \omega') \left(E'^2 (2 - \tilde{z})^2 + \omega^2 \right)}{2|\omega - (2 - \tilde{z})(\omega - \omega')|} - \frac{E' (E'^4 (2 - \tilde{z})^2 + E'^2 \omega^2 (3\tilde{z} - 5) + E' \omega^3 (1 - \tilde{z}) + \omega^4)}{2(\omega - E')^3} \right]$$

³In the following, we denote the limit of small electron mass compared to all other relevant energy scales as $\omega \gg m$.

⁴Note that suppressed terms in the lepton mass expansion of $\tilde{\text{I}}_L$ and $\tilde{\text{I}}_R$ contribute to the cross section at the same order as $\tilde{\text{I}}_R^L$. For a consistent power counting, one has either to neglect the interference term completely or to expand $\tilde{\text{I}}_L$ and $\tilde{\text{I}}_R$ further.

$$\begin{aligned}
& + \frac{E'^2 \omega' (2E'^3(1-\tilde{z})(2-\tilde{z}) + E'^2 \omega(13+2\tilde{z}(2\tilde{z}-7)) + 2E' \omega^2(4\tilde{z}-7) + 3\omega^3)}{2(\omega-E')^4} \\
& - \frac{E'^2 \omega'^2 (E'^3(1-\tilde{z})(2-\tilde{z}) + E'^2 \omega(8+\tilde{z}(4\tilde{z}-11)) + E' \omega^2(\tilde{z}^2 + \tilde{z}-4) + \omega^3 \tilde{z})}{2(\omega-E')^5} \Big] \mathcal{D}, \quad (62)
\end{aligned}$$

$$\tilde{\mathbb{I}}_{\text{R}} \xrightarrow{\omega \gg m} \frac{E'^2(1-\tilde{z})^2 + \omega'^2}{2} \left[\frac{\omega - \omega'}{|\omega - (2-\tilde{z})(\omega - \omega')|} - \frac{E'}{\omega - E'} \right] \mathcal{D}, \quad (63)$$

$$\tilde{\mathbb{I}}_{\text{R}}^{\text{L}} \xrightarrow{\omega \gg m} m \left[\frac{E'^2(2-\tilde{z})(\tilde{z}-1) + E'(3\omega' - \tilde{z}(\omega + \omega')) - \omega\omega'}{|\omega - (2-\tilde{z})(\omega - \omega')|} - \frac{E'(\omega - (3-\tilde{z})E')}{\omega - E'} \right] \mathcal{D}, \quad (64)$$

with the phase-space factor

$$\mathcal{D} = \frac{\pi^2}{\omega^3} \frac{d\tilde{z} dE' dk_\gamma}{k_\gamma}, \quad (65)$$

where $\omega' = \omega - k_\gamma - E'$ and the variable $\tilde{z} \leq 1$ is introduced to emphasize the forward direction of the relativistic electron:

$$1 - \cos \theta_e \equiv \frac{m}{\omega} (1 - \tilde{z}). \quad (66)$$

Note the difference between the electron scattering angle in the elastic process (Θ_e of Eq. (6)) and in the scattering process with radiation (θ_e). At $m \rightarrow 0$, the physical region of kinematical variables is given by

$$0 \leq E' \leq \omega, \quad 2 - \frac{\omega}{E'} \leq \tilde{z} \leq 1, \quad 0 \leq k_\gamma \leq \omega - E'. \quad (67)$$

In the vicinity of the elastic peak,

$$\tilde{z} \rightarrow \tilde{Z} = 1 - \frac{\omega'}{\omega - \omega'}, \quad (68)$$

the cross section of Eqs. (62-64) diverges. The small mass approximation in Eqs. (62-64) is valid only away from this region:

$$|\tilde{z} - \tilde{Z}| \gg \frac{m}{E'} \frac{k_\gamma^2}{(E' + k_\gamma)^2} \frac{\omega'}{\omega - \omega'}. \quad (69)$$

For a correct description in the elastic peak region, and to obtain distributions (such as energy spectra) that involve integration through this region, expressions with electron mass of Appendix B must be used.

4.3 Double-differential distribution in electron energy and electron angle

Integrating the triple-differential distribution over the photon energy k_γ , we obtain the double-differential cross section w.r.t. the recoil electron energy and electron angle. We provide the double-differential distribution in electron energy and electron angle keeping all electron mass terms in Appendix C. In the limit of small electron mass, the cross section is given by the following substitutions in Eqs. (56, 57):⁴

$$\tilde{\mathbb{I}}_i \xrightarrow{\omega \gg m} \frac{\pi^2}{\omega^2} \left(a_i + b_i \ln \frac{m}{2E'} + c_i \ln \frac{E' + \omega(1-z)}{\omega - E'} + d_i \ln \frac{2(E' - \omega)^2}{m(z\omega - E')} \right) \frac{dz dE'}{\omega - E'}, \quad (70)$$

with the coefficients a_i , b_i , c_i and d_i :

$$a_{\text{L}} = \frac{\omega^4 (E'(z(3-2(7-2z)z) + 16) - \omega(8-z(8-(7-3z)z)))}{4(\omega - E')^2(\omega z - E')}$$

$$\begin{aligned}
& + \frac{E'^2\omega (E'^2(4-z) + E'\omega(2 - (9-2z)z) - \omega^2(4-z)(5-z(z+3)))}{4(\omega - E')^2(\omega z - E')}, \\
a_R & = \frac{-\omega^6(1-z)^2(8-z(16-(15-4z)z)) - E'\omega^5(8-z(35-z(4z^3-14z^2+z+36))) - 4E'^2\omega^4}{4(E' + (1-z)\omega)^3(z\omega - E')} \\
& + \frac{E'^4\omega^2(6+(2-5z)z) + 3E'^3\omega^3(6-(2-z)(8-z)z) - E'^2\omega^4z(24-z(66-(46-9z)z))}{4(E' + (1-z)\omega)^3(z\omega - E')} \\
& - \frac{E'^5\omega(4-3z)}{4(E' + (1-z)\omega)^3(z\omega - E')}, \\
a_R^L & = m\omega \frac{E'(\omega(2-(2-z)z) - E'z)}{(E' + \omega(1-z))(\omega z - E')}, \\
b_L & = -\frac{(\omega - E')((E' + \omega(1-z))^2 + \omega^2)}{\omega z - E'}, \\
b_R & = -\frac{(\omega - E')((\omega - E')^2 + \omega^2(1-z)^2)}{\omega z - E'}, \\
b_R^L & = m \frac{2(\omega - E')(E'^2 + (\omega z - E')^2)}{E'(\omega z - E')}, \\
c_L & = \frac{(\omega - E')((E' + \omega(1-z))^2 + \omega^2)}{E' + \omega(1-z)}, \\
c_R & = \frac{(\omega - E')((\omega - E')^2 + \omega^2(1-z)^2)}{E' + \omega(1-z)} + \frac{E'\omega(\omega - E')(-2\omega^2(1-z) - E'(\omega z - E'))}{(E' + \omega(1-z))^3}, \\
c_R^L & = m \frac{2(\omega - E')(\omega z - 2E')}{E' + \omega(1-z)}, \\
d_L & = (\omega - E')(E' + \omega(1-z)) - \frac{E'^3\omega}{2(\omega - E')^2} + \frac{\omega^3(2E'^2(3-z) - 4E'\omega - \omega^2(2-z(6-(4-z)z)))}{2(E' - \omega)^2(E' + \omega(1-z))}, \\
d_R & = \frac{(E' - \omega)^2}{(E' + \omega(1-z))^2} d_L - \frac{(2-z)\omega(\omega z - E')^2((\omega z - E')^2 + 2\omega^2(1-z))}{2(E' + \omega(1-z))^3}, \\
d_R^L & = m \frac{(\omega z - 2E')^2}{E' + \omega(1-z)}. \tag{71}
\end{aligned}$$

The variable $z \leq 1$ is introduced to emphasize the forward direction of the relativistic electron:

$$1 - \cos \theta_e \equiv \frac{m}{E'} (1 - z). \tag{72}$$

At $m \rightarrow 0$, the physical region of kinematical variables is given by

$$m \leq E' \leq \omega, \quad \frac{E'}{\omega} \leq z \leq 1. \tag{73}$$

4.4 Double-differential distribution in electromagnetic energy and electron angle

To obtain the distribution w.r.t. the electromagnetic energy and electron angle, we use the neutrino energy ω' instead of k_γ in the triple-differential cross section, change the integration order and integrate first over the electron energy. The final neutrino energy determines the total electromagnetic energy E_{EM} : $E_{\text{EM}} = E' + k_\gamma = m + \omega - \omega'$ and can be used to obtain E_{EM} distributions since $dE_{\text{EM}} = -d\omega'$.

In the limit of small electron mass, the neutrino energy and electron angle distribution is given by the following substitutions in Eqs. (56, 57):⁴

$$\tilde{I}_i \xrightarrow{\omega \gg m} \frac{\pi^2}{\omega^3} \left(a_i + \frac{b_i}{|\omega - (2 - \tilde{z})(\omega - \omega')|} + c_i \ln \frac{1 - \tilde{z}}{2 - \tilde{z}} + \left(d_i + \frac{e_i}{|\omega - (2 - \tilde{z})(\omega - \omega')|} \right) \ln \left| \frac{\frac{1 - \tilde{z}}{2 - \tilde{z}} - \frac{\omega'}{\omega}}{1 - \frac{\omega'}{\omega}} \right| \right)$$

$$d\tilde{z}d\omega', \quad (74)$$

with the coefficients a_i , b_i , c_i , d_i and e_i :

$$\begin{aligned}
a_L &= \frac{(2\omega^3(1-\tilde{z}) - \omega^2\omega'(1-4\tilde{z}) - 9\omega\omega'^2(5-2\tilde{z}) - \omega'^3(23-18\tilde{z}))\omega}{4\omega'^2}, \\
a_R &= \frac{(1-\tilde{z})^2(-\omega(9-4\tilde{z}) + 2\omega'(2-\tilde{z}))\omega}{4(2-\tilde{z})^2}, \\
a_R^L &= \frac{3-\tilde{z}}{2-\tilde{z}}m\omega, \\
b_L &= \frac{1}{4}\omega(\omega-\omega')(-\omega(5-2\tilde{z}) + 2\omega'(2-\tilde{z})), \\
b_R &= \frac{(1-\tilde{z})^2\omega(\omega-\omega')(-\omega(5-2\tilde{z}) + 2\omega'(2-\tilde{z}))}{4(2-\tilde{z})^2}, \\
b_R^L &= \frac{\omega(5-(5-2\tilde{z})\tilde{z}) - 2\omega'(5-(4-\tilde{z})\tilde{z})}{2(2-\tilde{z})}m\omega, \\
c_L &= -\frac{\omega(\omega^3(1-\tilde{z}) + 2\omega^2\omega'\tilde{z} + \omega\omega'^2(31-(37-10\tilde{z})\tilde{z}) + \omega'^3(18-(26-9\tilde{z})\tilde{z}))}{2\omega'^2} \\
&\quad - \frac{\omega^2(\omega-\omega')^3(1-\tilde{z})^2}{2\omega'^3}, \\
c_R &= -\frac{\omega(\omega^2(1-\tilde{z})^2 + \omega'^2)}{2\omega'}, \\
c_R^L &= (2-\tilde{z})\frac{\omega}{\omega'}m\omega, \\
d_L &= \frac{(\omega-\omega')(\omega^4(1-\tilde{z})^2 - \omega^3\omega'(1-(3-2\tilde{z})\tilde{z}) + \omega^2\omega'^2(2-(1-\tilde{z})\tilde{z}) - \omega\omega'^3(3-\tilde{z}) + \omega'^4(2-\tilde{z}))}{2\omega'^3}, \\
d_R &= \frac{(\omega-\omega')(\omega^2(1-\tilde{z})^2 - 2\omega\omega'(1-\tilde{z})^2 + \omega'^2(2-(2-\tilde{z})\tilde{z}))}{2\omega'}, \\
d_R^L &= \frac{m(\omega-\omega')(-\omega(2-\tilde{z}) + \omega'(3-\tilde{z}))}{\omega'}, \\
e_L &= -\frac{1}{2}(\omega-\omega')(\omega^2(5-(4-\tilde{z})\tilde{z}) - 2\omega\omega'(2-\tilde{z})^2 + \omega'^2(2-\tilde{z})^2), \\
e_R &= -\frac{1}{2}(\omega-\omega')(\omega^2(1-\tilde{z})^2 - 2\omega\omega'(1-\tilde{z})^2 + \omega'^2(2-(2-\tilde{z})\tilde{z})), \\
e_R^L &= m(\omega^2(2-(2-\tilde{z})\tilde{z}) - 2\omega\omega'(3-(3-\tilde{z})\tilde{z}) + \omega'^2(5-(4-\tilde{z})\tilde{z})). \quad (75)
\end{aligned}$$

This approximation is valid only away from the elastic peak when $\tilde{z} \rightarrow \tilde{Z}$, cf. Eq. (68), when

$$|\tilde{z} - \tilde{Z}| \gg \frac{m}{E'} \frac{\omega'}{\omega - \omega'}. \quad (76)$$

At $m \rightarrow 0$, the physical region is given by

$$0 \leq \omega' \leq \omega, \quad 1 - \frac{\omega}{m} \leq \tilde{z} \leq 1. \quad (77)$$

We discuss the double-differential distribution in electromagnetic energy and electron angle keeping all electron mass terms in Appendix D.

4.5 Double-differential distribution in photon energy and electron energy

To obtain the distribution w.r.t. photon energy and electron energy, we can change the integration order and integrate the triple-differential cross section first over electron scattering angle. In the limit of small

electron mass, the leading terms of the photon energy and electron energy distribution are given by the following substitutions in Eqs. (56, 57):⁴

$$\tilde{\mathbb{I}}_{\text{L}} \xrightarrow{\omega \gg m} \left(\frac{-29E'^2 + 8E'k_\gamma \left(\frac{\omega'}{\omega} - 3 \right) + k_\gamma^2 \left(\frac{\omega'^2}{\omega^2} - 6 \right)}{12E_{\text{EM}}^2} + \frac{1}{2} \left(1 + \frac{E'^2}{E_{\text{EM}}^2} \right) \ln \frac{2E'E_{\text{EM}}}{mk_\gamma} \right) \mathcal{D}_\gamma, \quad (78)$$

$$\tilde{\mathbb{I}}_{\text{R}} \xrightarrow{\omega \gg m} \left(\frac{-29E'^2 \frac{\omega'^2}{\omega^2} + 8E'k_\gamma \left(1 - 3\frac{\omega'}{\omega} \right) \frac{\omega'}{\omega} + k_\gamma^2 \left(1 - 6\frac{\omega'^2}{\omega^2} \right)}{12E_{\text{EM}}^2} + \frac{1}{2} \left(1 + \frac{E'^2}{E_{\text{EM}}^2} \right) \frac{\omega'^2}{\omega^2} \ln \frac{2E'E_{\text{EM}}}{mk_\gamma} \right) \mathcal{D}_\gamma, \quad (79)$$

$$\tilde{\mathbb{I}}_{\text{R}}^{\text{L}} \xrightarrow{\omega \gg m} \left(\frac{E'^2 \left(4\frac{E_{\text{EM}}^2}{\omega^2} - \frac{\omega'}{\omega} \right) - E'k_\gamma \left(1 - 3\frac{\omega'}{\omega} \right) \left(\frac{\omega'}{\omega} - 3 \right) + 3k_\gamma^2 \frac{\omega'}{\omega}}{2E_{\text{EM}}^3} - \frac{E'}{\omega^2} \left(1 + \frac{k_\gamma^2 \omega \omega'}{E'E_{\text{EM}}^3} \right) \ln \frac{2E'E_{\text{EM}}}{mk_\gamma} \right) m\mathcal{D}_\gamma, \quad (80)$$

valid in the physical region, $0 \leq E' + k_\gamma \leq \omega$, with the phase-space factor \mathcal{D}_γ :

$$\mathcal{D}_\gamma = \pi^2 \frac{dk_\gamma}{k_\gamma} \frac{dE'}{\omega}. \quad (81)$$

We discuss the double-differential distribution in photon energy and electron energy keeping all electron mass terms in Appendix E.

4.6 Double-differential distribution in photon energy and photon angle

Besides the electron angle, the photon scattering angle θ_γ can be measured in principle. We consider the distribution w.r.t. the photon energy and the photon angle in the following. We present the double-differential distribution in photon energy and photon angle keeping all electron mass terms in Appendix F.

In the limit of small electron mass, the cross section is given by the following substitutions in Eqs. (56, 57):⁴

$$\tilde{\mathbb{I}}_i \xrightarrow{\omega \gg m} \frac{\pi^2}{\omega^3} \left(a_i + b_i \ln \frac{m/2}{\omega - k_\gamma(2 - \bar{z})} \right) \frac{dk_\gamma}{2k_\gamma} \frac{d\bar{z}}{(2 - \bar{z})^2}, \quad (82)$$

with coefficients:

$$\begin{aligned} a_{\text{L}} &= -k_\gamma^3(1 - \bar{z})(2 - \bar{z})^3 + k_\gamma^2\omega(2 - 3\bar{z})(2 - \bar{z})^2 + 4k_\gamma\omega^2\bar{z}(2 - \bar{z}) - 2\omega^3(1 + \bar{z}), \\ a_{\text{R}} &= \frac{k_\gamma^2(-2k_\gamma(1 - \bar{z})(2 - (2 - \bar{z})\bar{z})(2 - \bar{z}) - \omega(2 - (2 + (7 - 6\bar{z})\bar{z})\bar{z}))}{6} \\ &\quad + \frac{\omega^2(k_\gamma(2 - \bar{z})(10 - (24 - (9 + 4\bar{z})\bar{z})\bar{z}) - \omega(12 - (30 - (15 + 2\bar{z})\bar{z})\bar{z}))}{3(2 - \bar{z})^2}, \\ a_{\text{R}}^{\text{L}} &= \frac{m(k_\gamma^2(3 - 2\bar{z})(1 - \bar{z})(2 - \bar{z})^2 - k_\gamma\omega(6 - \bar{z})\bar{z}(2 - \bar{z}) + \omega^2(6 - \bar{z})\bar{z})}{2 - \bar{z}}, \\ b_{\text{L}} &= -\omega(k_\gamma^2(2 - \bar{z})^2 - 2k_\gamma\omega(2 - \bar{z}) + 2\omega^2), \\ b_{\text{R}} &= -\frac{(1 - \bar{z})^2\omega(k_\gamma^2(2 - \bar{z})^2 - 2k_\gamma\omega(2 - \bar{z}) + 2\omega^2)}{(2 - \bar{z})^2}, \\ b_{\text{R}}^{\text{L}} &= \frac{2m(k_\gamma^2(1 - \bar{z})(2 - \bar{z})^3 - k_\gamma\omega(2 - \bar{z}) + \omega^2)}{2 - \bar{z}}, \end{aligned} \quad (83)$$

where the variable $\bar{z} \leq 1$ is introduced to emphasize the forward direction of the photon:

$$1 - \cos \theta_\gamma \equiv \frac{m}{\omega} (1 - \bar{z}). \quad (84)$$

The photon angle w.r.t. the neutrino beam direction is bounded as

$$\cos \theta_\gamma \geq 1 - \frac{m}{k_\gamma} \left(1 - \frac{k_\gamma}{\omega} \right), \quad (85)$$

while the physical region for the photon energy is $0 \leq k_\gamma \leq \omega$.

4.7 Photon energy spectrum

Integrating the double-differential distribution in photon and electron energies over the electron energy, or the double-differential distribution in photon energy and photon scattering angle over the angle, we obtain the photon energy spectrum. We present the photon energy spectrum keeping all electron mass terms in Appendix G. The leading terms in the electron mass expansion are given by the following substitutions in Eqs. (56, 57):

$$\tilde{\text{I}}_{\text{L}} \xrightarrow{\omega \gg m} \frac{\pi^2}{\omega} g_{\text{L}} \left(\frac{k_\gamma}{\omega} \right) dk_\gamma, \quad (86)$$

$$\tilde{\text{I}}_{\text{R}} \xrightarrow{\omega \gg m} \frac{\pi^2}{\omega} g_{\text{R}} \left(\frac{k_\gamma}{\omega} \right) dk_\gamma, \quad (87)$$

$$\tilde{\text{I}}_{\text{R}}^{\text{L}} \xrightarrow{\omega \gg m} \frac{\pi^2}{\omega} \frac{m}{\omega} g_{\text{R}}^{\text{L}} \left(\frac{k_\gamma}{\omega} \right) dk_\gamma, \quad (88)$$

with functions $g_{\text{L}}(x)$, $g_{\text{R}}(x)$ and $g_{\text{R}}^{\text{L}}(x)$ derived first in the present paper:⁴

$$\begin{aligned} g_{\text{L}}(x) &= \frac{(1-x)(x^2 - 20x - 53)}{12x} - \left(3 + \frac{1}{x} \right) \ln x - \frac{x^2 + x - 2}{2x} \ln \frac{2\omega(1-x)}{m} \\ &+ \ln \frac{2\omega}{m} \ln x + \frac{\pi^2}{6} - \text{Li}_2 x, \end{aligned} \quad (89)$$

$$\begin{aligned} g_{\text{R}}(x) &= -\frac{(1-x)(37x^2 + 223x + 73)}{36x} - \left(\frac{1}{3x} + \frac{9+5x}{2} \right) \ln x + \frac{(1-x)(x^2 + 4x + 1)}{3x} \ln \frac{2\omega(1-x)}{m} \\ &+ \left(\ln \frac{2\omega}{m} \ln x + \frac{\pi^2}{6} - \text{Li}_2 x \right) (1+x), \end{aligned} \quad (90)$$

$$g_{\text{R}}^{\text{L}}(x) = \frac{(1-x)(11-13x)}{4x} + \frac{1-2x}{2x} \ln x - \frac{(1-x)^2}{x} \ln \frac{2\omega(1-x)}{m}. \quad (91)$$

The integral of the photon energy spectrum obtained from Eqs. (86-88) is infrared divergent if extended to arbitrary small photon energy. The total NLO cross section is obtained by implementing an infrared regulator and including the (separately infrared divergent) virtual correction from Section 3.

4.8 Electron energy spectrum

All of our following calculations for neutrino and antineutrino scattering contain the same IR contribution arising from the soft-photon phase space, when the elastic process (without radiation) and scattering with bremsstrahlung are experimentally indistinguishable. The soft-photon contribution has to be accounted for in differential cross sections w.r.t. one kinematical variable (except for the photon energy spectrum of Section 4.7, where one simply evaluates the spectrum above a chosen minimum photon energy). The amplitude $\text{T}_{\text{soft}}^{1\gamma}$ for the radiation of one soft photon with energy $k_\gamma \leq \varepsilon$, where $\varepsilon \ll m$, ω denotes a cutoff regulator, can be expressed in factorizable form as

$$\text{T}_{\text{soft}}^{1\gamma} = \left[\frac{(\varepsilon^* \cdot p')}{(k_\gamma \cdot p')} - \frac{(\varepsilon^* \cdot p)}{(k_\gamma \cdot p)} \right] e\text{T}, \quad (92)$$

where T corresponds to the amplitude without radiation. The corresponding contribution $d\sigma_{\text{soft}}^{\nu_\ell e \rightarrow \nu_\ell e \gamma}$ to the bremsstrahlung spectrum is given by

$$d\sigma_{\text{soft}}^{\nu_\ell e \rightarrow \nu_\ell e \gamma} = \frac{\alpha}{\pi} \delta_s d\sigma_{\text{LO}}^{\nu_\ell e \rightarrow \nu_\ell e}, \quad (93)$$

with the soft correction factor δ_s [21, 25, 29, 37]:

$$\delta_s = \frac{1}{\beta} \left(\text{Li}_2 \frac{1-\beta}{1+\beta} - \frac{\pi^2}{6} \right) - \frac{2}{\beta} \left(\beta - \frac{1}{2} \ln \frac{1+\beta}{1-\beta} \right) \ln \frac{2\varepsilon}{\lambda} + \frac{1}{2\beta} \ln \frac{1+\beta}{1-\beta} \left(1 + \ln \frac{\rho(1+\beta)}{4\beta^2} \right) + 1. \quad (94)$$

The velocity β of Eq. (32) (and $\rho = \sqrt{1-\beta^2}$),

$$\beta = \sqrt{1 - \frac{m^2}{\bar{E}^2}}, \quad (95)$$

now describes either electron or electromagnetic energy spectra and \bar{E} stands for the corresponding energy, i.e., $\bar{E} = E'$ or $\bar{E} = E_{\text{EM}}$. Note the exact cancellation of the IR divergence in the sum of vertex correction and soft-photon emission, i.e., $\delta_s + \delta_v$ does not depend on the fictitious photon mass λ [111–114]. The correction of Eq. (94) comes entirely from the first (factorizable) terms in Eqs. (59–61) and still contains an unphysical dependence on the photon energy cutoff ε .

For further evaluation of the electron angle distributions, we introduce the four-vector l [22]:

$$l = k + p - p' = (l_0, \vec{f}), \quad (96)$$

with the laboratory frame values:

$$l_0 = m + \omega - E', \quad (97)$$

$$f^2 = |\vec{f}|^2 = \omega^2 + \beta^2 E'^2 - 2\omega\beta E' \cos \theta_e. \quad (98)$$

Besides the soft-photon correction, the first factorizable terms in Eqs. (59–61) contribute from the region $k_\gamma \geq \varepsilon$. It is convenient to split this contribution into two parts. There are no restrictions on the phase-space integration in the region I: $l^2 = l_0^2 - f^2 \geq 2\varepsilon(l_0 + f)$. In the region II: $l^2 \leq 2\varepsilon(l_0 + f)$, which includes the region of scattering with elastic kinematics, the phase space of the final photon is bounded by

$$\cos \gamma \geq \frac{1}{f} \left(l_0 - \frac{l^2}{2\varepsilon} \right), \quad (99)$$

where γ is the angle between \vec{f} and \vec{k}_γ . The bremsstrahlung contribution from region I, $d\sigma_{\text{I}}^{\nu_\ell e \rightarrow \nu_\ell e \gamma}$, cancels the $\ln \varepsilon$ divergence of the soft-photon correction. It may be written as the sum of factorizable and nonfactorizable corrections,

$$d\sigma_{\text{I}}^{\nu_\ell e \rightarrow \nu_\ell e \gamma} = \frac{\alpha}{\pi} \delta_{\text{I}} d\sigma_{\text{LO}}^{\nu_\ell e \rightarrow \nu_\ell e} + d\sigma_{\text{I,NF}}^{\nu_\ell e \rightarrow \nu_\ell e \gamma}. \quad (100)$$

The factorizable correction δ_{I} is obtained from the first, factorizable, terms in Eqs. (59–61), evaluating kinematical factors I_{L} , I_{R} , I_{R}^{I} in the kinematics of elastic $2 \rightarrow 2$ process:

$$\delta_{\text{I}} = \frac{2}{\beta} \left(\beta - \frac{1}{2} \ln \frac{1+\beta}{1-\beta} \right) \ln \frac{2(1+\beta)\varepsilon}{\beta m(1+\cos \delta_0)}, \quad (101)$$

where the angle δ_0 is given by

$$\cos \delta_0 = \frac{\omega^2 - \beta^2 E'^2 - l_0^2}{2\beta E' l_0}. \quad (102)$$

The nonfactorizable part $d\sigma_{\text{I,NF}}^{\nu_\ell e \rightarrow \nu_\ell e \gamma}$ is discussed below. The bremsstrahlung contribution from region II can be expressed in factorizable form:

$$d\sigma_{\text{II}}^{\nu_\ell e \rightarrow \nu_\ell e \gamma} = \frac{\alpha}{\pi} \delta_{\text{II}} d\sigma_{\text{LO}}^{\nu_\ell e \rightarrow \nu_\ell e}, \quad (103)$$

where

$$\begin{aligned} \delta_{\text{II}} = & \frac{1}{\beta} \left(\left(\frac{1}{2} + \ln \frac{\rho(1 + \cos \delta_0)}{4\beta} \right) \ln \frac{1 - \beta}{1 + \beta} - \text{Li}_2 \frac{1 - \beta}{1 + \beta} - \text{Li}_2 \frac{\cos \delta_0 - 1}{\cos \delta_0 + 1} + \text{Li}_2 \left(\frac{\cos \delta_0 - 1}{\cos \delta_0 + 1} \frac{1 + \beta}{1 - \beta} \right) + \frac{\pi^2}{6} \right) \\ & + \ln \frac{1 - \beta \cos \delta_0}{\rho} - 1. \end{aligned} \quad (104)$$

Consequently, the complete electron energy spectrum is given by

$$d\sigma_{\text{LO}}^{\nu_\ell e \rightarrow \nu_\ell e \gamma} + d\sigma_{\text{NLO}}^{\nu_\ell e \rightarrow \nu_\ell e} = \left[1 + \frac{\alpha}{\pi} (\delta_v + \delta_s + \delta_{\text{I}} + \delta_{\text{II}}) \right] d\sigma_{\text{LO}}^{\nu_\ell e \rightarrow \nu_\ell e} + d\sigma_v^{\nu_\ell e \rightarrow \nu_\ell e} + d\sigma_{\text{dyn}}^{\nu_\ell e \rightarrow \nu_\ell e} + d\sigma_{\text{NF}}^{\nu_\ell e \rightarrow \nu_\ell e \gamma}, \quad (105)$$

and does not depend on the unphysical parameters ε and λ . We remark that although individual corrections contain double logarithms, i.e.,

$$\delta_v \underset{\beta \rightarrow 1}{\sim} -\frac{1}{8} \ln^2(1 - \beta), \quad \delta_s \underset{\beta \rightarrow 1}{\sim} -\frac{1}{4} \ln^2(1 - \beta), \quad \delta_{\text{II}} \underset{\beta \rightarrow 1}{\sim} \frac{3}{8} \ln^2(1 - \beta), \quad (106)$$

the complete cross-section correction is free from such Sudakov double logarithms [115, 116]. In Appendix H, we obtain the remaining nonfactorizable piece $d\sigma_{\text{NF}}^{\nu_\ell e \rightarrow \nu_\ell e \gamma}$ from the region of hard photons ($k_\gamma \geq \varepsilon$), which contains $d\sigma_{\text{I,NF}}^{\nu_\ell e \rightarrow \nu_\ell e \gamma}$ as well as the contribution beyond the first factorizable terms in Eqs. (59-61), integrating the electron angle and electron energy distribution over the variable f (equivalent to the electron scattering angle θ_e), and retaining all electron mass terms.

The resulting correction to the electron energy spectrum reproduces the result of Ref. [25] in the limit $m \rightarrow 0$, $E'/\omega = \text{const}$. Besides the closed fermion loop contribution of Sections 3.2 and 3.3, it is represented by the following substitutions in Eqs. (56, 57):

$$\tilde{\text{I}}_{\text{L}} \xrightarrow{\omega \gg m} \frac{\pi^2}{\omega} f_- \left(\frac{E'}{\omega} \right) dE', \quad (107)$$

$$\tilde{\text{I}}_{\text{R}} \xrightarrow{\omega \gg m} \frac{\pi^2}{\omega} \left(1 - \frac{E'}{\omega} \right)^2 f_+ \left(\frac{E'}{\omega} \right) dE', \quad (108)$$

$$\tilde{\text{I}}_{\text{R}}^{\text{L}} \xrightarrow{\omega \gg m} -\frac{\pi^2 m E'}{\omega \omega \omega} f_+^- \left(\frac{E'}{\omega} \right) dE', \quad (109)$$

with functions $f_-(x)$, $f_+(x)$ [25], and $f_+^-(x)$ derived first in the present paper:⁴

$$\begin{aligned} f_-(x) = & -\frac{2}{3} \ln \frac{2\omega}{m} + \left(\ln \frac{1-x}{\sqrt{x}} + \frac{x}{2} + \frac{1}{4} \right) \ln \frac{2\omega}{m} - \frac{1}{2} \left(\text{Li}_2(x) - \frac{\pi^2}{6} \right) + \frac{x^2}{24} - \frac{11x}{12} - \frac{47}{36} \\ & - \frac{1}{2} \ln^2 \frac{1-x}{x} - \left(\frac{x}{2} + \frac{23}{12} \right) \ln(1-x) + x \ln x, \end{aligned} \quad (110)$$

$$\begin{aligned} (1-x)^2 f_+(x) = & -\frac{2}{3} (1-x)^2 \ln \frac{2\omega}{m} + \left(\frac{x-1}{2} + (1-x)^2 \ln(1-x) \right) \ln \frac{2\omega}{m} - \frac{(1-x)^2}{2} \ln \frac{1-x}{x^2} \ln(1-x) \\ & + \left((1-x)x - \frac{1}{2} \right) \left(\text{Li}_2(x) + \ln \frac{2\omega x}{m} \ln x - \frac{\pi^2}{6} \right) + \left(x^2 + \frac{x}{2} - \frac{3}{4} \right) \ln x \\ & - \frac{31-49x}{72} (1-x) + \frac{1-x}{3} \left(5x - \frac{7}{2} \right) \ln(1-x), \end{aligned} \quad (111)$$

$$\begin{aligned}
-xf_+^-(x) &= 2 + 2\ln x + \left(x - \ln x - \frac{1}{2}\right) \ln \frac{2\omega x}{m} + \left(\frac{3}{2}x + \frac{1}{2} - x \ln \frac{2\omega x}{m}\right) \ln \frac{1-x}{x} + \frac{1}{2}x \ln^2(1-x) \\
&+ (x-1) \left(\text{Li}_2(x) - \frac{\pi^2}{6} + \frac{5}{4}\right).
\end{aligned} \tag{112}$$

We observe that in exactly forward kinematics at electron threshold, when $E' = m$, the energy spectrum is given by the nonfactorizable contribution from the electromagnetic vertex and closed fermion loops:

$$d\sigma_{\text{LO}}^{\nu_\ell e \rightarrow \nu_\ell e \gamma} + d\sigma_{\text{NLO}}^{\nu_\ell e \rightarrow \nu_\ell e} \xrightarrow{E' \rightarrow m} d\sigma_{\text{NLO}}^{\nu_\ell e \rightarrow \nu_\ell e} \rightarrow d\sigma_{\text{LO}}^{\nu_\ell e \rightarrow \nu_\ell e} + d\sigma_v^{\nu_\ell e \rightarrow \nu_\ell e} + d\sigma_{\text{dyn}}^{\nu_\ell e \rightarrow \nu_\ell e}, \tag{113}$$

with $f_2(0) = 1/2$ in Eqs. (33, 35, 36) and $\Pi(0, m_f)$, $\hat{\Pi}_{\gamma\gamma}^{(3)}(0)$, $\hat{\Pi}_{3\gamma}^{(3)}(0)$ of Eqs. (40, 45). This equation provides a universal limit for electron energy and electromagnetic energy spectra.

The electron energy spectrum has the following logarithmically-divergent behavior near its endpoint $E' \leq E'_0 = m + \frac{2\omega^2}{m+2\omega}$:

$$\frac{d\sigma_{\text{LO}}^{\nu_\ell e \rightarrow \nu_\ell e \gamma} + d\sigma_{\text{NLO}}^{\nu_\ell e \rightarrow \nu_\ell e}}{d\sigma_{\text{LO}}^{\nu_\ell e \rightarrow \nu_\ell e}} \approx -\frac{\alpha}{\pi} \frac{2}{\beta} \left(\beta - \frac{1}{2} \ln \frac{1+\beta}{1-\beta}\right) \ln \frac{E'_0 - E'}{m}, \tag{114}$$

as determined by infrared logarithms in Eqs. (34, 94).

4.9 Electromagnetic energy spectrum

We evaluate the bremsstrahlung cross section w.r.t. the sum of electron and photon energies considering the final neutrino energy spectrum instead of the electron energy spectrum [22], see Section 4.4 for explanations. For the neutrino scattering angle distributions, we introduce the four-vector \tilde{l} :

$$\tilde{l} = k + p - k' = (\tilde{l}_0, \vec{f}), \tag{115}$$

with the laboratory frame values:

$$\tilde{l}_0 = E_{\text{EM}}, \tag{116}$$

$$\vec{f}^2 = |\vec{f}|^2 = \omega^2 + \omega'^2 - 2\omega\omega' \cos \theta_\nu. \tag{117}$$

Note the difference between the neutrino scattering angle in the elastic process (Θ_ν of Eq. (3)) and in the scattering with radiation (θ_ν).

Below the endpoint of maximal electron energy, $E_{\text{EM}} \leq E'_0 = m + \frac{2\omega^2}{m+2\omega}$, we can use the same integration technique as in Ref. [22]. Above the endpoint, the photon energy is bounded from below $k_\gamma \geq E_{\text{EM}} - E'_0$ and there is no corresponding elastic process and no contribution from the soft region. We consider these two regions separately in the following.

4.9.1 Below electron endpoint: $E_{\text{EM}} \leq E'_0 = m + \frac{2\omega^2}{m+2\omega}$

The contribution from the soft-photon region $k_\gamma \leq \varepsilon$ is given by Eqs. (93, 94). We split the integration region with $k_\gamma \geq \varepsilon$ for factorizable terms in Eqs. (59-61) into two regions similar to Section 4.8. In region I: $\tilde{l}^2 - m^2 = \tilde{l}_0^2 - \vec{f}^2 - m^2 \geq 2\varepsilon(\tilde{l}_0 + \vec{f})$, there are no restrictions on the phase space. In region II: $\tilde{l}^2 - m^2 \leq 2\varepsilon(\tilde{l}_0 + \vec{f})$, the phase space of the final neutrino is restricted to

$$\cos \tilde{\gamma} \geq \frac{1}{\vec{f}} \left(\tilde{l}_0 - \frac{\tilde{l}^2 - m^2}{2\varepsilon}\right), \tag{118}$$

where $\tilde{\gamma}$ is the angle between \vec{f} and \vec{k}_γ . The correction factor from region II, δ_{II} , cf. Eq. (103), is given by

$$\delta_{\text{II}} = -\frac{1}{\beta} \left(\beta - \frac{1}{2} \ln \frac{1+\beta}{1-\beta} \right) \ln \frac{1+\beta}{1-\beta}. \quad (119)$$

Here β is expressed in terms of electromagnetic energy as in Eq. (95). As for the electron energy spectrum, the bremsstrahlung contribution from region I may be written as the sum of factorizable and nonfactorizable corrections, cf. Eq. (100). The factorizable correction δ_{I} is obtained from the first factorizable terms in Eqs. (59-61), evaluating kinematical factors I_{L} , I_{R} , I_{R}^{L} in the kinematics of elastic $2 \rightarrow 2$ process:

$$\delta_{\text{I}} = \frac{2}{\beta} \left(\beta - \frac{1}{2} \ln \frac{1+\beta}{1-\beta} \right) \ln \frac{\varepsilon}{m}. \quad (120)$$

In Appendix I we evaluate the remaining nonfactorizable piece $d\sigma_{\text{NF}}^{\nu_\ell e \rightarrow \nu_\ell e \gamma}$ of the electromagnetic energy spectrum below electron endpoint, performing straightforward integrations and keeping all electron mass terms. It accounts for the region of hard photons ($k_\gamma \geq \varepsilon$), and contains $d\sigma_{\text{I,NF}}^{\nu_\ell e \rightarrow \nu_\ell e \gamma}$ as well as the contribution beyond the first factorizable terms in Eqs. (59-61).

The resulting correction to the electromagnetic energy spectrum reproduces the result of Refs. [27, 28] in the limit $m \rightarrow 0$, $E_{\text{EM}}/\omega = \text{const}$. Besides the closed fermion loop contribution of Sections 3.2 and 3.3, it is represented by the following substitutions in Eqs. (56, 57):

$$\tilde{I}_{\text{L}} \xrightarrow{\omega \gg m} \frac{\pi^2}{\omega} f_{\text{L}} \left(\frac{E_{\text{EM}}}{\omega} \right) dE_{\text{EM}}, \quad (121)$$

$$\tilde{I}_{\text{R}} \xrightarrow{\omega \gg m} \frac{\pi^2}{\omega} \left(1 - \frac{E_{\text{EM}}}{\omega} \right)^2 f_{\text{R}} \left(\frac{E_{\text{EM}}}{\omega} \right) dE_{\text{EM}}, \quad (122)$$

$$\tilde{I}_{\text{R}}^{\text{L}} \xrightarrow{\omega \gg m} -\frac{\pi^2}{\omega} \frac{m}{\omega} \frac{E_{\text{EM}}}{\omega} f_{\text{R}}^{\text{L}} \left(\frac{E_{\text{EM}}}{\omega} \right) dE_{\text{EM}}, \quad (123)$$

with functions $f_{\text{L}}(x)$, $f_{\text{R}}(x)$ [27, 28], and $f_{\text{R}}^{\text{L}}(x)$ derived first in the present work:⁴

$$f_{\text{L}}(x) = \frac{3x^2 - 30x + 23}{72} - \frac{2}{3} \ln \frac{2\omega x}{m} - \frac{\pi^2}{6}, \quad (124)$$

$$f_{\text{R}}(x) = \frac{-4x^2 - 16x + 23}{72(1-x)^2} - \frac{2}{3} \ln \frac{2\omega x}{m} - \frac{\pi^2}{6}, \quad (125)$$

$$f_{\text{R}}^{\text{L}}(x) = \frac{x^2 + 3x - 3}{4x^2} - \frac{3}{2} \ln \frac{2\omega x}{m} - \frac{\pi^2}{6}. \quad (126)$$

In exactly forward kinematics at electromagnetic energy threshold when $E_{\text{EM}} = m$, the electromagnetic energy spectrum coincides with the electron energy spectrum, see Eq. (113).

Just below electron endpoint ($E_{\text{EM}} < E'_0 = m + \frac{2\omega^2}{m+2\omega} \approx \omega$), the electromagnetic energy spectrum, besides the closed fermion loop contribution, is given by the following substitutions in the nonfactorizable correction:⁴

$$\tilde{I}_{\text{L}} \xrightarrow{\omega \gg m} -\frac{\pi^2}{3} \left(\ln \frac{4\omega^2}{m^2} + \frac{\pi^2}{2} + \frac{1}{6} \right) \frac{dE_{\text{EM}}}{\omega}, \quad (127)$$

$$\tilde{I}_{\text{R}} \xrightarrow{\omega \gg m} \frac{\pi^2}{24} \frac{dE_{\text{EM}}}{\omega}, \quad (128)$$

$$\tilde{I}_{\text{R}}^{\text{L}} \xrightarrow{\omega \gg m} \frac{\pi^2}{4} \frac{m}{\omega} \left(3 \ln \frac{4\omega^2}{m^2} + \frac{2\pi^2}{3} - 1 \right) \frac{dE_{\text{EM}}}{\omega}. \quad (129)$$

Equations (127, 128) are in agreement with the similar limit taken from the result of Refs. [27, 28].

4.9.2 Above electron endpoint: $E_{\text{EM}} > E'_0 = m + \frac{2\omega^2}{m+2\omega}$

Above the electron endpoint energy, the corresponding elastic process is kinematically forbidden. For $\omega \gg m$, this region is relatively small but finite:

$$E_{\text{EM}} - E'_0 \leq \frac{1}{1 + \frac{m}{2\omega}} \frac{m}{2} < \frac{m}{2}. \quad (130)$$

Since the photon energy is bounded from below in this region, $k_\gamma > E_{\text{EM}} - E'_0$, the calculation does not require IR regularization. We present the electromagnetic energy spectrum above electron endpoint keeping all electron mass terms in Appendix J.

The electromagnetic energy spectrum has the following logarithmically divergent behavior just above the electron endpoint $E_{\text{EM}} > E'_0 = m + \frac{2\omega^2}{m+2\omega}$:

$$\frac{d\sigma_{\text{LO}}^{\nu_\ell e \rightarrow \nu_\ell e \gamma}}{d\sigma_{\text{LO}}^{\nu_\ell e \rightarrow \nu_\ell e}} \approx \frac{\alpha}{\pi} \frac{2}{\beta} \left(\beta - \frac{1}{2} \ln \frac{1+\beta}{1-\beta} \right) \ln \frac{E_{\text{EM}} - E'_0}{m}. \quad (131)$$

4.10 Absolute cross section

The resulting total cross-section correction, besides closed fermion loop contributions, in the ultrarelativistic limit is given by the following substitutions in Eqs. (56, 57) for $\tilde{\text{I}}_{\text{L}}$, $\tilde{\text{I}}_{\text{R}}$ [25], and $\tilde{\text{I}}_{\text{R}}^{\text{L}}$ derived first in the present paper:⁴

$$\tilde{\text{I}}_{\text{L}} \xrightarrow{\omega \gg m} \frac{\pi^2}{24} \left(19 - 4\pi^2 - 16 \ln \frac{2\omega}{m} \right), \quad (132)$$

$$\tilde{\text{I}}_{\text{R}} \xrightarrow{\omega \gg m} \frac{\pi^2}{72} \left(19 - 4\pi^2 - 16 \ln \frac{2\omega}{m} \right) + \frac{\pi^2}{3}, \quad (133)$$

$$\tilde{\text{I}}_{\text{R}}^{\text{L}} \xrightarrow{\omega \gg m} -\frac{\pi^2}{24} \frac{m}{\omega} \left(15 - 2\pi^2 - 36 \ln \frac{2\omega}{m} \right). \quad (134)$$

Factors $\tilde{\text{I}}_{\text{L}}$ and $\tilde{\text{I}}_{\text{R}}$ of Eqs. (132, 133) can be obtained integrating Eqs. (124, 125) or Eqs. (110, 111) over the energy variable. To evaluate the factor $\tilde{\text{I}}_{\text{R}}^{\text{L}}$, one has to regulate the logarithmic mass singularity properly or take the limit from the general expression of Section K. Note the absence of double logarithms in the resulting cross-section correction in Eqs. (124-126) and (132-134), although individual corrections contain them, cf. Eq. (106). Note that the total elastic cross section at leading order is given by the following substitutions in Eqs. (14, 15):

$$\int d\omega' \text{I}_{\text{L}} \xrightarrow{\omega \gg m} \omega, \quad \int d\omega' \text{I}_{\text{R}} \xrightarrow{\omega \gg m} \frac{\omega}{3}, \quad \int d\omega' \text{I}_{\text{R}}^{\text{L}} \xrightarrow{\omega \gg m} -\frac{m}{2}. \quad (135)$$

Results for the absolute cross section including the electron mass dependence are presented in Appendix K.

5 Illustrative results

Our results may be used to compute absolute and differential cross sections for neutrino-electron scattering over a broad range of energies and experimental setups. We focus on the application to flux normalization at accelerator-based neutrino experiments in this Section.

5.1 Total cross section: energy dependence and error analysis

The total cross sections for $\nu_\mu e$, $\nu_e e$, $\bar{\nu}_\mu e$ and $\bar{\nu}_e e$ scattering are shown in Figure 8. For $\omega \gg m$, cross sections grow approximately linearly with neutrino beam energy. As a benchmark point, we determine at $\omega = 1$ GeV:

$$\sigma[\nu_\mu e \rightarrow \nu_\mu e(\gamma)] = [1.5724 \times 10^{-42} \text{ cm}^2] \times [1 \pm 0.0037_{\text{had}} \pm 0.0003_{\text{EW}} \pm 0.00007_{\text{pert}}]. \quad (136)$$

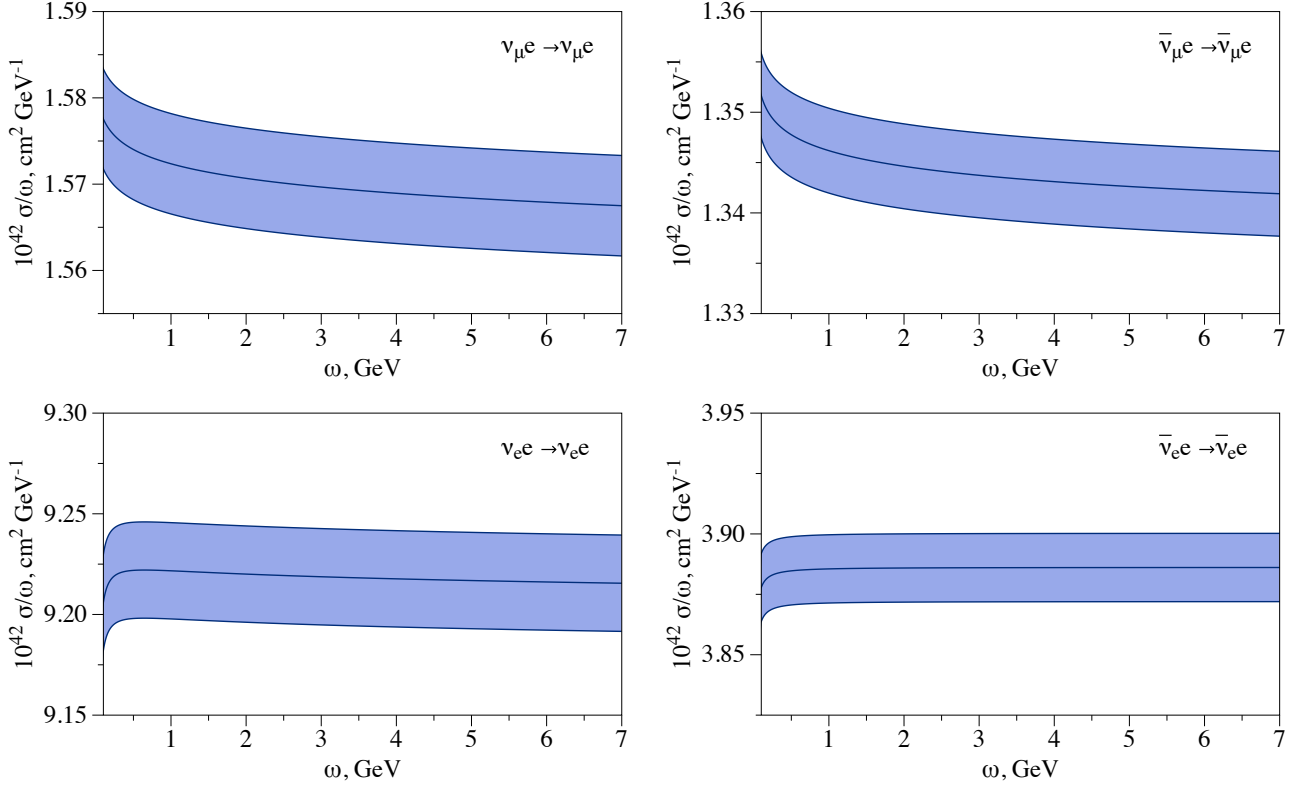


Figure 8: Total cross section in the (anti-)neutrino-electron scattering processes $\nu_\mu e \rightarrow \nu_\mu e(X_\gamma)$, $\nu_e e \rightarrow \nu_e e(X_\gamma)$, $\bar{\nu}_\mu e \rightarrow \bar{\nu}_\mu e(X_\gamma)$ and $\bar{\nu}_e e \rightarrow \bar{\nu}_e e(X_\gamma)$ as a function of (anti-)neutrino beam energy.

The cross section is evaluated using four-flavor QCD, with running QED and QCD couplings $\alpha(\mu)$ and $\alpha_s(\mu)$ evaluated using 2 and 5 loop running, respectively, with $\alpha(2 \text{ GeV}) = 1/133.307$ and $\alpha_s(2 \text{ GeV}) = 0.3065$. The uncertainties in Eq. (136) are from: (i) the hadronic parameter $\hat{\Pi}_{3\gamma}^{(3)}(0)/\hat{\Pi}_{\gamma\gamma}^{(3)}(0)$ in Eq. (52) and from $\hat{\Pi}_{\gamma\gamma}^{(3)}(0)$ in Eq. (51);⁵ (ii) from uncertainties in the four-fermion operator coefficients $c_L^{\nu\ell\ell'}$, c_R in Table 1; and (iii) from higher-order perturbative corrections, estimated by varying renormalization scale $\mu_0^2/2 < \mu^2 < 2\mu_0^2$, where $\mu_0 = 2 \text{ GeV}$. For simplicity, we evaluate the light-quark contribution of Eq. (45) neglecting NLO electroweak corrections and renormalization group corrections to the four-fermion operator coefficients, taking for definiteness $G_F = 1.166379 \times 10^{-5} \text{ GeV}^{-2}$ and $\sin^2 \theta_W = 0.23112$ in Eqs. (45) and (46); it is straightforward to include these corrections, whose impact is given by the few permille shift in the coefficients [47], times the $\sim 1\%$ fractional contribution of light quarks to the cross section. The charm-quark contribution in Eq. (40) is evaluated including the $\mathcal{O}(\alpha_s)$ and $\mathcal{O}(\alpha_s^2)$ corrections from Appendix A and using the $\overline{\text{MS}}$ mass $\hat{m}_c(2 \text{ GeV}) = 1.084 \text{ GeV}$ (corresponding to $\hat{m}_c(\hat{m}_c) = 1.27(2) \text{ GeV}$ [117]). The fractional uncertainty coming from the charm quark mass error is $\approx 2 \times 10^{-5}$ and is not displayed in Eq. (136), nor is the uncertainty of similar magnitude coming from higher orders in G_F expansion. The e -, μ - and τ -lepton contributions in Eq. (40) are evaluated using lepton pole masses and the complete kinematic dependence of $\Pi(q^2, m_\ell)$ in Eq. (39).⁶

For $\omega \gg m$, the relative cross section error is approximately constant, independent of neutrino energy. Relative uncertainties on total cross sections from different sources are summarized in Table 2. The dominant uncertainty from the light-quark contribution in differential and absolute cross sections can be

⁵The error of $\hat{\Pi}_{\gamma\gamma}^{(3)}(0)$ in Eq. (51) contributes ± 0.00006 .

⁶One can safely evaluate τ -lepton contribution considering $\Pi(0, m_\tau)$ since $|q^2| \ll m_\tau^2$.

Table 2: Relative errors of the total neutrino-electron scattering cross section.

	light-quark correction	effective couplings	higher orders
$\nu_\mu e \rightarrow \nu_\mu e (X_\gamma)$	0.37 %	0.034 %	$\lesssim 0.008$ %
$\bar{\nu}_\mu e \rightarrow \bar{\nu}_\mu e (X_\gamma)$	0.31 %	0.029 %	$\lesssim 0.005$ %
$\nu_e e \rightarrow \nu_e e (X_\gamma)$	0.26 %	0.024 %	$\lesssim 0.007$ %
$\bar{\nu}_e e \rightarrow \bar{\nu}_e e (X_\gamma)$	0.36 %	0.033 %	$\lesssim 0.006$ %

expressed as⁷

$$\delta \left(\frac{d\sigma_{\text{uds}}^{\nu_\ell e \rightarrow \nu_\ell e}}{dE'} \right) \approx \eta \frac{G_F m}{\sqrt{2}\pi} \frac{\alpha}{\pi} \hat{\Pi}_{\gamma\gamma}^{(3)}(0) \left| c_L^{\nu_\ell e} \mathbf{I}_L + c_R \mathbf{I}_R + \frac{c_L^{\nu_\ell e} + c_R}{2} \mathbf{I}_R^L \right|, \quad (138)$$

$$\delta \sigma_{\text{uds}}^{\nu_\ell e \rightarrow \nu_\ell e} \approx \eta \frac{G_F m \omega}{\sqrt{2}\pi} \frac{\alpha}{\pi} \hat{\Pi}_{\gamma\gamma}^{(3)}(0) \left(\frac{2\omega c_L^{\nu_\ell e}}{m + 2\omega} + \left(1 - \frac{m^3}{(m + 2\omega)^3} \right) \frac{c_R}{3} - \frac{m\omega (c_L^{\nu_\ell e} + c_R)}{(m + 2\omega)^2} \right), \quad (139)$$

with the relative uncertainty $\eta = (\hat{\Pi}_{3\gamma}^{(3)}(0) / \hat{\Pi}_{\gamma\gamma}^{(3)}(0) - 1.0) \approx 0.2$ and the substitution $c_L^{\nu_\ell e} \leftrightarrow c_R$ in the case of antineutrino scattering.

5.2 Electron and total electromagnetic energy spectra

Figures 9 and 10 display the typical size of the radiative corrections to energy spectra w.r.t. the final electron energy ($\bar{E} = E'$), and w.r.t. the total electromagnetic energy (i.e., the electron energy plus photon energy, $\bar{E} = E' + k_\gamma$). We consider muon type neutrinos and antineutrinos, the primary component in the accelerator neutrino beam. In these Figures, we show the quantity δ representing the radiative correction normalized to the leading-order elastic cross section:

$$\delta = \frac{d\sigma_{\text{LO}}^{\nu_\ell e \rightarrow \nu_\ell e \gamma} + d\sigma_{\text{NLO}}^{\nu_\ell e \rightarrow \nu_\ell e} - d\sigma_{\text{LO}}^{\nu_\ell e \rightarrow \nu_\ell e}}{d\sigma_{\text{LO}}^{\nu_\ell e \rightarrow \nu_\ell e}}. \quad (140)$$

The correction to the electromagnetic energy spectrum is relatively flat over a wide energy, whereas the correction to the electron energy spectrum is logarithmically divergent below electron endpoint, cf. Eq. (114). The logarithmic divergence of the electromagnetic energy spectrum above the electron endpoint, cf. Eq. (131), is not seen in Figure 9 due to the small size of the region in Section 4.9.2 compared to the scale of the Figure. Both corrections start from the limit of Eq. (113) at $\bar{E} = m$. Note that the correction δ depends on the renormalization scale μ since the numerator does not contain the leading-order elastic process, rather just the virtual correction to it, leaving the scale dependence of the closed fermion loops (Sections 3.2 and 3.3) without cancellations. The large renormalization scale dependence in Figures 9 and 10 illustrates the cancellations occurring between LO and NLO in arriving at the total cross section in Eq. (136). Other uncertainties are not shown in the figure.

5.3 Electron angular spectrum

In this Section, we consider the angular smearing of differential cross sections. It can be presented as a function of the variable X :

$$X = 2m \left(1 - \frac{\bar{E}}{\omega} \right), \quad (141)$$

⁷It can be seen, cf. Eq. (138), that the muon antineutrino-electron scattering cross section is free from hadronic uncertainty, and also effective coupling uncertainty induced by c_R , at the particular recoil antineutrino energy $\tilde{\omega}$:

$$\tilde{\omega} = \frac{\sqrt{(c_L^{\nu_\mu e} + c_R)^2 m^2 + 8c_L^{\nu_\mu e} (c_L^{\nu_\mu e} + c_R) m\omega - 16c_L^{\nu_\mu e} c_R \omega^2 - (c_L^{\nu_\mu e} + c_R) m}}{4c_L^{\nu_\mu e}} \xrightarrow{\omega \gg m} \sqrt{\frac{-c_R}{c_L^{\nu_\mu e}}} \omega. \quad (137)$$

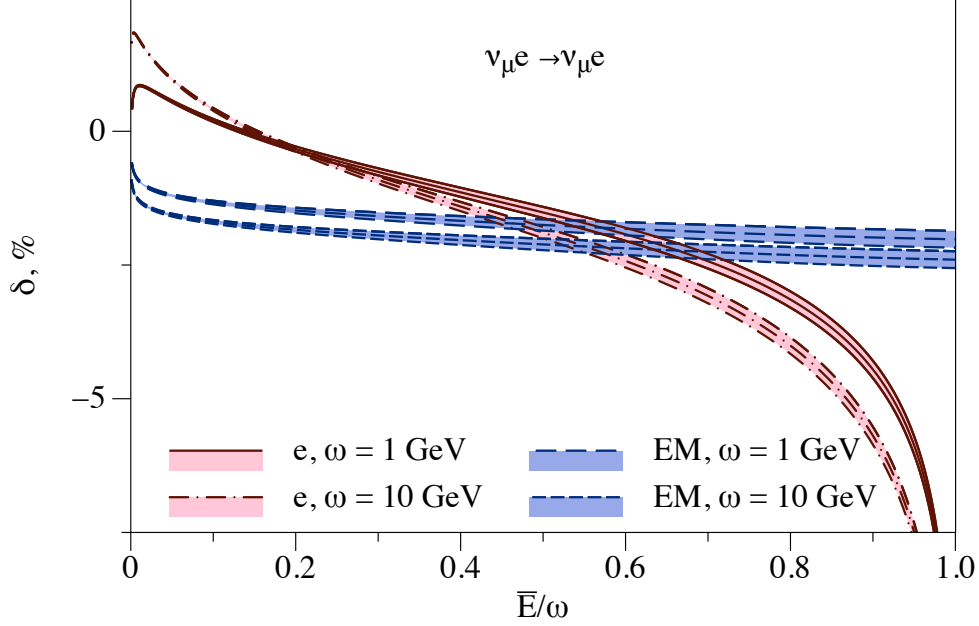


Figure 9: Radiative corrections to the neutrino-electron scattering process $\nu_\mu e \rightarrow \nu_\mu e(X_\gamma)$ for two neutrino beam energies $\omega = 1, 10$ GeV. The quantity δ is defined in Eq. (140) and strongly depends on the $\overline{\text{MS}}$ scale μ . Three curves for $\mu = \mu_0/\sqrt{2}$, $\mu = \mu_0$ and $\mu = \sqrt{2}\mu_0$ with $\mu_0 = 2$ GeV are presented. The solid and dashed-dotted curves correspond with electron spectrum, i.e., $\bar{E} = E'$, dashed curves with electromagnetic spectrum, i.e., $\bar{E} = E' + k_\gamma$. Uncertainties are not shown on this plot with a scale-dependent quantity. Lower curves correspond to larger value of μ .

which becomes $X \approx E'\theta_e^2$ for (anti-)neutrinos of high energy in case of the electron energy spectrum. We present the resulting NLO spectrum in Figures 11 and 12 for two (anti-)neutrino beam energies: $\omega = 1$ GeV and 10 GeV. Although the electromagnetic and electron energy spectra integrate to the same total cross section, shape effects induced by radiative corrections can potentially impact the calibration of neutrino flux. For example, experimental cuts requiring a minimum observed energy will result in different numbers of accepted events depending on which distribution (electromagnetic or electron energy) is chosen. In a practical analysis, neither the electron spectrum nor the electromagnetic spectrum will perfectly represent the experimental conditions, and the more general distributions presented elsewhere in this paper can be used.

Results comparing E' and E_{EM} distributions after averaging over typical experimental flux profiles are collected in Appendix L.

6 Conclusions and outlook

In this work, we have presented analytical results for elastic (anti-)neutrino-electron scattering starting from four-fermion effective field theory. Total cross sections, the electron and electromagnetic energy spectra as well as double- and triple-differential cross sections were presented in a relatively compact form. Our results can be applied to improve constraints of neutrino flux measurements via elastic neutrino-electron scattering. All expressions were obtained for finite electron mass and can also be used in low energy applications such as oscillation measurements with solar and reactor (anti-)neutrinos.

Next-to-leading order corrections with bremsstrahlung of one photon are typically of order few percent and depend on the experimental setup. For instance, as discussed in Section 5.3, electron and electromagnetic energy spectra differ significantly. Although these two spectra integrate to the same total

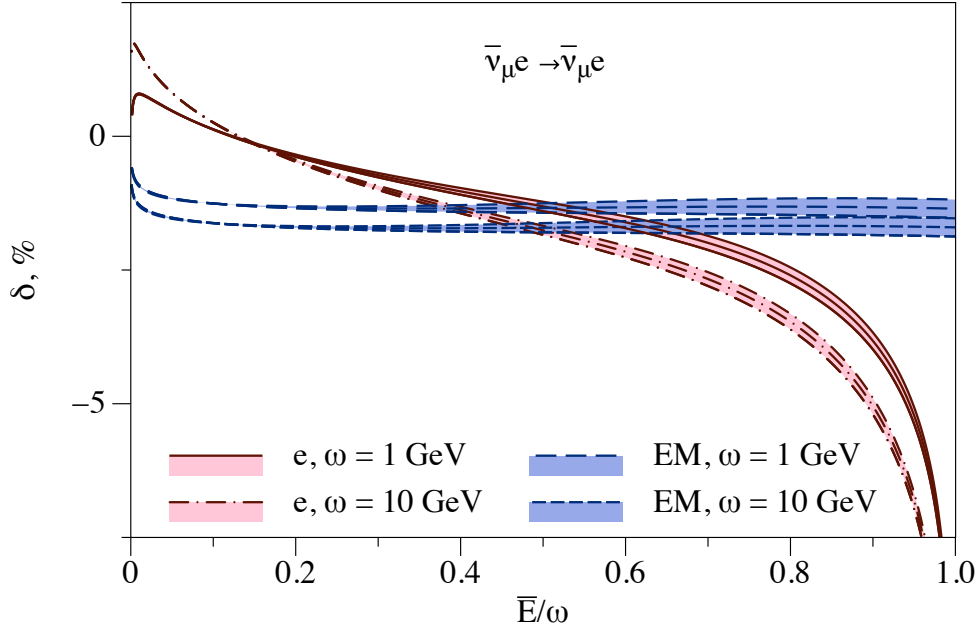


Figure 10: Same as Figure 9 for antineutrino-electron scattering process $\bar{\nu}_\mu e \rightarrow \bar{\nu}_\mu e(X_\gamma)$. Uncertainties are not shown on this plot with a scale-dependent quantity. Lower curves correspond to large value of μ for $\bar{E}/\omega \lesssim 0.07 - 0.1$ and to smaller value of μ above.

cross section, kinematical cuts can alter inferred flux constraints if radiative corrections are not matched correctly to experimental conditions. Future precise measurements of the electron angular spectrum in neutrino-electron scattering can provide energy-dependent neutrino flux constraints. Our results provide a complete description of the kinematic dependence of radiative corrections needed to control uncertainties in neutrino energy reconstruction.

We provided a complete error budget for neutrino-electron scattering observables. The light-quark contribution to the radiative correction is the dominant source of uncertainty. We have expressed this contribution in terms of well-defined Standard Model observables, independent of “constituent quark” models used in previous treatments, and determined the relevant hadronic parameter, denoted $\hat{\Pi}_{3\gamma}^{(3)}(0)$, using $SU(3)_f$ symmetry to relate it to the experimentally constrained parameter $\hat{\Pi}_{\gamma\gamma}^{(3)}(0)$. To further pin down the uncertainty of this light-quark contribution, one can evaluate closed fermion loop contribution within the dispersion relation approach decomposing e^+e^- cross section data and measurements of hadronic τ decays into flavor components [106, 107, 110, 118–120] or perform a calculation in lattice QCD [121].

We note that due to the restrictive kinematics of neutrino-electron scattering ($|q^2| < 2m\omega$ for the elastic process) the light-quark contribution enters as a single constant, representing the $q^2 \rightarrow 0$ limit of the relevant hadronic tensor. This single constant will also impact (and may be constrained by) other low q^2 processes such as coherent neutrino-nucleus scattering.

Besides its phenomenological relevance, the neutrino-electron scattering process provides an analytically calculable prototype for the more complicated case of neutrino-nucleus scattering [122]. In general, radiative corrections can be decomposed (“factorized”) into soft and hard functions using effective field theory [123]. The soft functions depend on experimental configuration but are independent of hadronic physics and describe universal large logarithms that are present in general kinematics. The hard functions are independent of experimental configuration and describe hadronic physics. In neutrino-electron scattering the analogous hard functions are perturbatively calculable whereas in neutrino-nucleus scattering they must be parameterized and experimentally constrained.

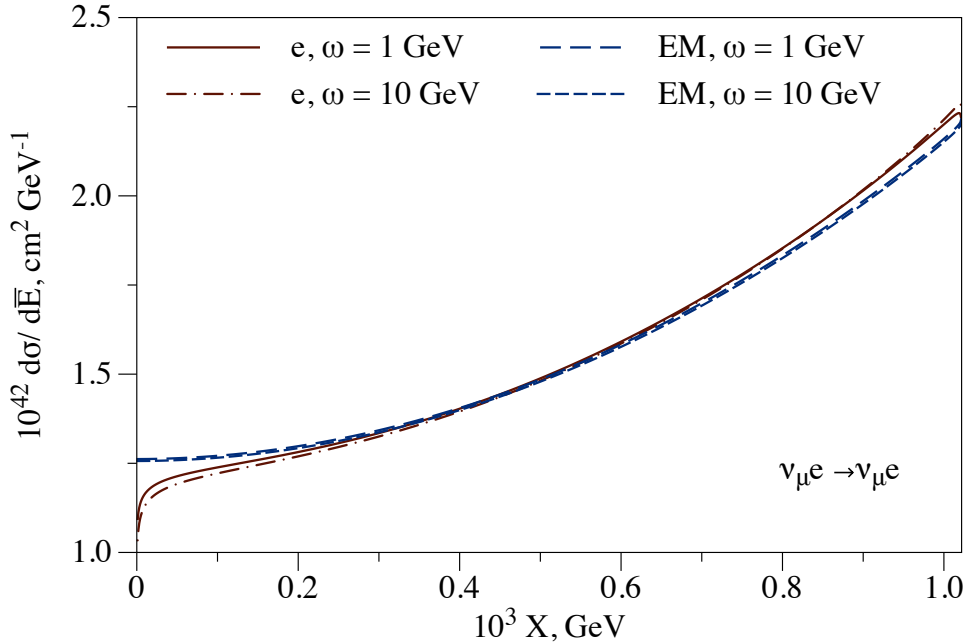


Figure 11: Energy spectrum in the neutrino-electron scattering $\nu_\mu e \rightarrow \nu_\mu e(\gamma)$, plotted as a function of $X = 2m(1 - \bar{E}/\omega)$ for two neutrino beam energies $\omega = 1, 10$ GeV. The solid and dashed-dotted curves correspond with electron spectrum, i.e., $\bar{E} = E'$, dashed curves with electromagnetic spectrum, i.e., $\bar{E} = E' + k_\gamma$.

Acknowledgments

We thank K. McFarland for useful discussions. O. T. thanks Matthias Heller for useful discussions regarding radiative corrections in QED. Work supported by the U.S. Department of Energy, Office of Science, Office of High Energy Physics, under Award Number DE-SC0019095 and by the Deutsche Forschungsgemeinschaft DFG through the Collaborative Research Center [The Low-Energy Frontier of the Standard Model (SFB 1044)]. FeynCalc [124, 125], LoopTools [126], JaxoDraw [127], Mathematica [128] and DataGraph were extremely useful in this work.

A QCD correction to QED vacuum polarization

For quark loop contributions in Section 3.2, we include the leading QCD correction due to one exchanged gluon inside the quark loop. This correction modifies the form factor Π in Eq. (39) as $\Pi \rightarrow \Pi + \Pi^{\text{QCD}}$ with Π^{QCD} from Refs. [102–105]:⁸

$$\Pi^{\text{QCD}} = \frac{\alpha_s}{3\pi} \left(\ln \frac{\mu^2}{m_f^2} - 4\zeta(3) + \frac{55}{12} + \frac{4m_f^2}{q^2} V_1 \left(\frac{q^2}{4m_f^2} \right) \right), \quad (142)$$

where α_s is a strong coupling constant, $\zeta(s)$ denotes the Riemann zeta functions and the function $V(r)$ is given by (for spacelike momentum transfer, $r < 0$)

$$V(r) = \sqrt{1 - \frac{1}{r}} \left(\frac{8}{3} \left(r + \frac{1}{2} \right) \left(\text{Li}_2(r_-^2) - \text{Li}_2(r_-^4) + \ln \frac{-64(1-r)^2 r}{r_+^3} \ln r_+ \right) - 2 \left(r + \frac{3}{2} \right) \ln r_+ \right)$$

⁸Note that the color factor applies as $N_c(\Pi + \Pi^{\text{QCD}})$.

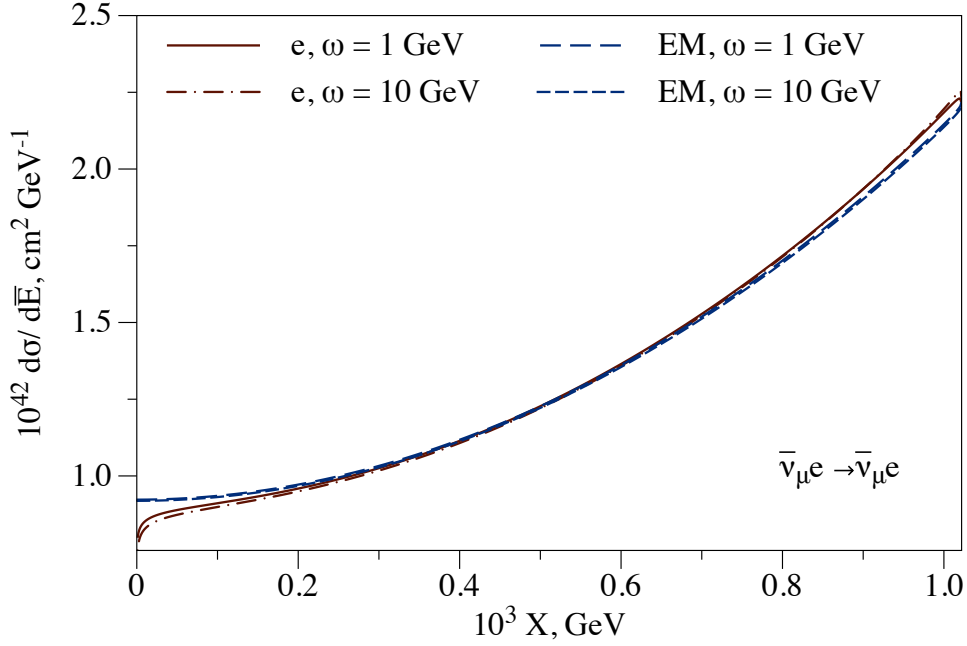


Figure 12: Same as Figure 11 for antineutrino-electron scattering process $\bar{\nu}_\mu e \rightarrow \bar{\nu}_\mu e(X_\gamma)$.

$$\begin{aligned}
& + 4 \left(r - \frac{1}{4r} \right) \left(2\text{Li}_3(r_-^2) - \text{Li}_3(r_+^4) + \frac{8}{3} (\text{Li}_2(r_-^2) - \text{Li}_2(r_+^4)) \ln r_+ \right) + \frac{13}{6} + \frac{\zeta(3)}{r} \\
& + \frac{16}{3} \left(r - \frac{1}{4r} \right) \ln \frac{8(1-r)\sqrt{-r}}{r_+^3} \ln^2 r_+ - 8 \left(r - \frac{1}{6} - \frac{7}{48r} \right) \ln^2 r_+, \tag{143}
\end{aligned}$$

with notations $r_\pm = \sqrt{1-r} \pm r$. As discussed at the end of Section 3.2, the relevant limit for neutrino-electron scattering is $-q^2 \rightarrow 0$, corresponding with

$$\Pi^{\text{QCD}} \Big|_{q^2 \rightarrow 0} = \frac{\alpha_s}{3\pi} \left(\ln \frac{\mu^2}{m_f^2} + \frac{15}{4} \right). \tag{144}$$

For practical evaluation of c-quark contribution, we take the well-convergent expression in terms of $\overline{\text{MS}}$ quark mass \hat{m}_c from Refs. [108, 129–131]:

$$\begin{aligned}
\Pi & = \frac{1}{3} \ln \frac{\mu^2}{\hat{m}_c^2} + \frac{\alpha_s}{3\pi} \left(-\ln \frac{\mu^2}{\hat{m}_c^2} + \frac{13}{12} \right) \\
& + \frac{\alpha_s^2}{3\pi^2} \left(\frac{655}{144} \zeta(3) - \frac{3847}{864} - \frac{5}{6} \ln \frac{\mu^2}{\hat{m}_c^2} - \frac{11}{8} \ln^2 \frac{\mu^2}{\hat{m}_c^2} + n_q \left(\frac{361}{1296} - \frac{1}{18} \ln \frac{\mu^2}{\hat{m}_c^2} + \frac{1}{12} \ln^2 \frac{\mu^2}{\hat{m}_c^2} \right) \right), \tag{145}
\end{aligned}$$

where $n_q = 4$ denotes the number of active quarks. The correction of order α_s^2 in Eq. (145) does not change our results within significant digits.

B Triple-differential distribution

We evaluate the bremsstrahlung cross section following Ref. [22]. For the electron angle distributions, we introduce the four-vector l :

$$l = k + p - p' = (l_0, \vec{f}), \tag{146}$$

with the laboratory frame values:

$$l_0 = m + \omega - E', \quad (147)$$

$$f^2 = |\vec{f}|^2 = \omega^2 + \beta^2 E'^2 - 2\omega\beta E' \cos \theta_e. \quad (148)$$

Note the difference between electron scattering angle in the elastic process (Θ_e of Eq. (6)) and in the scattering with radiation (θ_e).

The triple-differential cross section w.r.t. electron angle, electron energy and photon energy is given by the following substitutions in Eqs. (56, 57):

$$\begin{aligned} \tilde{\mathbb{I}}_{\text{L}} \rightarrow & \left(\frac{l^2 f^2 ((m + \rho k_\gamma) l^2 - 2\rho m^2 k_\gamma)}{4\sqrt{d}} - \frac{m\omega f^2 ((m + \rho k_\gamma) (\rho (l^2 - 2ml_0) - 2m^2) + 2\rho m^3)}{\rho\sqrt{d}} \right. \\ & + \frac{(\rho m (k_\gamma^2 - m^2) - \rho (m + k_\gamma) (l^2 - 2ml_0 + m^2) + (2m + 3k_\gamma) m^2) \sigma}{8\rho^2 m k_\gamma f^2} - \frac{(m + k_\gamma) \sigma^2}{32\rho^2 m k_\gamma f^4} \\ & - \frac{4(1 - \rho) m (m + k_\gamma) l^2 (l^2 - 4k_\gamma l_0 + 4k_\gamma^2) (\rho (m + \omega) l^2 + (1 - \rho) m (m + \omega)^2 - (1 + \rho) m\omega^2)}{64\rho^2 k_\gamma m f^4} \\ & - \frac{(l^2 - 2m\omega)^2}{8k_\gamma} + \frac{k_\gamma (l^2 - m(m + 2\omega))}{2} - \frac{\rho l^4 - 2m(2\rho\omega + (2 + \rho)m)l^2 + 8m^2\omega(\rho l_0 + 2m)}{8\rho m} \\ & \left. - \frac{\rho^2 k_\gamma m^4 \omega^2 f^4 \sigma}{d^{3/2}} - \frac{l^6 (m + k_\gamma) (l^2 - 4k_\gamma l_0 + 4k_\gamma^2)}{64k_\gamma m f^4} \right) \mathcal{D}_m, \quad (149) \end{aligned}$$

$$\begin{aligned} \tilde{\mathbb{I}}_{\text{R}} \rightarrow & \left(\frac{f^2 ((\rho k_\gamma + m) (l^2 - 2ml_0)^2 + 4m^2 (\rho k_\gamma ((l_0 - k_\gamma)^2 - m(2l_0 - k_\gamma)) + m(l_0 - k_\gamma)^2))}{4\sqrt{d}} \right. \\ & + \frac{\rho m^2 f^2 l^2 k_\gamma}{2\sqrt{d}} - \frac{(l^2 - 2ml_0)^2}{8k_\gamma} - \frac{l^4}{8m} - \frac{\rho^2 k_\gamma m^4 f^4 (l_0 - k_\gamma)^2 \sigma}{d^{3/2}} + \frac{(2l_0 - m) l^2}{4} \\ & \left. + \frac{1}{2} k_\gamma m (2l_0 - k_\gamma - m) - ml_0 (l_0 - m) \right) \mathcal{D}_m, \quad (150) \end{aligned}$$

$$\begin{aligned} \tilde{\mathbb{I}}_{\text{R}}^{\text{L}} \rightarrow & \left(\frac{m (m ((1 - \rho) (4m^2 l_0^2 - 2m(l_0 + m) l^2) - \rho l^4) + 4k_\gamma \rho (-f^2 - m^2 + \frac{ml_0}{2}) l^2)}{8\rho k_\gamma f^2} \right. \\ & - \frac{f^2 m (\rho^2 (l^2 + m^2 - 2mk_\gamma) (l^2 - m^2) + 4\rho k_\gamma m^3 + (2 - \rho)^2 m^4)}{2\rho\sqrt{d}} + \frac{\rho(1 - \rho) k_\gamma m^6 f^4 \sigma}{d^{3/2}} \\ & \left. + \frac{\rho^2 k_\gamma^2 m^5 f^4 \sigma}{d^{3/2}} + \frac{m^3 (l_0^2 + f^2 + (\rho - 1) ml_0)}{2\rho f^2} \right) \mathcal{D}_m, \quad (151) \end{aligned}$$

with the kinematical notations:

$$\sigma = 2(\beta\rho E' (l^2 - 2k_\gamma l_0) (\omega \cos \theta_e - \beta E') + 2k_\gamma m f^2), \quad (152)$$

$$d = \beta^2 m^2 l^2 \omega^2 (l^2 + 4k_\gamma^2 - 4k_\gamma l_0) \sin^2 \theta_e + \frac{\sigma^2}{4}, \quad (153)$$

where the phase-space factor \mathcal{D}_m is given by

$$\mathcal{D}_m = \frac{\pi^2}{m^2 \omega^2} df \frac{dk_\gamma}{k_\gamma} \frac{dE'}{\omega}. \quad (154)$$

The physical region of variables corresponding to the radiation of hard photons with energy $k_\gamma \geq \varepsilon$ ($\varepsilon \ll m$, ω), is the following (see Section 4.8 for a description of hard and soft-photon regions):

$$m + \frac{2\varepsilon^2}{m - 2\varepsilon} \leq E' \leq m + \frac{2(\omega - \varepsilon)^2}{m + 2(\omega - \varepsilon)}, \quad (155)$$

$$|\omega - |\vec{p}'|| \leq f \leq l_0 - 2\varepsilon, \quad (156)$$

$$\frac{l_0 - f}{2} \leq k_\gamma \leq \frac{l_0 + f}{2}. \quad (157)$$

We keep the exact dependence on the unphysical parameter ε which is important in the evaluation of electron energy spectrum in Section 4.8. Our integration region in Eqs. (155-157) corresponds to the region I in Section 4.8.

C Double-differential distribution in electron energy and electron angle

Integrating Eqs. (149-151) over the photon energy k_γ , we obtain the double-differential cross section w.r.t. the recoil electron energy and angle. The result is given by the following substitutions in Eqs. (56, 57):

$$\begin{aligned} \tilde{\text{I}}_i &\rightarrow \frac{\pi^2 m}{\omega^3} \left(a_i + b_i \ln \frac{1 + \beta}{1 - \beta} + c_i \ln \frac{l_0 + f}{l_0 - f} + d_i \ln \frac{l_0 - \beta f \cos \delta - \sqrt{g}}{l_0 - \beta f \cos \delta + \sqrt{g}} \right) df dE' \\ &- \frac{\pi^2}{\omega} \frac{2}{\beta} \left(\beta - \frac{1}{2} \ln \frac{1 + \beta}{1 - \beta} \right) \text{I}_i \frac{df^2}{l^2} dE', \end{aligned} \quad (158)$$

with $g = (f \cos \delta - \beta l_0)^2 + \rho^2 f^2 \sin^2 \delta$ and the angle δ between vectors \vec{l} and \vec{p}' :

$$\cos \delta = \frac{\omega^2 - \beta^2 E'^2 - f^2}{2\beta E' f}. \quad (159)$$

Kinematical factors I_L , I_R , I_R^{I} in Eq. (158) correspond to $2 \rightarrow 2$ process.

The coefficients in integrals $\tilde{\text{I}}_i$ are given by

$$\begin{aligned} a_L &= \frac{f(2\omega - m)}{2m^2} - \frac{\beta \cos \delta \left(\frac{3}{4}l^2 - \frac{f^2}{2\rho} - E'l_0 - 2m\omega \right)}{\rho m^2} - \frac{(1 + \beta^2 \cos^2 \delta) f(l_0 + 2m)}{4\rho^2 m^2} \\ &- \frac{\beta^2 l^2 (1 - 3 \cos^2 \delta) (l_0 - 4m)}{8\rho^2 m^2 f} - \frac{(f - \beta l_0 \cos \delta) (l^2 - m(\frac{5}{2}l_0 - m + 3E'))}{2\rho m^3}, \\ b_L &= \frac{fl^2}{4\beta m^3} - \frac{\omega f}{\beta m^2}, \\ c_L &= \frac{\beta^2 l^2 (1 - 3 \cos^2 \delta) (l^2 - 4l_0 m)}{16\rho^2 f^2 m^2} - \frac{l^2 (l^2 - 2s)}{8m^4} - \frac{\omega (m + \omega)}{m^2} \\ &- \frac{\beta \cos \delta (l^2 (l^2 - 4l_0 m - mE' + m^2) + 4m^2 \omega l_0)}{4\rho f m^3}, \\ d_L &= -\frac{\rho f \left((l^2 - s)^2 + s(s - 2m^2) \right)}{8\sqrt{g} m^4} - \frac{f\rho\omega}{2\sqrt{g} m}, \\ a_R &= \frac{3\beta^2 \rho^2 f^3 l^2 \sin^2 \delta \left(\frac{l_0 - \beta f \cos \delta}{4m\rho} + 1 \right)}{2g^2 m} - \frac{f \left(l^2 - \frac{11l_0 m}{2} + m^2 \right)}{2m^3} + \frac{\beta^2 f (2f^2 + 3l_0^2)}{2gm} \\ &+ \frac{f^2 \rho (\beta \cos \delta (f^2 + 2l_0 (\omega - 6E')) + f(2m - 3l_0))}{4gm^2}, \end{aligned}$$

$$\begin{aligned}
b_R &= \frac{l^2 f}{4\beta m^3} - \frac{l_0 f}{\beta m^2}, \\
c_R &= -\frac{l^2 (l^2 - 4m(l_0 - \frac{m}{2}))}{8m^4} - \frac{l_0 (l_0 - m)}{m^2}, \\
d_R &= \frac{\beta f l^2 ((2l_0 \rho - m(-2\rho^2 + \rho + 1))(\beta l_0 - f \cos \delta) - \frac{1}{2}\beta \rho l^2)}{4g^{3/2} m^2} - \frac{\rho^2 f l_0 (f(f - \beta l_0 \cos \delta) + \frac{1}{2}\beta^2 l^2)}{g^{3/2} m} \\
&\quad - \frac{\rho f (l^2 (l^2 - 4l_0 m + 2m^2) + 8l_0 m^2 (\omega - 2E'))}{8\sqrt{g} m^4} + \frac{3\beta^2 \rho^3 f^3 l^2 \sin^2 \delta (l^2 + 4E' (l_0 - \beta f \cos \delta))}{16g^{5/2} m^2}, \\
a_R^L &= \frac{\beta f (\beta l_0 - f \cos \delta)}{g} - \frac{\beta \cos \delta}{\rho}, \\
b_R^L &= -\frac{\rho f l^2}{2\beta m^3}, \\
c_R^L &= \frac{\beta l_0 \cos \delta}{2\rho f} - \frac{l^2 - m(m + E')}{2m^2}, \\
d_R^L &= \frac{\rho f ((m + 2E')m - l^2)}{2m^2 \sqrt{g}} - \frac{\rho^2 f^2 (f - \beta l_0 \cos \delta)}{2g^{3/2}}.
\end{aligned}$$

D Double-differential distribution in electromagnetic energy and electron angle

To obtain neutrino energy (equivalently, electromagnetic energy) and electron angle distribution, Eqs. (149-151) can be integrated over the electron energy, exploiting the energy conservation: $k_\gamma = m + \omega - \omega' - E'$. The integration measure of Eq. (154) is replaced as

$$\mathcal{D}_m = \frac{\pi^2}{m^2 \omega^2} df \frac{dk_\gamma}{k_\gamma} \frac{dE'}{\omega} \rightarrow \frac{\pi^2}{m^2 \omega^2} d \cos \theta_e \frac{d\omega'}{k_\gamma} \frac{\beta E' dE'}{f}. \quad (160)$$

The physical integration region is contained in

$$0 \leq \omega' \leq \omega, \quad (161)$$

$$0 \leq \cos \theta_e \leq 1, \quad (162)$$

$$m \leq E' \leq m \frac{(m + \omega)^2 + \omega^2 \cos^2 \theta_e}{(m + \omega)^2 - \omega^2 \cos^2 \theta_e}, \quad (163)$$

which is actually larger than the physical region. The extraneous regions I and II are above the electron endpoint ($E_{EM} \geq E'_0 = m + \frac{2\omega^2}{m+2\omega}$) and below it ($E_{EM} \leq E'_0 = m + \frac{2\omega^2}{m+2\omega}$):

$$\text{region I :} \quad 0 \leq \omega' \leq \frac{m\omega}{m+2\omega}, \quad (164)$$

$$\frac{2\sqrt{\omega' (m - \omega') (\omega - \omega') (m + \omega - \omega')}}{m\omega} \leq \cos \theta_e \leq 1, \quad (165)$$

$$E'_- (\omega') \leq E' \leq E'_+ (\omega'), \quad (166)$$

$$\text{region II :} \quad \frac{m\omega}{m+2\omega} \leq \omega' \leq \omega, \quad (167)$$

$$\frac{m + \omega}{\omega} \sqrt{\frac{\omega - \omega'}{2m + \omega - \omega'}} \leq \cos \theta_e \leq 1, \quad (168)$$

$$E'_- (\omega') \leq E' \leq m \frac{(m + \omega)^2 + \omega^2 \cos^2 \theta_e}{(m + \omega)^2 - \omega^2 \cos^2 \theta_e}. \quad (169)$$

Here E'_\pm (ω') stand for two solutions ($E_+ \geq E_-$) of

$$\cos \theta_e = \frac{E'(m + \omega - 2\omega') - m^2 + m(2\omega' - \omega) + 2\omega'(\omega - \omega')}{\omega\sqrt{E'^2 - m^2}}. \quad (170)$$

The presentation here in terms of a larger region (161-163) and subtractions (164-169) is designed as a simple description of the actual physical region. In practice, one may perform the integration over this larger region and use subtractions above the electron endpoint $E_{\text{EM}} \geq E'_0 = m + \frac{2\omega^2}{m+2\omega}$; or one may break up the integration region (161-163) and integrate once only over the physical region in any case.

E Double-differential distribution in photon energy and electron energy

To obtain the distribution w.r.t. the photon energy and electron energy, Eqs. (149-151) can be integrated first over the variable f after the change of the integration order. The kinematical region of electron energy is bounded as

$$m \leq E' \leq m + \frac{2\omega^2}{m+2\omega}. \quad (171)$$

The physical region of f for different values of k_γ is then given by

$$0 \leq k_\gamma \leq \frac{l_0 - |\omega - |\vec{p}'||}{2}, \quad l_0 - 2k_\gamma \leq f \leq l_0; \quad (172)$$

$$\frac{l_0 - |\omega - |\vec{p}'||}{2} \leq k_\gamma \leq \frac{l_0 + |\omega - |\vec{p}'||}{2}, \quad |\omega - |\vec{p}'|| \leq f \leq l_0; \quad (173)$$

$$\frac{l_0 + |\omega - |\vec{p}'||}{2} \leq k_\gamma \leq l_0, \quad -l_0 + 2k_\gamma \leq f \leq l_0. \quad (174)$$

F Double-differential distribution in photon energy and photon angle

We evaluate the bremsstrahlung cross section w.r.t. photon energy and photon angle considering the final photon energy spectrum instead of the electron spectrum [22], see Section 4.4 for explanations. For the photon scattering angle (w.r.t. neutrino beam direction) distributions, we introduce the four-vector \vec{l} :

$$\vec{l} = k + p - k_\gamma = (\bar{l}_0, \vec{f}), \quad (175)$$

with the laboratory frame values:

$$\bar{l}_0 = m + \omega - k_\gamma, \quad (176)$$

$$\vec{f}^2 = |\vec{f}|^2 = \omega^2 + k_\gamma^2 - 2\omega k_\gamma \cos \theta_\gamma, \quad (177)$$

where θ_γ denotes the photon scattering angle.

The photon energy spectrum accounting for electron mass terms is given by the following substitutions in Eqs. (56, 57):

$$\tilde{I}_i \rightarrow \frac{\pi^2}{2m\omega^2} \left(a_i (\bar{l}^2 - m^2) + b_i \ln \frac{m^2}{\bar{l}^2} \right) \frac{\bar{f} d\bar{f}}{(\bar{l}^2 - s)^2} dk_\gamma, \quad (178)$$

with $s = m^2 + 2m\omega$ and coefficients a_i and b_i in Eq. (178):

$$a_L = \frac{(\bar{l}^2 - m^2)^2 (2\bar{l}^2 (k_\gamma \bar{l}_0 + m(2\bar{l}_0 - m)) + m(-2\bar{l}_0^2(2\omega + m) + \bar{l}_0 m(6\omega + m) - 3m^2\omega))}{4k_\gamma^2 \bar{l}^2 m\omega}$$

$$\begin{aligned}
& - \frac{4m\omega^3 (m(2k_\gamma - \omega + m) + \bar{l}^2) - \omega(\omega - k_\gamma) (3\bar{l}^4 - 6\bar{l}^2\bar{l}_0m - m^3(2\bar{l}_0 - 5m))}{k_\gamma^2\bar{l}^2} \\
& - \frac{2\omega^2 (\bar{l}^4 - \bar{l}^2m(5\bar{l}_0 - 3m) + m^2(2\bar{l}_0 - 3m)(\bar{l}_0 - 2m))}{k_\gamma^2\bar{l}^2} - \frac{(\bar{l}^2 - m^2)^2 \bar{l}^2(k_\gamma + m)}{4k_\gamma^2m^2\omega}, \\
\frac{a_R / (\bar{l}^2 - m^2)}{\bar{f}^2 - (\bar{l}_0 - m)^2} &= - \frac{m(\bar{l}^2 - s) (-4k_\gamma^3(11\omega + 17m) - 4k_\gamma^2(35\omega^2 + 103m^2) - 3k_\gamma m^2(12\omega + 29m))}{12k_\gamma^2\bar{l}^6\omega} \\
& - \frac{2m^3s (k_\gamma^2(344\omega^2 + 1116m\omega + 537m^2) + m(312\omega^3 + 501m\omega^2 + 342m^2\omega + 72m^3))}{3\bar{l}^6\omega (\bar{l}^2 - m^2) (\bar{f}^2 - (\bar{l}_0 - m)^2)} \\
& - \frac{4m^2s^2 (6k_\gamma^2m(27\omega^2 + 93m\omega + 46m^2) + k_\gamma s(51\omega^2 + 154m\omega + 108m^2) - 3sm\omega^2)}{3\bar{l}^6\omega (\bar{l}^2 - m^2) (\bar{l}^2 - s) (\bar{f}^2 - (\bar{l}_0 - m)^2)} \\
& - \frac{m^3(\bar{l}^2 - s) (4k_\gamma^2(64\omega^2 + 197m\omega + 96m^2) + k_\gamma m(2950\omega^2 + 3376m\omega + 1191m^2))}{3\bar{l}^6\omega (\bar{l}^2 - m^2) (\bar{f}^2 - (\bar{l}_0 - m)^2)} \\
& - \frac{m^2(\bar{l}^2 - s) (-4k_\gamma^2\omega + k_\gamma(268\omega^2 + 794m\omega + 384m^2) + 2m^2(785\omega + 327m))}{6\bar{l}^6\omega (\bar{f}^2 - (\bar{l}_0 - m)^2)} \\
& - \frac{2m^2s (k_\gamma^2m(590\omega^3 + 2106m\omega^2 + 2144m^2\omega + 617m^3) + 92k_\gamma m\omega^4 - 2s^2\omega^2)}{3k_\gamma\bar{l}^6\omega (\bar{l}^2 - m^2) (\bar{f}^2 - (\bar{l}_0 - m)^2)} \\
& - \frac{m^2(\bar{l}^2 - s) (2\omega^2k_\gamma(162\omega + 579m) - m(16\omega^3 - 18m\omega^2 - 105m^2\omega - 64m^3))}{6k_\gamma\bar{l}^6\omega (\bar{f}^2 - (\bar{l}_0 - m)^2)} \\
& - \frac{4m^3(\bar{l}^2 - s) (193k_\gamma^2\omega^3 - m(4\omega^2 + 2m\omega - 3m^2)(\omega^2 + m\omega + m^2))}{3k_\gamma\bar{l}^6\omega (\bar{l}^2 - m^2) (\bar{f}^2 - (\bar{l}_0 - m)^2)} + \frac{11(\bar{l}^2 - m^2)}{6\bar{l}^4} \\
& - \frac{m^3(\bar{l}^2 - s) (184\omega^4 + 740m\omega^3 + 1344m^2\omega^2 + 1167m^3\omega + 405m^4)}{3\bar{l}^6\omega (\bar{l}^2 - m^2) (\bar{f}^2 - (\bar{l}_0 - m)^2)} + \frac{106m^2(\bar{l}^2 - s)}{3\bar{l}^6} \\
& + \frac{(\bar{l}^2 - m^2) (k_\gamma^2 + 11k_\gamma m + (\omega^2 + 6m^2))}{3k_\gamma\bar{l}^4\omega} + \frac{(k_\gamma + m) (\bar{l}^2 - m^2) (\bar{f}^2 - (\bar{l}_0 - m)^2)^2}{12k_\gamma^2m^2\omega (\bar{l}^2 - s)^2} \\
& - \frac{8k_\gamma m^3 s^3 (48k_\gamma s + \omega^2(27k_\gamma - m))}{3\bar{l}^6\omega (\bar{l}^2 - m^2) (\bar{l}^2 - s)^2 (\bar{f}^2 - (\bar{l}_0 - m)^2)} - \frac{1}{6k_\gamma^2} - \frac{m^5(\bar{l}^2 - s)}{12k_\gamma^2\bar{l}^6\omega}, \\
a_R^L &= \frac{\bar{l}^2m(8k_\gamma^2 + 14k_\gamma\bar{l}_0 - 9k_\gamma m - 2\bar{l}_0m)}{2k_\gamma^2\omega} - \frac{m^4s^2(2k_\gamma - m)^2(2\bar{l}_0 - m)}{4k_\gamma^2\bar{l}^4\omega (\bar{l}^2 - s)} \\
& + \frac{m^3(8k_\gamma^3(2\omega + 5m) - 8k_\gamma^2(6(\omega + m)^2 + m(\omega + 2m)) + 4k_\gamma(8(\omega + m)^3 - 3s\omega))}{4k_\gamma^2\bar{l}^2\omega} \\
& + \frac{m^2(-4k_\gamma^3 + 2k_\gamma^2(8\omega - 7m) - k_\gamma(28\omega^2 + 34m\omega + 15m^2) + m(3(\omega + m)^2 - \omega^2))}{2k_\gamma^2\omega} \\
& - \frac{m^3(8k_\gamma^2(16k_\gamma\omega + 13k_\gamma m + m^2) - s(2k_\gamma - m)^2 + 2k_\gamma m(4k_\gamma - m)^2)}{4k_\gamma^2\omega (\bar{l}^2 - s)} \\
& - \frac{\bar{l}^4(4k_\gamma - m)}{4k_\gamma^2\omega} - \frac{m^3s(2s + 3m^2)}{4k_\gamma^2\bar{l}^2\omega}, \\
b_L &= -(\bar{l}^2 - m^2)^2 - 4m^2\omega(\omega + 2m), \\
\frac{b_R}{\bar{f}^2 - (\bar{l}_0 - m)^2} &= \frac{16k_\gamma m^3(\omega + m)((\omega + 2m)^2 + 4m\omega)}{\omega(\bar{l}^2 - s)^2} + \frac{\bar{l}^2(k_\gamma(\omega + 2m) + m^2)}{k_\gamma\omega}
\end{aligned}$$

$$\begin{aligned}
& + \frac{m(2k_\gamma^2(\omega+m) + (2\omega+3m)(k_\gamma(\omega+4m) + m^2))}{k_\gamma\omega} \\
& - \frac{8m^2(\bar{l}_0((\omega+2m)^2 + m(\omega-m)) - 2(\omega+m)^2(\omega+4m))}{\omega(\bar{l}^2-s)}, \\
b_{\text{R}}^{\text{L}} = & - \frac{\bar{l}^4(m^2(-12k_\gamma\omega + 20\omega(\omega+m) + 7m^2) - 2\bar{l}^2m(\bar{l}_0+\omega) + (\bar{l}^2-s)^2)}{k_\gamma\omega(\bar{l}^2-s)} \\
& - \frac{2\bar{l}^2m^2(2k_\gamma^2m(2\omega+3m) + k_\gamma m(7m^2 + 10m\omega + 12\omega^2) - 4s((\omega+m)^2 + \omega^2))}{k_\gamma\omega(\bar{l}^2-s)} \\
& - \frac{m^2(4k_\gamma^2m^3(8\omega+5m) - 8k_\gamma ms(m^2 + (\omega+m)^2) + s^2(2m^2 + (2\omega+m)^2))}{k_\gamma\omega(\bar{l}^2-s)}.
\end{aligned}$$

G Photon energy spectrum

The photon energy spectrum accounting for electron mass terms is given by the following substitutions in Eqs. (56, 57):

$$\begin{aligned}
\tilde{\text{I}}_i \rightarrow & \frac{\pi^2}{\omega^3} \left[a_i + b_i \ln \frac{k_\gamma}{\omega} + c_i \ln \frac{2\bar{l}_0 - m}{m} - d_i \ln \frac{2k_\gamma}{2\omega + m} \ln \frac{2\bar{l}_0 - m}{m} \right. \\
& \left. + d_i \sum_{\sigma_1, \sigma_2=\pm} \Re \left(\text{Li}_2 \frac{\bar{l}_0 + \sigma_1 \sqrt{\bar{l}_0^2 - m^2}}{\bar{l}_0 + \sigma_2 \sqrt{(\bar{l}_0 - m)^2 - 2mk_\gamma}} - \text{Li}_2 \frac{\bar{l}_0 + \sigma_1 (\bar{l}_0 - m)}{\bar{l}_0 + \sigma_2 \sqrt{(\bar{l}_0 - m)^2 - 2mk_\gamma}} \right) \right] dk_\gamma, \quad (179)
\end{aligned}$$

with coefficients a_i , b_i , c_i and d_i in Eq. (179):

$$\begin{aligned}
a_{\text{L}} & = \frac{(\omega - k_\gamma)(2k_\gamma^3 - k_\gamma^2 m + 6k_\gamma m^2 - 2\omega^2(53k_\gamma + 2m) - \omega(8k_\gamma - m)(5k_\gamma + 3m) - 3m^3)}{24k_\gamma^2}, \\
\frac{a_{\text{R}}}{\omega - k_\gamma} & = \frac{m^5}{24k_\gamma^2(2\omega + m)^2} + \frac{m^3(-36k_\gamma^2 - 10k_\gamma m + m^2)}{96k_\gamma^3(2\omega + m)} - \frac{m(k_\gamma^3 m + (k_\gamma - \frac{m}{4})(4k_\gamma^3 - 2k_\gamma^2 m - m^3))}{24k_\gamma^3(2\omega - 2k_\gamma + m)} \\
& + \frac{m^2\omega}{12(2\omega - 2k_\gamma + m)^2} - \frac{\omega^2(73k_\gamma + 2m)}{36k_\gamma^2} - \frac{m(656\omega + 897m)}{144k_\gamma} - \frac{37k_\gamma}{36} - \frac{892\omega + 1184m}{144}, \\
a_{\text{R}}^{\text{L}} & = \frac{m^2\omega(\omega - k_\gamma)(2\omega + 3m)}{8k_\gamma^2(2\omega + m)} - \frac{m(\omega - k_\gamma)(26k_\gamma^2 - k_\gamma(22\omega - 13m) + 3m^2)}{8k_\gamma^2}, \\
b_{\text{L}} & = - \frac{\omega^2(3k_\gamma(2\omega + m) + 2\omega(\omega + m))}{k_\gamma(2\omega + m)}, \\
b_{\text{R}} & = \frac{4m\omega^4(\omega + m)}{3k_\gamma(2\omega + m)^3} - \frac{6\omega^4}{(2\omega + m)^2} + \frac{\omega^2(3k_\gamma^2 + 14\omega^2)}{3k_\gamma(2\omega + m)} - \frac{14\omega^3}{3k_\gamma} \\
& - \frac{\omega(8k_\gamma m + 3k_\gamma(k_\gamma + \omega) - 2(\omega^2 - m^2))}{k_\gamma}, \\
b_{\text{R}}^{\text{L}} & = - \frac{m\omega(k_\gamma(2\omega + m)(2\omega + 3m) - 2\omega^3 + 3m^2\omega + m^3)}{k_\gamma(2\omega + m)^2}, \\
c_{\text{L}} & = \frac{m^2(4\omega^2 - 3m^2)}{16k_\gamma(2\omega + m)} - \frac{8k_\gamma^3\omega + 2k_\gamma^2(4\omega^2 - m^2) - 16k_\gamma\omega^2(\omega + m) - m^4}{16k_\gamma^2}, \\
c_{\text{R}} & = - \frac{m^4(36\omega^2 + 30m\omega + 7m^2)}{24k_\gamma(2\omega + m)^3} + \frac{3m^4}{8(2\omega + m)^2} - \frac{3m^3}{2(2\omega + m)} - k_\gamma \left(\frac{\omega^2}{2\omega + m} + \frac{1}{4}(2\omega + 15m) \right)
\end{aligned}$$

$$\begin{aligned}
& + \frac{\omega^3 - k_\gamma^3}{3k_\gamma} + \frac{m(72\omega^2 + 204m\omega + 123m^2)}{48k_\gamma} + \frac{m^4}{48k_\gamma^2} - \frac{13m^2}{8} + \omega(\omega + 3m), \\
c_R^L &= \frac{m\omega(8k_\gamma(\omega + m)(2\omega + m) - \omega(8\omega^2 + 12m\omega + 3m^2))}{2k_\gamma(2\omega + m)^2} - \frac{m(2k_\gamma - m)(8k_\gamma(k_\gamma + m) + 3m^2)}{16k_\gamma^2}, \\
d_L &= -\omega^2, \\
d_R &= -\frac{k_\gamma^2(2\omega + 3m) + 2k_\gamma(\omega + 2m)^2 + 2m^2(\omega + m)}{2k_\gamma}, \\
d_R^L &= -\frac{m^2(3k_\gamma + m)}{2k_\gamma}.
\end{aligned}$$

H Electron energy spectrum

The nonfactorizable contribution to the electron energy spectrum $d\sigma_{\text{NF}}^{\nu_\ell e \rightarrow \nu_\ell e \gamma}$ from Eq. (105), is given by the following substitutions in Eqs. (56, 57):

$$\begin{aligned}
\tilde{I}_i &\rightarrow \frac{\pi^2}{\omega^3} \left(z_i + y_i \ln \frac{\frac{2\omega}{m}}{-1 + \frac{\rho}{1+\beta} \left(1 + \frac{2\omega}{m}\right)} + x_i \ln \frac{\frac{2l_0}{m}}{\left(1 + \frac{2\omega}{m}\right) - \frac{1+\beta}{\rho}} + r_i \ln \frac{1 - \frac{1+\beta}{\rho}}{\frac{1+\beta}{1-\beta} - \frac{1+\beta}{\rho} \left(1 + \frac{2\omega}{m}\right)} \right) dE' \\
&+ \frac{\pi^2}{\omega^3} \left(q_i \ln \frac{1+\beta}{1-\beta} + v_i \left(\text{Li}_2 \frac{1+\beta}{\rho} - \text{Li}_2 \left(1 + \frac{2\omega}{m}\right) + \text{Li}_2 \frac{\left(1 + \frac{2\omega}{m}\right)\rho}{1+\beta} - \frac{\pi^2}{6} \right) \right) dE'. \quad (180)
\end{aligned}$$

Exact expressions for coefficients z_i , y_i , x_i , r_i , q_i and v_i in Eq. (180) are given by

$$\begin{aligned}
v_L &= \frac{1}{2} \left(\frac{m^2}{2} + 2m\omega + \omega^2 \right), & v_R &= \frac{1}{2} \left(l_0^2 + \frac{\beta^2 + \rho}{\rho^2} m^2 \right), & v_R^L &= \frac{1}{2} m(2l_0 - m), \\
x_L &= -\frac{2}{15} \frac{\omega^5}{m^3} + \frac{1}{3} \frac{\omega^3}{m} + \left(\frac{1+3\beta^2}{3\rho^3} - \frac{4\beta^4 - 11\beta^2 + 7}{3\rho^4} \right) \omega^2 + \left(\frac{2}{\rho^3} - \frac{\beta^4 - \beta^2 + 2}{\rho^4} \right) m\omega \\
&+ \left(\frac{-7\beta^4 + 14\beta^2 - 22}{15\rho^4} + \frac{15\beta^4 - 25\beta^2 + 22}{15\rho^5} \right) m^2, \\
x_R &= -\frac{l_0^2(35l_0m^2 - 10l_0^2m + 2l_0^3 - 30m^3)}{15m^3}, \\
x_R^L &= \frac{3l_0m^2 - 3l_0^2m - 2l_0^3 + 3m^2\omega}{3m}, \\
y_L &= \frac{1}{2} \omega(\omega - m), \\
y_R &= \frac{-\omega^4 - 2 \left(5 - \frac{1}{\rho}\right) m\omega^3 + \frac{12\beta^2 + 11\rho - 16}{\rho^2} m^2\omega^2 + \frac{6\beta^2 + 9\rho - 10}{\rho^2} m^3\omega + \frac{\beta^2 + 2\rho - 2}{\rho^2} m^4}{(m + 2\omega)^2}, \\
y_R^L &= mE' \left(1 - \frac{(m + 2\omega)^2 - m\omega}{E'(m + 2\omega)} \right), \\
r_L &= \left(-\frac{2+\beta}{3} \frac{\rho}{(1+\beta)^2} + \frac{1}{6} \frac{4+\beta}{1+\beta} \right) \omega^2 + \left(\frac{\beta - \rho^2}{\rho(1+\beta)} + \frac{1}{2} \left(1 + \frac{1}{(1+\beta)^2} \right) \right) m\omega \\
&+ \left(-\frac{(17\beta^2 + 36\beta + 22)\rho}{30(1+\beta)^3} + \frac{14\beta^2 + 43\beta + 44}{60(1+\beta)^2} \right) m^2, \\
r_R &= \left(-\frac{2+\beta}{3} \frac{\rho}{(1+\beta)^2} + \frac{1}{6} \frac{4+\beta}{1+\beta} \right) \omega^2 + \left(\frac{\beta^2 - 5\beta + 1}{3\rho(1+\beta)} + \frac{1}{6} \frac{7\beta^2 + 8\beta - 2}{(1+\beta)^2} \right) m\omega'
\end{aligned}$$

$$\begin{aligned}
& + \left(\frac{-23\beta^3 + 14\beta^2 + 41\beta - 2}{30\rho(1+\beta)^2} + \frac{-28\beta\rho^2 + 43\beta^2 + 2}{30\rho^2(1+\beta)} \right) m^2, \\
r_{\text{R}}^{\text{L}} &= \frac{1}{6} \left(14 + 5\beta + 2\frac{2\beta^2 - 4\beta - 7}{\rho} \right) \frac{m^2}{1+\beta} + \left(1 + \frac{1-2\rho}{1+\beta} \right) m\omega, \\
q_{\text{L}} &= \left(\frac{1}{2\beta} \frac{\rho}{1+\beta} - \frac{1+\beta}{2\beta} \right) \omega^2 + \frac{\beta}{2\rho} m\omega + \frac{1-\rho}{2\beta} m^2, \\
q_{\text{R}} &= \left(\frac{1}{2\beta} \frac{\rho}{1+\beta} - \frac{1+\beta}{2\beta} \right) \omega'^2 + \left(2 - \frac{1}{1+\beta} - \frac{2-\beta}{2\rho} \right) m\omega' \\
& + \left(\frac{4\beta^3 + \beta^2 - 4\beta + 2}{4\beta\rho^2} + \frac{-\beta^3 + 2\beta^2 + \beta - 1}{2\beta\rho(1+\beta)} \right) m^2, \\
q_{\text{R}}^{\text{L}} &= \frac{(1-\beta)\omega^2 - 2\rho m\omega + \left(1 + \frac{\beta}{2}\right) m^2}{\beta} \frac{l_0 - \omega}{m} + \beta m E', \\
z_{\text{L}} &= \frac{z^{\omega^4} \omega^4 + z_{\text{L}}^{\omega^3} m\omega^3 + z_{\text{L}}^{\omega^2} m^2 \omega^2 + z_{\text{L}}^{\omega} m^3 \omega + z_{\text{L}}^0 m^4}{m^2}, \\
z_{\text{R}} &= \frac{2z^{\omega^4} \omega^5 + z_{\text{R}}^{\omega^4} m\omega^4 + z_{\text{R}}^{\omega^3} m^2 \omega^3 + z_{\text{R}}^{\omega^2} m^3 \omega^2 + z_{\text{R}}^{\omega} m^4 \omega + z_{\text{R}}^0 m^5}{m^2(m+2\omega)}, \\
z_{\text{R}}^{\text{L}} &= \frac{2l_0 + 9m}{6} \left(l_0 - \frac{\rho\omega}{1+\beta} \right), \\
z^{\omega^4} &= \frac{1}{15} - \frac{1}{15} \frac{\rho}{1+\beta}, & z_{\text{L}}^0 &= \frac{25\beta^2 - 49}{60\rho^3} \left(1 - \frac{1}{\rho} \right) - \frac{8\beta^2}{15\rho^2}, \\
z_{\text{L}}^{\omega^3} &= \frac{3-\beta}{30\rho} - \frac{3+2\beta}{30(1+\beta)}, & z_{\text{L}}^{\omega^2} &= \frac{7\beta^2 + 8\beta - 23}{30(1+\beta)\rho} - \frac{15\beta^2 + 6\beta - 23}{30\rho^2}, \\
z_{\text{L}}^{\omega} &= \frac{-20\beta^3 + 51\beta^2 + 38\beta - 105}{60\rho^3} - \frac{55\beta^3 + 54\beta^2 - 82\beta - 105}{60\rho^2(1+\beta)}, \\
z_{\text{R}}^{\omega^4} &= -\frac{8}{15\rho} + \frac{1}{15} \frac{8-\beta}{1+\beta}, & z_{\text{R}}^{\omega^3} &= \frac{113\beta^2 - 2\beta - 133}{30(1+\beta)\rho} - \frac{143\beta^2 - 34\beta - 133}{30\rho^2}, \\
z_{\text{R}}^{\omega^2} &= -\frac{339\beta^3 - 805\beta^2 - 353\beta + 851}{60\rho^3} + \frac{-760\beta^3 - 825\beta^2 + 778\beta + 851}{60\rho^2(1+\beta)}, \\
z_{\text{R}}^{\omega} &= \frac{\beta((433 - 45\beta)\beta + 44) - 439}{30\rho^3} + \frac{\beta(\beta(9\beta(33\beta + 3) - 730) - 29) + 439}{30\rho^4}, \\
z_{\text{R}}^0 &= \frac{270\beta^2 - 269}{60\rho^3} + \frac{309\beta^4 - 839\beta^2 + 538}{120\rho^4},
\end{aligned}$$

where $l_0 = m + \omega - E'$ and $\omega' = l_0$. Our result agrees numerically with Refs. [29, 38]. Integrated over the electron energy, it agrees with the total cross section of Appendix K.

I Electromagnetic energy spectrum below electron endpoint

For the remaining nonfactorizable contribution to the electromagnetic energy spectrum $d\sigma_{\text{NF}}^{\nu_\ell e \rightarrow \nu_\ell e \gamma}$, it is convenient to express the result as

$$d\sigma_{\text{NF}}^{\nu_\ell e \rightarrow \nu_\ell e \gamma} = \frac{\alpha}{\pi} \delta_\gamma d\sigma_{\text{LO}}^{\nu_\ell e \rightarrow \nu_\ell e} + (d\sigma_{\text{NF}}^{\nu_\ell e \rightarrow \nu_\ell e \gamma})', \quad (181)$$

where in the first term the cross section of elastic process is expressed as a function of the final state neutrino energy, and

$$\begin{aligned}\delta_\gamma &= \frac{1}{2\beta} \ln \frac{1-\beta}{1+\beta} \left(1 + \ln \frac{\rho^{17/2}}{4\beta^4 (1-\beta)^{9/2}} \right) - 1 - 2 \ln \frac{1-\rho}{\rho} \\ &- \frac{1}{\beta} \left(\text{Li}_2 \frac{-\rho^3}{(1+\beta)^3} + \frac{1}{2} \text{Li}_2 \frac{1-\beta}{1+\beta} - \text{Li}_2 \frac{\rho}{1+\beta} + \frac{\pi^2}{6} \right).\end{aligned}\quad (182)$$

As for the electron energy spectrum, individual corrections contain double logarithms:

$$\delta_v \underset{\beta \rightarrow 1}{\sim} -\frac{1}{8} \ln^2(1-\beta), \quad \delta_s \underset{\beta \rightarrow 1}{\sim} -\frac{1}{4} \ln^2(1-\beta), \quad \delta_\Pi \underset{\beta \rightarrow 1}{\sim} \frac{1}{2} \ln^2(1-\beta), \quad \delta_\gamma \underset{\beta \rightarrow 1}{\sim} -\frac{1}{8} \ln^2(1-\beta), \quad (183)$$

but the complete electromagnetic energy spectrum is free from Sudakov double logarithms [115]. The residual nonfactorizable piece of the bremsstrahlung contribution, $(d\sigma_{\text{NF}}^{\nu_\ell e \rightarrow \nu_\ell e \gamma})'$ is given by the following substitutions in Eqs. (56, 57):

$$\tilde{\mathbf{I}}_i \rightarrow \frac{\pi^2}{\omega^3} \left(a_i + b_i \ln \frac{1+\beta}{1-\beta} + c_i \ln \frac{2-\rho}{1-\beta} \right) d\omega', \quad (184)$$

where coefficients a_i , b_i and c_i can be expressed in terms of the initial and final neutrino energies, ω and ω' respectively, in the following form:

$$\begin{aligned}f_L(\omega) &= f^{\omega^2} \omega^2 + f^\omega m\omega + f^0 m^2, \\ f_R(\omega) = f_L(-\omega') &= f^{\omega^2} \omega'^2 - f^\omega m\omega' + f^0 m^2,\end{aligned}$$

with dimensionless coefficients:

$$\begin{aligned}c^{\omega^2} &= \frac{3\beta^2 + 1}{3\rho^3} - \frac{7\beta^2 + 8}{3\rho^2}, \\ c^\omega &= \frac{2(\beta^2 + 4)}{\rho^3} + \frac{17\beta^4 + 22\beta^2 - 55}{8\rho^4}, \\ c^0 &= \frac{112 - 15\beta^4 - 85\beta^2}{15\rho^5} + \frac{31\beta^4 + 118\beta^2 - 449}{60\rho^4}, \\ b^{\omega^2} &= \frac{(\beta - 3)(2\beta - 1)\rho}{6(1-\beta)^2\beta} + \frac{\beta + 14}{6(1-\beta)}, \\ b^\omega &= \frac{((\beta - 4)\beta - 2)\rho}{2(1-\beta)^2\beta} + \frac{55 - \beta(17\beta + 30)}{16(1-\beta)^2} + \frac{1}{\beta}, \\ b^0 &= \frac{\rho(\beta(\beta + 1)(23 - 2\beta) - 45)}{30(1-\beta)^3\beta} + \frac{-31\beta^3 - 88\beta^2 + 89\beta + 180}{120(1-\beta)^2\beta}, \\ a^{\omega^2} &= \frac{\rho(11\beta^2 + 21)}{3(\beta^4 + 2\beta^2 - 3)} + \frac{2(3\beta^4 + 8\beta^2 - 15)}{3(\beta^4 + 2\beta^2 - 3)}, \\ a^\omega &= \frac{23\beta^4 + 34\beta^2 - 73}{4\rho^3(\beta^2 + 3)} + \frac{-2\beta^4 + 13\beta^2 + 73}{-4\beta^4 - 8\beta^2 + 12}, \\ a^0 &= \frac{85\beta^2 - 163}{30\rho^3} + \frac{15\beta^4 - 166\beta^2 + 163}{30\rho^4}.\end{aligned}$$

The interference part of the energy spectrum is determined by

$$a_{\text{R}}^{\text{L}} = \left(-\frac{\rho}{2-\rho} \frac{2\omega\omega'}{m^2} - \frac{1}{3\rho} + 4 \right) \omega^2 \text{I}_{\text{R}}^{\text{L}},$$

$$\begin{aligned}
b_{\text{R}}^{\text{L}} &= \left(\frac{1+\beta}{2\beta} \frac{2\omega\omega'}{m^2} - \frac{1}{3\beta^2} + \frac{1}{3(1-\beta)} + \frac{7}{6} - \frac{1+\beta}{\rho} \left(\frac{1}{3\beta^2} + \frac{7}{6\beta} + \frac{1}{6} \right) \right) \omega^2 \text{I}_{\text{R}}^{\text{L}}, \\
c_{\text{R}}^{\text{L}} &= \left(-\frac{2\omega\omega'}{m^2} + \frac{\beta^4 - 5\beta^2 + 2}{3\beta^2\rho^2} + \frac{2(1+4\beta^2)}{3\beta^2\rho} \right) \omega^2 \text{I}_{\text{R}}^{\text{L}},
\end{aligned}$$

where $\text{I}_{\text{R}}^{\text{L}}$ is given by Eq. (20).

Our result agrees with numerical evaluation in Ref. [29].

J Electromagnetic energy spectrum above electron endpoint

The electromagnetic energy spectrum above electron endpoint can be conveniently expressed as a sum of the factorizable and nonfactorizable corrections,

$$d\sigma^{\nu_\ell e \rightarrow \nu_\ell e \gamma} = \frac{\alpha}{\pi} \delta_\gamma d\sigma_{\text{LO}}^{\nu_\ell e \rightarrow \nu_\ell e} + (d\sigma^{\nu_\ell e \rightarrow \nu_\ell e \gamma})' . \quad (185)$$

The factorizable part is given by

$$\begin{aligned}
\delta_\gamma &= \frac{1}{\beta} \left(-\frac{\pi^2}{3} + \frac{7}{8} \ln^2 \frac{1+\beta}{1-\beta} + 2 \ln \left(1 + \frac{2\omega}{m} \right) \ln \frac{1+\beta}{1-\beta} - \frac{3}{2} \ln \frac{1+\beta}{1-\beta} \ln \frac{2-\rho}{1-\beta} + 2 \text{Li}_2 \frac{\rho}{1+\beta} \right. \\
&+ \ln \frac{2-\rho(1+\frac{2\omega}{m})}{\rho(1+\frac{2\omega}{m})} \ln \left(\frac{1+\beta}{1-\beta} \frac{1+\beta-\rho(1+\frac{2\omega}{m})}{-1+\beta+\rho(1+\frac{2\omega}{m})} \right) - \text{Li}_2 \frac{\rho(1+\frac{2\omega}{m})}{1+\beta} - \text{Li}_2 \frac{2-\rho(1+\frac{2\omega}{m})}{1+\beta} \\
&+ \text{Li}_2 \frac{2-\rho}{1+\beta} + \Re \left(\text{Li}_2 \frac{\rho(1+\frac{2\omega}{m})}{1-\beta} + \text{Li}_2 \frac{2-\rho(1+\frac{2\omega}{m})}{1-\beta} - \text{Li}_2 \frac{2-\rho}{1-\beta} \right) \\
&+ \left. 2 \ln \left(\frac{2-\rho(1+\frac{2\omega}{m})}{1-\rho} \frac{2\omega\omega' + m(\omega' - \omega)}{-m^2} \right) \right), \quad (186)
\end{aligned}$$

where the elastic cross section $d\sigma_{\text{LO}}^{\nu_\ell e \rightarrow \nu_\ell e}$ is expressed in terms of ω' . The nonfactorizable part is given by the following substitutions in Eqs. (56, 57):

$$\tilde{\text{I}}_i \rightarrow \frac{\pi^2}{\omega^3} \left(a_i + b_i \ln \frac{2-\rho(1+\frac{2\omega}{m})}{\rho} + c_i \ln \left(1 + \frac{2\omega}{m} \right) + d_i \ln \frac{2-\rho(1+\frac{2\omega}{m})}{2-\rho} \right) d\omega', \quad (187)$$

with coefficients a_i , b_i , c_i and d_i :

$$\begin{aligned}
a_{\text{L}} &= \frac{\omega \left(\frac{30m^4(2\omega+m)}{m+2\omega-2\omega'} - \frac{15m^5}{m-2\omega'} - 15m^4 + 4(109m^2 + 78m\omega + 2\omega^2)\omega'^2 - 2(m-2\omega)(11m^2 + 4\omega^2)\omega' \right)}{120m^3} \\
&+ \frac{\omega\omega'^3(8\omega - 7m - 4\omega')}{5m^3}, \\
b_{\text{L}} &= \frac{2\omega^5}{15m^3} - \frac{\omega^3}{3m} - 2\omega^2, \\
c_{\text{L}} &= -b_{\text{L}} + \frac{m^2}{60} - \frac{9m\omega}{8} - \frac{11\omega^2}{3}, \\
d_{\text{L}} &= \frac{m^2(6\omega'^2 + 6\omega\omega' - 5\omega^2) + m(\omega - \omega')(\omega^2 + 7\omega\omega' + 13\omega'^2) + 3\omega'^2(\omega - \omega')^2}{3m^2} \\
&+ \frac{2m^5 - 135m^4\omega - 16(\omega - \omega')^3(\omega^2 + 3\omega\omega' + 6\omega'^2)}{120m^3}, \\
a_{\text{R}} &= a_{\text{L}}(\omega \leftrightarrow -\omega'),
\end{aligned}$$

$$\begin{aligned}
b_R &= b_L(\omega \leftrightarrow \omega') + b_L(\omega \leftrightarrow -\omega') + c_L(\omega \leftrightarrow -\omega') - d_L(\omega \leftrightarrow -\omega') + 2\omega'^2, \\
c_R &= d_R + \frac{\omega'^3}{3m} - \frac{2\omega'^5}{15m^3}, \\
d_R &= d_L(\omega \leftrightarrow -\omega'), \\
a_R^L &= \frac{4\omega\omega'((\omega - \omega' - 3m)^2 - 13m^2)}{3m(2E_{\text{EM}} - m)}, \\
b_R^L &= 2\left(\frac{\omega^3}{3m} - m\omega' - \omega^2 + \omega\omega'\right), \\
c_R^L &= \frac{2m^2}{3} - \frac{2\omega^3}{3m} + m(3\omega - \omega') + 2\omega(\omega - \omega'), \\
d_R^L &= c_R^L + \frac{2}{3}\omega'\left(\frac{\omega'^2}{m} - 3E_{\text{EM}}\right),
\end{aligned}$$

where $E_{\text{EM}} = m + \omega - \omega'$, and as explained in Section 2.2 $d\sigma/dE' = d\sigma/d\omega'$. Our result agrees with a numerical evaluation of Ref. [29]. The total cross section from both regions of Sections 4.9.1 and 4.9.2 is in agreement with Ref. [31]. Correcting obvious typos, the function $\tilde{\text{I}}_L^{\text{R}}$ and only the function $\tilde{\text{I}}_L$ of Eq. (187) with the interchange $\tilde{\text{I}}_L \leftrightarrow \tilde{\text{I}}_R$ are in agreement with Ref. [31]. For all other kinematical factors of Sections 4.9.1 and 4.9.2, we find nontrivial discrepancies with Ref. [31].

K Total cross section

The total cross-section correction including both real and virtual contributions, besides closed fermion loop correction of Sections 3.2 and 3.3, is given by the following substitutions in Eqs. (56, 57) [31]:

$$\frac{\tilde{\text{I}}_L}{\pi^2} \rightarrow (1+R)\text{L}_2 + \frac{r^2(1-r)}{2}\ln^2 R + 4(1-R)\ln r - \left(r^2 - \frac{r}{2} + \frac{3R}{2} + \frac{10}{3}\right)\ln R - \frac{r}{2} + \frac{19(1-R)}{24}, \quad (188)$$

$$\begin{aligned}
\frac{\tilde{\text{I}}_R}{\pi^2} &\rightarrow -4r^2(2r+1)\text{L}_3 + \left(8r^2 + \frac{R^3}{3} + 2R + \frac{1}{3}\right)\text{L}_2 - \frac{7r^3}{6}\ln^2 R + \left(8r - \frac{8R^3}{9} + \frac{R^2}{3} - \frac{16R}{3} + \frac{17}{9}\right)\ln r \\
&- \left(\frac{31r^2}{3} - \frac{7r}{3} - \frac{R^3}{18} + \frac{35R}{6} + \frac{5}{3}\right)\ln R - \frac{7r}{6} - \frac{11R^3}{8} + \frac{13R^2}{12} + \frac{73R}{36} + \frac{43}{72}, \quad (189)
\end{aligned}$$

$$\begin{aligned}
\frac{\tilde{\text{I}}_R^L}{\pi^2} &\rightarrow -4r^3\text{L}_3 - (-4r^2 + 2r + R^2 - R)\text{L}_2 - r^2(2+5r)\ln^2 R + (4r + 3R^2 - 7R)\ln r \\
&+ 7(-2r^2 + r - R)\ln R - 5r + \frac{13}{4}R^2 + \frac{15}{4}R, \quad (190)
\end{aligned}$$

with additional definitions:

$$\text{L}_2 = \frac{\text{Li}_2(1-1/R^2) - \text{Li}_2(1-R^2)}{2} + \Re\left(\text{Li}_2\left(1 + \frac{1}{R}\right) - \text{Li}_2(1+R)\right) + \text{Li}_2\left(-\frac{1}{r}\right) + 2\ln R \ln r, \quad (191)$$

$$\begin{aligned}
\text{L}_3 &= \frac{\text{Li}_3(1-1/R^2) + \text{Li}_3(1-R^2)}{2} + 2\left(\text{Li}_2(-R) + \frac{1}{2}\text{Li}_2(R^2)\right)\ln R - \text{Li}_2\left(-\frac{1}{r}\right)\ln R - \ln^2 R \ln r \\
&- \frac{\text{Li}_3(R^2)}{4} - \text{Li}_3(-R) - \text{Li}_3\left(-\frac{1}{R}\right) + \ln[(1-R^2)(1+R)]\ln^2 R - \pi^2 \ln \frac{1+R}{2\sqrt{R}} - \zeta(3) \\
&+ \Re\left(2\left(\text{Li}_3\left(1 + \frac{1}{R}\right) + \text{Li}_3(1+R)\right) - \frac{1}{4}\text{Li}_3\left(\frac{1}{R^2}\right) - 4\text{Li}_3(2)\right), \quad (192)
\end{aligned}$$

$$R = \frac{m}{m+2\omega}, \quad r = \frac{m}{2\omega}. \quad (193)$$

Note that the total elastic cross section at leading order is given by the following substitutions in Eqs. (14, 15),

$$\int d\omega' I_L \rightarrow \omega(1-R), \quad \int d\omega' I_R \rightarrow \frac{\omega(1-R^3)}{3}, \quad \int d\omega' I_R^L \rightarrow -\frac{\omega R^2}{r}. \quad (194)$$

L Averaged over flux neutrino cross sections

In the following, we average the energy spectrum with anticipated flux profiles of the DUNE Near Detector [132, 133] at Fermilab. In Figures 13 and 14, we show the resulting electron and electromagnetic energy spectra for neutrino and antineutrino beam modes.

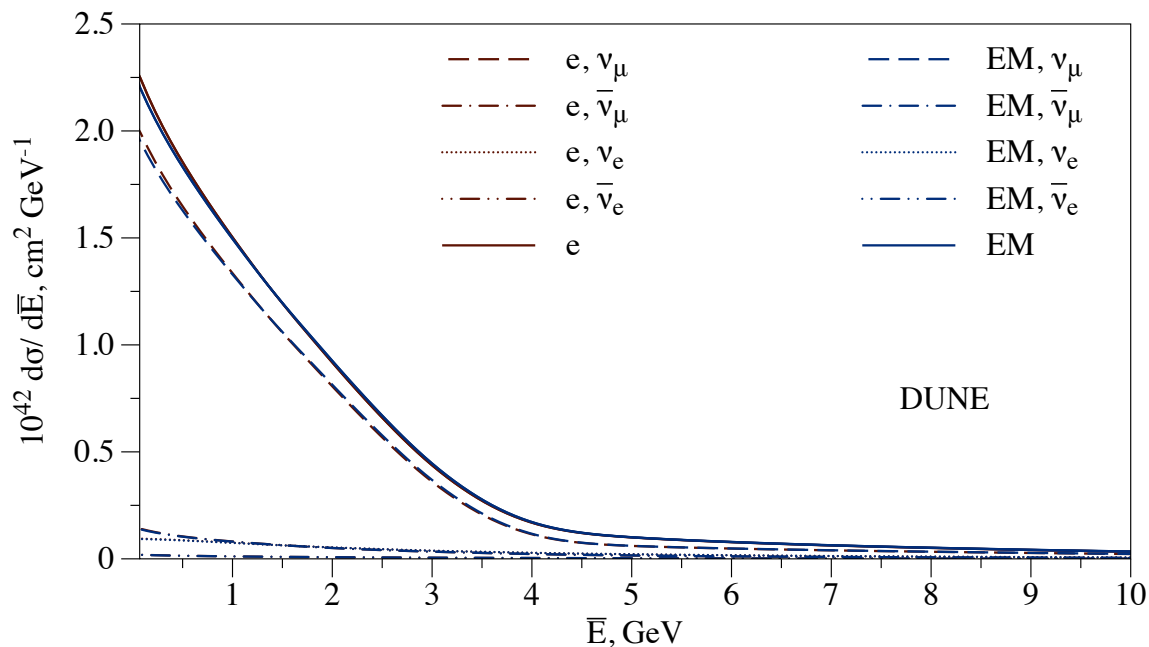


Figure 13: Electron (e) and electromagnetic (EM) energy spectra in elastic neutrino-electron scattering for neutrino beam mode of DUNE experiments. Electron energy spectrum is above at low energy. Electron and muon (anti-)neutrino contributions are shown as well.

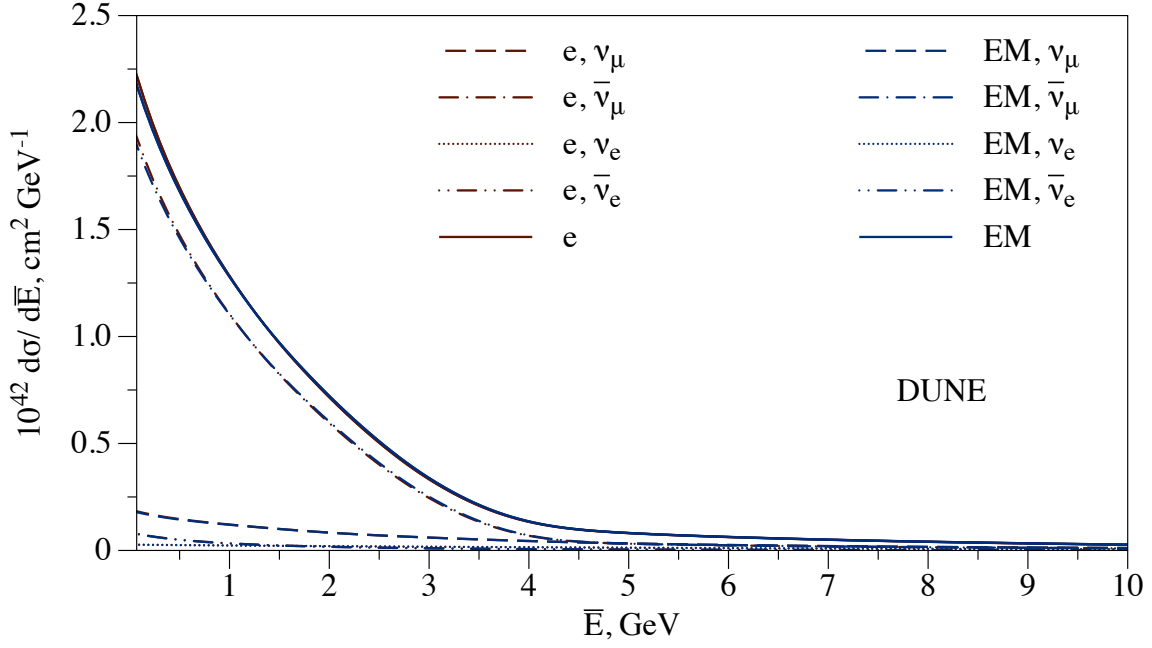


Figure 14: Same as Figure 13 for the antineutrino beam mode.

The corresponding Figures for MINERvA [19, 20, 134–136], NOvA [137], and T2K [138, 139] experiments are shown in Figures 15–20. The difference between the electron and electromagnetic energy spectra slightly washes out after averaging over the typical neutrino flux. It is larger at low energies, where it can reach an effect of the relative order 1–3 %, and smaller at higher energies reflecting the dependence in Figure 11.

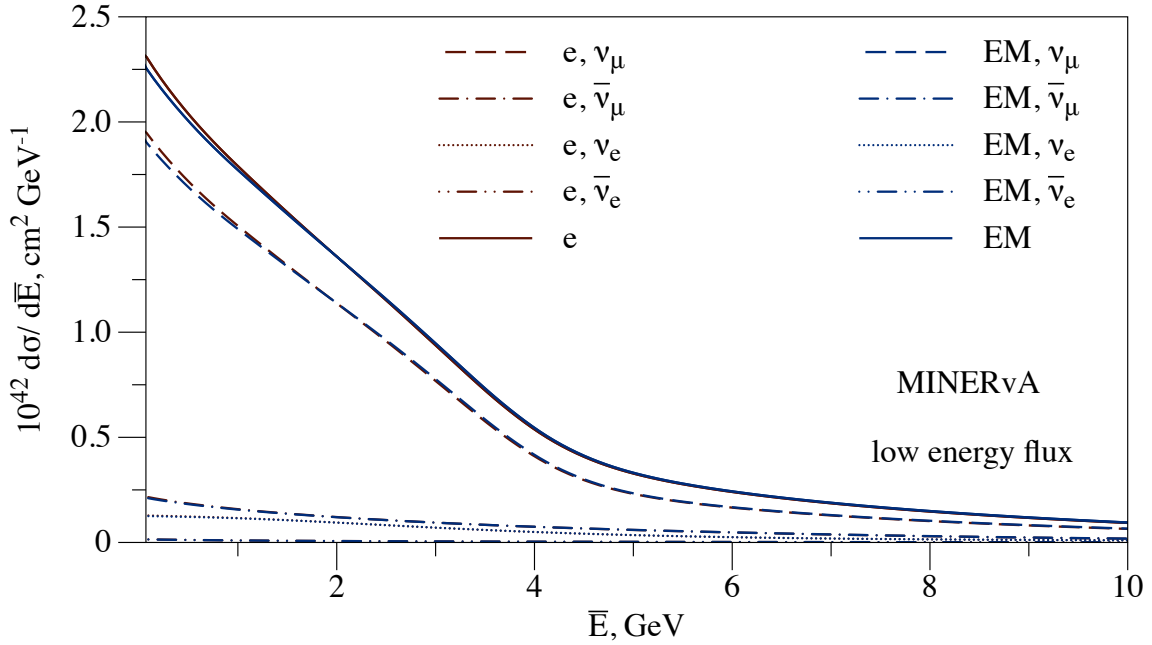


Figure 15: Same as Figure 13 for MINERvA experiment.

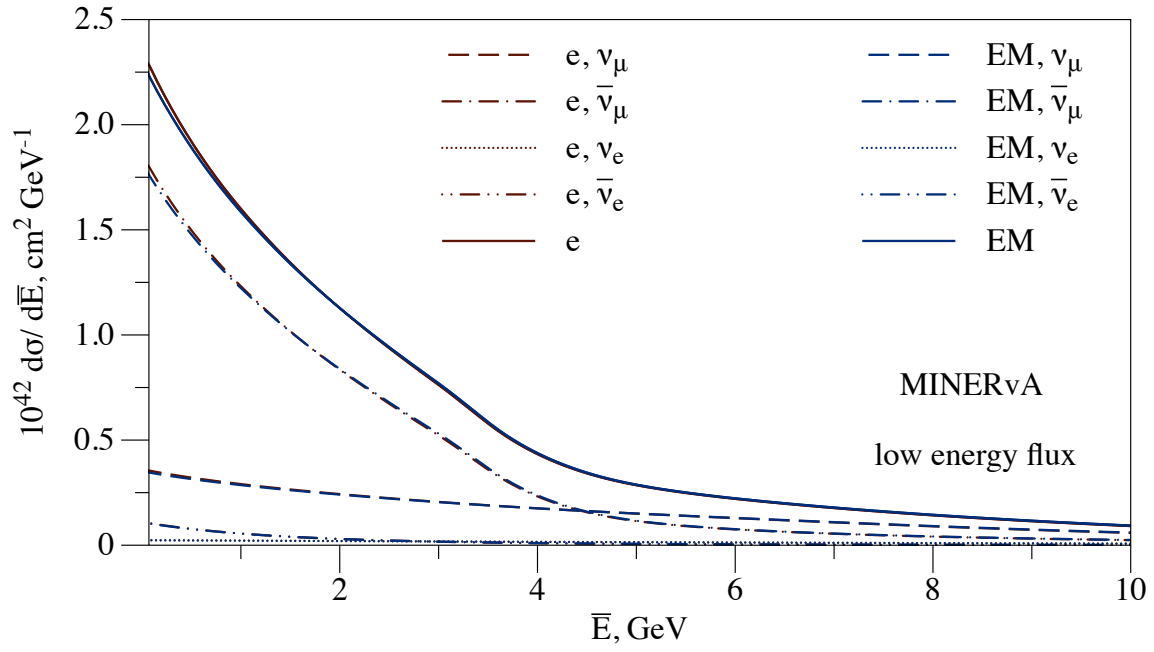


Figure 16: Same as Figure 14 for MINERvA experiment.

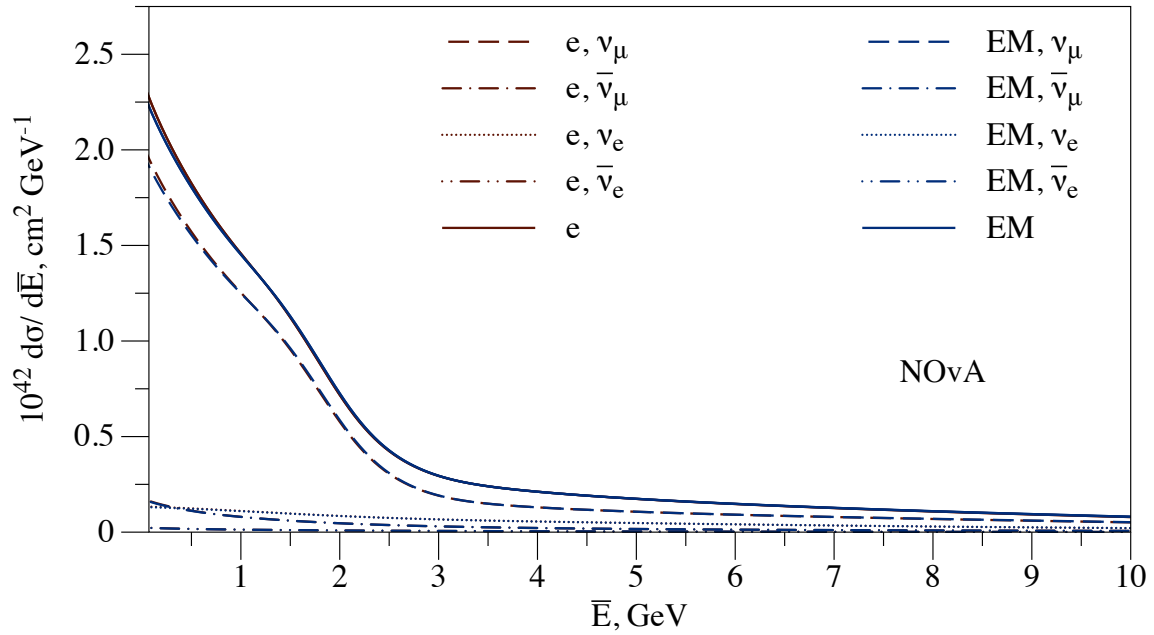


Figure 17: Same as Figure 13 for NOvA experiment.

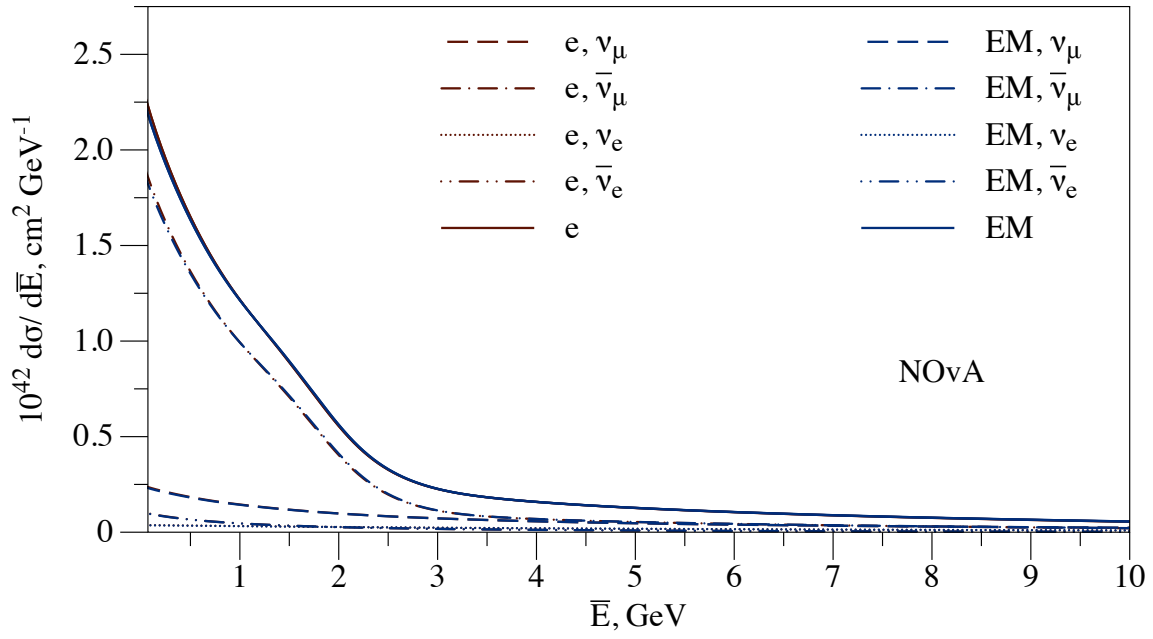


Figure 18: Same as Figure 14 for NOvA experiment.

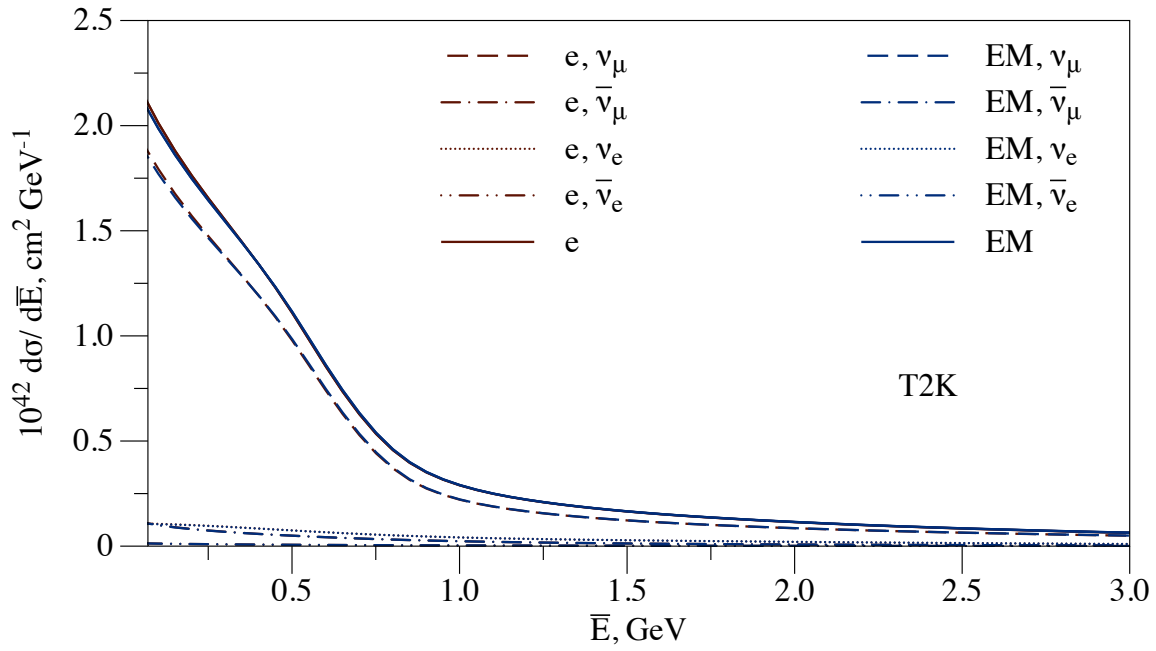


Figure 19: Same as Figure 13 for T2K experiment.

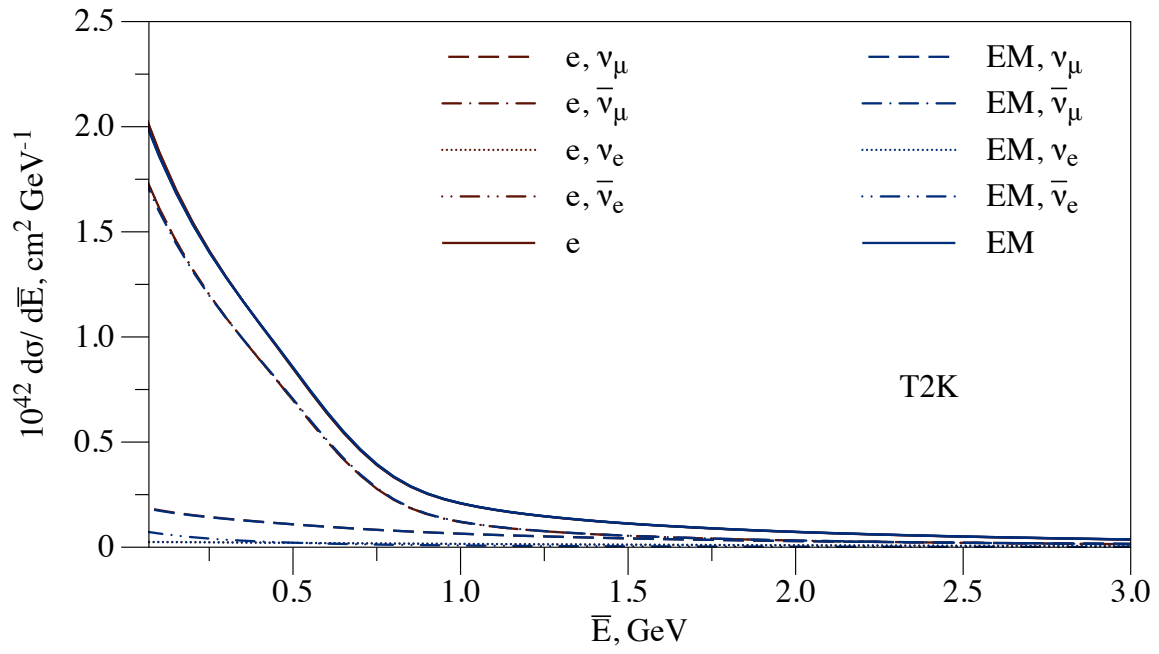


Figure 20: Same as Figure 14 for T2K experiment.

References

- [1] B. T. Cleveland, T. Daily, R. Davis, Jr., J. R. Distel, K. Lande, C. K. Lee, P. S. Wildenhain, and J. Ullman, *Astrophys. J.* **496**, 505 (1998).
- [2] W. Hampel *et al.* (GALLEX), *Phys. Lett.* **B447**, 127 (1999).
- [3] Q. R. Ahmad *et al.* (SNO), *Phys. Rev. Lett.* **89**, 011301 (2002).
- [4] J. N. Abdurashitov *et al.* (SAGE), *J. Exp. Theor. Phys.* **95**, 181 (2002), [*Zh. Eksp. Teor. Fiz.* 122, 211 (2002)].
- [5] S. Fukuda *et al.* (Super-Kamiokande), *Phys. Rev. Lett.* **86**, 5651 (2001).
- [6] S. N. Ahmed *et al.* (SNO), *Phys. Rev. Lett.* **92**, 181301 (2004).
- [7] Y. Fukuda *et al.* (Super-Kamiokande), *Phys. Rev. Lett.* **81**, 1562 (1998).
- [8] Y. Ashie *et al.* (Super-Kamiokande), *Phys. Rev. Lett.* **93**, 101801 (2004).
- [9] K. Eguchi *et al.* (KamLAND), *Phys. Rev. Lett.* **90**, 021802 (2003).
- [10] T. Araki *et al.* (KamLAND), *Phys. Rev. Lett.* **94**, 081801 (2005).
- [11] Y. Abe *et al.* (Double Chooz), *Phys. Rev.* **D86**, 052008 (2012).
- [12] J. K. Ahn *et al.* (RENO), *Phys. Rev. Lett.* **108**, 191802 (2012).
- [13] F. P. An *et al.* (Daya Bay), *Chin. Phys.* **C37**, 011001 (2013).
- [14] M. H. Ahn *et al.* (K2K), *Phys. Rev. Lett.* **90**, 041801 (2003).
- [15] D. G. Michael *et al.* (MINOS), *Phys. Rev. Lett.* **97**, 191801 (2006).
- [16] K. Abe *et al.* (T2K), *Phys. Rev.* **D88**, 032002 (2013).
- [17] B. Pontecorvo, *Sov. Phys. JETP* **6**, 429 (1957), [*Zh. Eksp. Teor. Fiz.* 33, 549 (1957)].
- [18] B. Pontecorvo, *Sov. Phys. JETP* **26**, 984 (1968), [*Zh. Eksp. Teor. Fiz.* 53, 1717 (1967)].
- [19] J. Park *et al.* (MINERvA), *Phys. Rev.* **D93**, 112007 (2016).
- [20] E. Valencia *et al.* (MINERvA), (2019), [arXiv:1906.00111](https://arxiv.org/abs/1906.00111) [hep-ex].
- [21] T. D. Lee and A. Sirlin, *Rev. Mod. Phys.* **36**, 666 (1964).
- [22] M. Ram, *Phys. Rev.* **155**, 1539 (1967).
- [23] S. Weinberg, *Phys. Rev. Lett.* **19**, 1264 (1967).
- [24] G. 't Hooft, *Phys. Lett.* **37B**, 195 (1971).
- [25] S. Sarantakos, A. Sirlin, and W. J. Marciano, *Nucl. Phys.* **B217**, 84 (1983).
- [26] J. N. Bahcall, M. Kamionkowski, and A. Sirlin, *Phys. Rev.* **D51**, 6146 (1995).
- [27] D. Yu. Bardin and V. A. Dokuchaeva, *Nucl. Phys.* **B246**, 221 (1984).
- [28] D. Yu. Bardin and V. A. Dokuchaeva, *Sov. J. Nucl. Phys.* **43**, 975 (1986), [*Yad. Fiz.* 43, 1513 (1986)].

- [29] M. Passera, *Phys. Rev.* **D64**, 113002 (2001).
- [30] M. Green, *J. Phys.* **G7**, 1169 (1981).
- [31] D. Yu. Bardin and V. A. Dokuchaeva, *Sov. J. Nucl. Phys.* **39**, 563 (1984), [*Yad. Fiz.* 39, 888 (1984)].
- [32] P. Salomonson and Y. Ueda, *Phys. Rev.* **D11**, 2606 (1975).
- [33] E. D. Zhizhin, R. V. Konoplich, and Yu. P. Nikitin, (1975), [*Izv. Vuz. Fiz.* 1975, no. 12, 82 (1975)].
- [34] N. Byers, R. Ruckl, and A. Yano, *Physica* **A96**, 163 (1979).
- [35] M. Green and M. J. G. Veltman, *Nucl. Phys.* **B169**, 137 (1980), [Erratum: *Nucl. Phys.* B175, 547 (1980)].
- [36] W. J. Marciano and A. Sirlin, *Phys. Rev.* **D22**, 2695 (1980), [Erratum: *Phys. Rev.* D31, 213 (1985)].
- [37] K.-i. Aoki, Z. Hioki, R. Kawabe, M. Konuma, and T. Muta, *Prog. Theor. Phys.* **65**, 1001 (1981).
- [38] K.-i. Aoki and Z. Hioki, *Prog. Theor. Phys.* **66**, 2234 (1981).
- [39] Z. Hioki, *Prog. Theor. Phys.* **67**, 1165 (1982).
- [40] A. M. Mourao, L. Bento, and B. K. Kerimov, *Phys. Lett.* **B237**, 469 (1990).
- [41] A. Weber and L. M. Sehgal, *Nucl. Phys.* **B359**, 262 (1991).
- [42] F. Buccella, C. Gualdi, G. Miele, and P. Santorelli, *Nuovo Cim.* **B107**, 1343 (1992).
- [43] J. Bernabeu, S. M. Bilenky, F. J. Botella, and J. Segura, *Nucl. Phys.* **B426**, 434 (1994).
- [44] E. Akhmedov, G. Arcadi, M. Lindner, and S. Vogl, *JHEP* **10**, 045 (2018).
- [45] W. J. Marciano and Z. Parsa, *J. Phys.* **G29**, 2629 (2003).
- [46] A. Sirlin and A. Ferroglia, *Rev. Mod. Phys.* **85**, 263 (2013).
- [47] O. Tomalak and R. J. Hill, “On effective theory of neutrino-electron and neutrino-quark scattering,” In preparation.
- [48] D. Akimov *et al.* (COHERENT), *Science* **357**, 1123 (2017).
- [49] D. S. Ayres *et al.* (NOvA), (2007), 10.2172/935497.
- [50] R. Acciarri *et al.* (DUNE), (2015), arXiv:1512.06148 [physics.ins-det].
- [51] K. Abe *et al.*, (2011), arXiv:1109.3262 [hep-ex].
- [52] K. Abe *et al.* (Super-Kamiokande), *Phys. Rev.* **D83**, 052010 (2011).
- [53] M. Wurm *et al.* (LENA), *Astropart. Phys.* **35**, 685 (2012).
- [54] Y.-F. Li, J. Cao, Y. Wang, and L. Zhan, *Phys. Rev.* **D88**, 013008 (2013).
- [55] C. Giunti and A. Studenikin, *Rev. Mod. Phys.* **87**, 531 (2015).
- [56] C. Giunti, K. A. Kouzakov, Y.-F. Li, A. V. Lokhov, A. I. Studenikin, and S. Zhou, *Annalen Phys.* **528**, 198 (2016).
- [57] E. Fermi, *Z. Phys.* **88**, 161 (1934).

- [58] R. P. Feynman and M. Gell-Mann, *Phys. Rev.* **109**, 193 (1958).
- [59] E. C. G. Sudarshan and R. E. Marshak, *Phys. Rev.* **109**, 1860 (1958).
- [60] M. E. Nahmias, *Math. Proc. Cambridge Phil. Soc.* **31**, 99 (1935).
- [61] H. R. Crane, *Rev. Mod. Phys.* **20**, 278 (1948).
- [62] J. H. Barrett, *Phys. Rev.* **79**, 907 (1950).
- [63] J. L. Kulp and L. E. Tyron, *Rev. Sci. Instr.* **23**, 296 (1952).
- [64] F. G. Houtermans and W. Thirring, *Helv. Phys. Acta* **27**, 81 (1954).
- [65] C. L. Cowan, F. Reines, and F. B. Harrison, *Phys. Rev.* **96**, 1294 (1954).
- [66] J. Bernstein, M. Ruderman, and G. Feinberg, *Phys. Rev.* **132**, 1227 (1963).
- [67] F. J. Hasert *et al.*, *Phys. Lett.* **B46**, 121 (1973).
- [68] F. Reines, H. S. Gurr, and H. W. Sobel, *Phys. Rev. Lett.* **37**, 315 (1976).
- [69] L. Wolfenstein, *Phys. Rev.* **D17**, 2369 (1978).
- [70] L. Wolfenstein, *Phys. Rev.* **D20**, 2634 (1979).
- [71] L. B. Okun, *Leptons and Quarks* (North-Holland, Amsterdam, Netherlands, 1982).
- [72] R. C. Allen *et al.*, *Phys. Rev. Lett.* **55**, 2401 (1985).
- [73] S. P. Mikheyev and A. Yu. Smirnov, *Sov. J. Nucl. Phys.* **42**, 913 (1985).
- [74] H. A. Bethe, *Phys. Rev. Lett.* **56**, 1305 (1986).
- [75] S. J. Parke, *Solar Neutrinos: An Overview*, *Phys. Rev. Lett.* **57**, 1275 (1986).
- [76] S. P. Rosen and J. M. Gelb, *Phys. Rev.* **D34**, 969 (1986).
- [77] J. Dorenbosch *et al.* (CHARM), *Z. Phys.* **C41**, 567 (1989), [Erratum: *Z. Phys.* C51, 142 (1991)].
- [78] R. C. Allen *et al.*, *Phys. Rev. Lett.* **64**, 1330 (1990).
- [79] L. A. Ahrens *et al.*, *Phys. Rev.* **D41**, 3297 (1990).
- [80] G. S. Vidyakin, V. N. Vydrov, I. I. Gurevich, Yu. V. Kozlov, V. P. Martemyanov, S. V. Sukhotin, V. G. Tarasenkov, E. V. Turbin, and S. K. Khakhimov, *JETP Lett.* **55**, 206 (1992), [*Pisma Zh. Eksp. Teor. Fiz.* 55, 212 (1992)].
- [81] R. C. Allen *et al.*, *Phys. Rev.* **D47**, 11 (1993).
- [82] A. I. Derbin, A. V. Chernyi, L. A. Popeko, V. N. Muratova, G. A. Shishkina, and S. I. Bakhlanov, *JETP Lett.* **57**, 768 (1993), [*Pisma Zh. Eksp. Teor. Fiz.* 57, 755 (1993)].
- [83] J. Horejsi, *Introduction to electroweak unification: Standard model from tree unitarity* (1993).
- [84] P. Vilain *et al.* (CHARM-II), *Phys. Lett.* **B335**, 246 (1994).
- [85] L. B. Auerbach *et al.* (LSND), *Phys. Rev.* **D63**, 112001 (2001).
- [86] D. W. Liu *et al.* (Super-Kamiokande), *Phys. Rev. Lett.* **93**, 021802 (2004).

- [87] Z. Daraktchieva *et al.* (MUNU), *Phys. Lett.* **B615**, 153 (2005).
- [88] A. G. Beda, V. B. Brudanin, E. V. Demidova, V. G. Egorov, M. G. Gavrilov, M. V. Shirchenko, A. S. Starostin, and T. Vylov, *Phys. Atom. Nucl.* **70**, 1873 (2007).
- [89] C. Arpesella *et al.* (Borexino), *Phys. Rev. Lett.* **101**, 091302 (2008).
- [90] M. Deniz *et al.* (TEXONO), *Phys. Rev.* **D81**, 072001 (2010).
- [91] A. G. Beda, V. B. Brudanin, V. G. Egorov, D. V. Medvedev, V. S. Pogosov, M. V. Shirchenko, and A. S. Starostin, *Adv. High Energy Phys.* **2012**, 350150 (2012).
- [92] J. A. Formaggio and G. P. Zeller, *Rev. Mod. Phys.* **84**, 1307 (2012).
- [93] J. Segura, J. Bernabeu, F. J. Botella, and J. Penarrocha, *Phys. Rev.* **D49**, 1633 (1994).
- [94] J. Bernabeu, J. Papavassiliou, and M. Passera, *Phys. Lett.* **B613**, 162 (2005).
- [95] J. S. Schwinger, *Phys. Rev.* **76**, 790 (1949).
- [96] R. Barbieri, J. A. Mignaco, and E. Remiddi, *Nuovo Cim.* **A11**, 824 (1972).
- [97] W. Pauli and M. E. Rose, *Phys. Rev.* **49**, 462 (1936).
- [98] R. P. Feynman, *Phys. Rev.* **76**, 769 (1949).
- [99] Y. S. Tsai, *Phys. Rev.* **120**, 269 (1960).
- [100] M. Vanderhaeghen, J. M. Friedrich, D. Lhuillier, D. Marchand, L. Van Hoorebeke, and J. Van de Wiele, *Phys. Rev.* **C62**, 025501 (2000).
- [101] M. Heller, O. Tomalak, M. Vanderhaeghen, and S. Wu, (2019), [arXiv:1906.02706](https://arxiv.org/abs/1906.02706) [hep-ph].
- [102] A. Djouadi and C. Verzegnassi, *Phys. Lett.* **B195**, 265 (1987).
- [103] A. Djouadi, *Nuovo Cim.* **A100**, 357 (1988).
- [104] B. A. Kniehl, *Nucl. Phys.* **B347**, 86 (1990).
- [105] S. Fanchiotti, B. A. Kniehl, and A. Sirlin, *Phys. Rev.* **D48**, 307 (1993).
- [106] F. Jegerlehner, *Z. Phys.* **C32**, 195 (1986).
- [107] F. Jegerlehner, *Workshop on New Physics: complementarities between direct and indirect searches (LC10) Frascati, Italy, November 30-December 3, 2010*, *Nuovo Cim.* **C034S1**, 31 (2011).
- [108] J. Erler, *Phys. Rev.* **D59**, 054008 (1999).
- [109] J. Erler and M. J. Ramsey-Musolf, *Phys. Rev.* **D72**, 073003 (2005).
- [110] J. Erler and R. Ferro-Hernández, *JHEP* **03**, 196 (2018).
- [111] F. Bloch and A. Nordsieck, *Phys. Rev.* **52**, 54 (1937).
- [112] N. Nakanishi, *Prog. Theor. Phys.* **19**, 159 (1958).
- [113] T. Kinoshita, *J. Math. Phys.* **3**, 650 (1962).
- [114] T. D. Lee and M. Nauenberg, *Phys. Rev.* **133**, B1549 (1964).

- [115] V. V. Sudakov, Sov. Phys. JETP **3**, 65 (1956), [Zh. Eksp. Teor. Fiz.30,87(1956)].
- [116] D. R. Yennie, S. C. Frautschi, and H. Suura, *Annals Phys.* **13**, 379 (1961).
- [117] M. Tanabashi *et al.* (Particle Data Group), *Phys. Rev.* **D98**, 030001 (2018).
- [118] W. Wetzel, *Z. Phys.* **C11**, 117 (1981).
- [119] N. A. Papadopoulos, J. A. Penarrocha, F. Scheck, and K. Schilcher, *Nucl. Phys.* **B258**, 1 (1985).
- [120] N. A. Papadopoulos, J. A. Penarrocha, F. Scheck, and K. Schilcher, *Phys. Lett.* **149B**, 213 (1984).
- [121] M. Cè, A. Gèrardin, K. Ottnad, and H. B. Meyer, *Proceedings, 36th International Symposium on Lattice Field Theory (Lattice 2018): East Lansing, MI, United States, July 22-28, 2018*, **PoS LATTICE2018**, 137 (2018).
- [122] R. J. Hill, K. S. McFarland, and O. Tomalak, “Radiative corrections to neutrino scattering,” In preparation.
- [123] R. J. Hill, *Phys. Rev.* **D95**, 013001 (2017).
- [124] R. Mertig, M. Bohm, and A. Denner, *Comput. Phys. Commun.* **64**, 345 (1991).
- [125] V. Shtabovenko, R. Mertig, and F. Orellana, *Comput. Phys. Commun.* **207**, 432 (2016).
- [126] T. Hahn and M. Perez-Victoria, *Comput. Phys. Commun.* **118**, 153 (1999).
- [127] D. Binosi and L. Theussl, *Comput. Phys. Commun.* **161**, 76 (2004).
- [128] W. R. Inc., “Mathematica, Version 11.0.1.0,” Champaign, IL, 2016.
- [129] K. G. Chetyrkin, J. H. Kuhn, and A. Kwiatkowski, *Phys. Rept.* **277**, 189 (1996).
- [130] K. G. Chetyrkin, J. H. Kuhn, and M. Steinhauser, *Nucl. Phys.* **B482**, 213 (1996).
- [131] K. G. Chetyrkin, B. A. Kniehl, and M. Steinhauser, *Nucl. Phys.* **B510**, 61 (1998).
- [132] T. Alion *et al.* (DUNE), (2016), [arXiv:1606.09550](https://arxiv.org/abs/1606.09550) [physics.ins-det].
- [133] “Dune fluxes,” <http://home.fnal.gov/~ljf26/DUNEFluxes/>, accessed: 2019-04-15.
- [134] J. Devan *et al.* (MINERvA), *Phys. Rev.* **D94**, 112007 (2016).
- [135] L. Aliaga *et al.* (MINERvA), *Phys. Rev.* **D94**, 092005 (2016), [Addendum: *Phys. Rev.* D95, no. 3, 039903 (2017)].
- [136] L. A. Soplín, *Neutrino Flux Prediction for the NuMI Beamline*, Ph.D. thesis, The College of William and Mary (2016).
- [137] “Nova fluxes,” <http://nova-docdb.fnal.gov/cgi-bin/ShowDocument?docid=25266>, accessed: 2019-04-24.
- [138] K. Abe *et al.* (T2K), *Phys. Rev.* **D87**, 012001 (2013), [Addendum: *Phys. Rev.* D87, no. 1, 019902 (2013)].
- [139] K. Abe *et al.* (T2K), *Phys. Rev.* **D91**, 072010 (2015).